

**Electromagnetic Nucleus - Nucleus Cross Sections  
using Energy Dependent Branching Ratios**

by

**Anne Marie Adamczyk**

A Dissertation

Submitted to the Faculty

of the

Worcester Polytechnic Institute

in partial fulfillment of the requirements for the

Degree of Doctor of Philosophy

in

Physics

April 2009

# Electromagnetic Nucleus - Nucleus Cross Sections using Energy Dependent Branching Ratios

by

Anne Marie Adamczyk

A Dissertation

Submitted to the Faculty

of the

Worcester Polytechnic Institute

in partial fulfillment of the requirements for the

Degree of Doctor of Philosophy

in

Physics

April 2009

APPROVED:

---

Dr. John W. Norbury, Major Advisor

---

Dr. Padmanabhan K. Aravind, Co - Advisor

---

Dr. Steve R. Blattnig, Committee Member  
NASA Langley Research Center

## Abstract

It is important that accurate estimates of crew exposure to radiation are obtained for future long - term space missions. To predict the radiation environment, a few space radiation transport codes exist, all of which use basic nuclear cross section information for transport of radiation through materials.

Little theoretical and experimental work has been conducted on reactions induced by the electromagnetic (EM) force, especially with regard to differential cross sections. Therefore, radiation transport codes have typically neglected to incorporate EM nuclear collision cross sections. EM cross sections for single nucleon removal have been included in some radiation codes, but better values can be obtained by using an energy dependent branching ratio. Most previous theoretical and experimental work has been devoted to total cross sections. Therefore, the energy dependent branching ratios presented can be extensively compared to past theory and experiment. Such comparisons indicate that using energy dependent branching ratios yield better estimates of total cross sections.

Differential cross sections for electromagnetic dissociation in nuclear collisions are calculated for the first time. In order to be useful for three - dimensional transport codes, these cross sections have been calculated in both the projectile and lab frames. The formulas for these cross sections are such that they can be immediately used in space radiation transport codes. Only a limited amount of data exists, but the comparison between theory and experiment is good.

## Acknowledgments

There are several people and organizations without whom this thesis would not have been possible and to whom I need to thank.

- I would like to thank NASA Langley Research Center for their financial support through the NASA Graduate Student Research Program Fellowship, of which I was a recipient for the past four years.
- I am grateful to Arvid E. Anderson for establishing the Arvid and Marietta Anderson Fellowship at Worcester Polytechnic Institute to honor his wife's memory. I benefited from the fellowship during the first year of my Ph.D. studies.
- I would like to acknowledge my advisor Dr. John Norbury for his advice, comments, and willingness to discuss any questions or ideas. I would like to express my gratitude for all that he has enabled me to accomplish.
- My thanks and appreciation goes to Dr. Padmanabhan Aravind, a thesis committee member, a co - advisor, and one of the kindest people I have ever met. He stepped in and provided mentorship, encouragement, and assistance when needed.
- Special thanks goes to two individuals at NASA Langley Research Center, Dr. Martha Cloudsley for her mentorship and Dr. Steve Blattnig, a committee member, who provided many valuable suggestions and comments.
- I am grateful for the friendship, entertainment, and caring nature of Merrill Lamont. His proofreading and contributions to this document are invaluable.

- I would like to thank Ken Pan for his love, emotional support, help through the difficult times, and belief in me. He was extremely influential in helping me achieve this step in my life.
- Lastly, I wish to thank my parents. Thank you for providing understanding, support, endless patience, and encouragement when it was most needed. To them I dedicate this thesis.

## List of symbols

Symbol	Description
$a$	Incident particle
$a$	Level density parameter ( $\text{MeV}^{-1}$ )
$\tilde{a}$	Asymptotic level density parameter ( $\text{MeV}^{-1}$ )
$\tilde{a}_B$	Asymptotic level density parameter of the residual nucleus $B$ ( $\text{MeV}^{-1}$ )
$A$	Incident Nucleus or Parent Nucleus
$A^*$	Compound nucleus excited state
$A_P$	Atomic mass number of the projectile
$\mathcal{A}$	Atomic mass number
$\mathcal{A}_B$	Atomic mass number of the residual nucleus $B$
$(A - N)_0$	Daughter Nucleus in the ground state
$b$	Emitted Particle
$b$	Impact Parameter (fm)
$b_{\min}$	Minimum Impact Parameter (fm)
$B$	Residual nucleus
$c$	Speed of light (m/s)
$C$	Compound nucleus
$C^*$	Excited compound nucleus
$C_n$	Parameter for $\sigma_{\text{inv},n}$
$\mathcal{C}$	Constant for the spectral distribution
$d$	Deuteron
$d_{\text{overlap}}$	Overlap distance (fm)

Continued on Next Page...

List of Symbols – Continued

Symbol	Description
$\mathcal{D}$	Constant used in the nuclear temperature formula
$e$	Electron charge (C)
$E$	Total energy (MeV)
$E_b$	Kinetic energy of emitted particle $b$ (MeV)
$E_{b,\max}$	Maximum kinetic energy of emitted particle $b$ (MeV)
$E_c$	Kinetic energy of an emitted charged particle (MeV)
$E_{\text{deform}}$	Deformation energy (MeV)
$E_{\text{exp}}$	Experimental atomic mass excess (MeV)
$E_{jl}$	Energy of particle $j$ in the lab frame (MeV)
$E_l$	Energy in the lab frame (MeV)
$E_{\text{ld}}$	Energy calculated with liquid drop formula (MeV)
$E_{\max}$	Maximum Energy (MeV)
$E_{\min}$	Minimum Energy (MeV)
$E_n$	Kinetic energy of an emitted neutron (MeV)
$E_{\text{threshold}}$	Threshold energy (MeV)
$E^*$	Excitation energy (MeV)
$E_B^*$	Excitation energy of nucleus $B$ (MeV)
$E_C^*$	Excitation energy of the compound nucleus $C$ (MeV)
$E_{\text{GDR}}$	Giant dipole resonance energy (MeV)
$E_N$	Total Energy (MeV)
$E_{\text{Th},b}$	Threshold energy for emitting particle $b$ (MeV)
$E_\gamma$	Photon Energy (MeV)

Continued on Next Page . . .

List of Symbols – Continued

Symbol	Description
$g_b$	Branching ratio for the emission of particle $b$
$g_n$	Neutron branching ratio
$g_p$	Proton branching ratio
$g_X$	Branching ratio for producing particle $X$
$h$	Plank's Constant, taken as $4.13566733 \times 10^{-21}$ MeV s
$H_{B \rightarrow C}$	Hamiltonian for a transition from state $B$ to $C$
$H_{C \rightarrow B}$	Hamiltonian for a transition from state $C$ to $B$
${}^3He$	Helion
$\mathcal{I}$	Intensity, energy per unit area per unit frequency interval
$j$	Particle
$J$	Nuclear liquid drop parameter, taken as 36.8 Mev
$\mathcal{J}$	Flux, number of incident particles per second per unit area
$k$	Boltzmann constant, taken to be 1
$k_c$	Penetrability coefficient for charged particles
$K$	Constant for an isotropic angular distribution
$K_0$	Modified Bessel function
$K_1$	Modified Bessel function
$m_a$	Nuclear mass of particle $a$ (MeV/c <sup>2</sup> )
$m_{\text{nucleon}}$	Nucleon mass, taken as 938.95 MeV/c <sup>2</sup>
$m_A$	Nuclear mass of nucleus $A$ (MeV/c <sup>2</sup> )
$m_N$	Atomic Mass of the emitted particle $N$ (MeV/c <sup>2</sup> )
$m^*$	7/10 nucleon mass (MeV/c <sup>2</sup> )

Continued on Next Page. . .

List of Symbols – Continued

Symbol	Description
$M_b$	Mass of emitted particle $b$ (MeV/c <sup>2</sup> )
$M_c$	Mass of an emitted charged particle (MeV/c <sup>2</sup> )
$M_n$	Mass of an emitted neutron (MeV/c <sup>2</sup> )
$M_B$	Mass of residual nucleus $B$ (MeV/c <sup>2</sup> )
$N$	Particle with mass number $N$
$N_P$	Neutron number of the projectile
$N(E_\gamma)$	Virtual photon spectrum (MeV <sup>-1</sup> )
$N(E_\gamma, \theta)$	Number of equivalent photons incident per unit area
$\mathcal{N}$	Number of events per second per nucleus
$p$	Proton
$p_b$	Momentum of emitted particle $b$ (MeV/c)
$p_{jl}$	Momentum of particle $j$ in the lab frame (MeV/c)
$p_B$	Momentum of residual nucleus $B$ (MeV/c)
$p_N$	Momentum of particle $N$ (MeV/c)
$p_T$	Momentum of the target (MeV/c)
$p_{Tl}$	Momentum of the target in the lab frame (MeV/c)
$P_{B \rightarrow C}$	Probability of a transition from state $B$ to $C$
$P_{C \rightarrow B}$	Probability of a transition from state $C$ to $B$
$Q'$	Nuclear liquid drop parameter, taken as 17 MeV
$r_0$	Radius parameter, taken to be 1.18 fm
$R_{0,B}$	Nuclear radius of residual nucleus $B$ (fm)
$R_{0.1,P}$	10% charge density radii for the projectile nucleus (fm)

Continued on Next Page . . .

List of Symbols – Continued

Symbol	Description
$R_{0.1,T}$	10% charge density radii for the target nucleus (fm)
$s$	Spin
$s_b$	Spin of emitted particle $b$
$s_c$	Spin of a charged particle
$s_n$	Spin of a neutron
$S$	Entropy
$t$	Triton
$T_{\text{lab}}$	Kinetic energy per particle $N$ of the projectile (MeV/Nucleon)
$T_{\text{max}}$	Kinetic energy maximum (MeV/Nucleon)
$T_{\text{min}}$	Kinetic energy minimum (MeV/Nucleon)
$T_N$	Kinetic energy of the emitted particle $N$ (MeV/Nucleon)
$T_B$	Temperature of residual nucleus $B$ (MeV)
$u$	Nuclear liquid drop parameter
$V_0$	Classical Coulomb barrier (MeV)
$V_{\text{Coulomb},b}$	Coulomb potential barrier for particle $b$ (MeV)
$\mathcal{V}_b$	Volume of normalization
$x$	Energy Parameter
$Z$	Atomic number
$Z_b$	Atomic number of the emitted particle $b$
$Z_B$	Atomic number of the residual nucleus $B$
$Z_P$	Atomic number of the projectile
$Z_T$	Atomic number of the target

Continued on Next Page. . .

List of Symbols – Continued

Symbol	Description
$\alpha$	Alpha particle
$\alpha_{\text{fsc}}$	Electromagnetic fine structure constant, taken to be 1/137
$\alpha_{jl}$	Ratio of the lab frame velocity to velocity of particle $j$
$\alpha_{jp}$	Ratio of the projectile frame velocity to velocity of particle $j$
$\alpha_v$	Volume component coefficient for $\tilde{a}$ (MeV <sup>-1</sup> )
$\beta$	Velocity in units of $c$
$\beta_{cl}$	Velocity in units of $c$ , in the center of mass frame relative to the lab frame
$\beta_{\text{deform}}$	Liquid drop deformation energies (MeV)
$\beta_n$	Parameter for $\sigma_{\text{inv},n}$ (MeV)
$\beta_{pl}$	Velocity in units of $c$ , in the projectile frame relative to the lab frame
$\beta_s$	Surface component coefficient for $\tilde{a}$ (MeV <sup>-1</sup> )
$\delta E_0$	Shell correction energy (MeV)
$\delta E_{0,B}$	Shell correction energy for residual nucleus $B$ (MeV)
$\epsilon$	Nuclear liquid drop parameter, taken to be 0.0768
$\epsilon_b$	Binding energy of particle $b$ (MeV)
$\epsilon_c$	Binding energy of an emitted charged particle (MeV)
$\epsilon_n$	Binding energy of an emitted neutron (MeV)
$\gamma$	Photon
$\gamma'$	Lorentz factor
$\gamma_{cl}$	Lorentz factor in the center of mass frame relative to the lab frame
$\gamma_{\text{damp}}$	Damping parameter (MeV <sup>-1</sup> )
$\gamma_{\text{damp},0}$	Phenomenological constant for the damping parameter (MeV <sup>-1</sup> )

Continued on Next Page . . .

List of Symbols – Continued

Symbol	Description
$\gamma_{jl}$	Lorentz factor particle $j$ in the lab frame
$\gamma_{pl}$	Lorentz factor in the projectile frame relative to the lab frame
$\Gamma$	Width of the electric dipole (E1) giant dipole resonance (MeV)
$\Gamma_b$	Partial width of decay for emitted particle $b$
$\Gamma_{\text{tot}}$	Total width of the state $C$
$\Gamma_{B \rightarrow C}$	Partial width of a transition from state $B$ to $C$
$\Gamma_{C \rightarrow B}$	Partial width of a transition from state $C$ to $B$
$\hbar$	Reduced Plank's constant, taken as $6.58211899 \times 10^{-22}$ MeV s
$\kappa$	Coulomb's constant, taken as $8.9876 \times 10^9$ (N m <sup>2</sup> /C <sup>2</sup> )
$\omega$	State density
$\omega_b$	Density of continuum states for emitted particle $b$
$\omega_B$	State density of state $B$
$\omega_C$	State density of state $C$
$\Omega_l$	Direction in the lab frame
$\Omega_{jl}$	Direction of particle $j$ in the lab frame
$\Omega_N$	Direction of particle $N$
$\psi_B$	Wavefunction of state $B$
$\psi_B^*$	Wavefunction of excited state $B$
$\psi_C$	Wavefunction of state $C$
$\psi_C^*$	Wavefunction of excited state $C$
$\rho$	Level density
$\rho_B$	Level density of state $B$

Continued on Next Page. . .

List of Symbols – Continued

Symbol	Description
$\rho_C$	Level density of state $C$
$\sigma_{abs}$	Absorption cross section (mb)
$\sigma_{geo,c}$	Geometrical cross section for an emitted charged particle (fm <sup>2</sup> )
$\sigma_{geo,n}$	Geometrical cross section for an emitted neutron (fm <sup>2</sup> )
$\sigma_{geo,B}$	Geometrical cross section for residual nucleus $B$ (fm <sup>2</sup> )
$\sigma_{inv}$	Inverse reaction cross section (fm <sup>2</sup> )
$\sigma_{inv,c}$	Inverse reaction cross section for charged particles (fm <sup>2</sup> )
$\sigma_{inv,n}$	Inverse reaction cross section for an emitted neutron (fm <sup>2</sup> )
$\sigma_m$	Cross section parameter (mb)
$\sigma_{tot}$	Photonuclear total cross section (mb)
$\sigma_{AA}$	Total nucleus - nucleus cross section (mb)
$\sigma_{A \rightarrow B}$	Cross section for the transition from state $A$ to $B$ (mb)
$\sigma_{A \rightarrow C}$	Cross section for the transition from state $A$ to $C$ (mb)
$\sigma_{TRK}$	Thomas - Reiche - Kuhn cross section (mb)
$\sigma_{\gamma A}(E_\gamma)$	Photonuclear total cross section (mb)
$v_b$	Velocity of emitted particle $b$ (MeV c)
$v_B$	Velocity of residual nucleus $B$ (MeV c)
$v_{bB}$	Relative velocity between particle $b$ and residual nucleus $B$ (MeV c)
$\theta_{jl}$	Angle of particle $j$ in the lab frame (rad)
$\theta_{jp}$	Angle of particle $j$ in the projectile frame (rad)
$\theta_l$	Angle in the lab frame (rad)
$\theta_N$	Angle of nucleus $N$ (rad)

Continued on Next Page . . .

List of Symbols – Continued

---



---

Symbol	Description
$\Theta$	Nuclear Temperature (MeV)
$\xi$	Adiabacity parameter
$\zeta$	Level density pre - factor
$d\tau$	Volume element
$\frac{dn}{dE}$	Density of continuum states
$\frac{d\sigma}{dE}$	Spectral Distribution (mb/MeV)
$\frac{d\sigma}{d\Omega}$	Angular Distribution (mb/sr)
$\frac{d^2\sigma}{dEd\Omega}$	Double differential cross section (mb/MeV sr)

---



---

# Contents

<b>1</b>	<b>Introduction</b>	<b>8</b>
1.1	Electromagnetic Dissociation cross sections . . . . .	9
1.2	Branching ratios for cross sections . . . . .	10
1.3	Differential cross sections . . . . .	11
1.4	Cross sections for transport codes . . . . .	12
<b>2</b>	<b>Compound nuclear reactions</b>	<b>13</b>
2.1	Weisskopf - Ewing theory . . . . .	14
2.2	Partial width of decay . . . . .	15
2.2.1	Density of continuum states . . . . .	16
2.2.2	Relative velocity . . . . .	19
2.2.3	Partial width of decay formula . . . . .	22
<b>3</b>	<b>Components of the partial width of decay</b>	<b>25</b>
3.1	Limits of integration . . . . .	25
3.1.1	Binding energy of emitted particles . . . . .	26
3.1.2	Coulomb potential barrier . . . . .	27
3.2	Cross section of an inverse reaction . . . . .	29
3.3	Nuclear level density . . . . .	30
3.3.1	Theoretical level density evaluation . . . . .	31
3.3.2	Level density experimental sources . . . . .	33
3.3.3	Level density parameter . . . . .	34
<b>4</b>	<b>Branching ratios</b>	<b>39</b>
4.1	Energy dependent branching ratio . . . . .	39

4.1.1	Approximate analytic partial width of decay formula . . . . .	40
4.2	Energy independent branching ratio . . . . .	42
<b>5</b>	<b>Photonuclear cross sections</b>	<b>44</b>
5.1	Relationship of compound nucleus decay and differential cross sections . .	44
5.2	Two - body final state . . . . .	45
5.3	Three - body final state . . . . .	46
5.4	Angular distribution . . . . .	48
5.5	Spectral distribution . . . . .	49
5.5.1	Useful integrals . . . . .	50
5.5.2	Spectral distribution in terms of total cross section . . . . .	51
5.6	Double differential cross section . . . . .	53
5.7	Lorentz invariant differential cross section . . . . .	53
5.8	Total cross section . . . . .	54
<b>6</b>	<b>Nucleus - nucleus cross sections</b>	<b>57</b>
6.1	Total cross section . . . . .	58
6.1.1	Weizsacker - Williams virtual photon spectrum . . . . .	59
6.2	Angular distribution . . . . .	62
6.3	Spectral distribution . . . . .	63
6.4	Double differential cross section . . . . .	63
6.5	Lorentz invariant differential cross section . . . . .	64
<b>7</b>	<b>Lorentz transformation of cross sections</b>	<b>65</b>
7.1	Discussion of photonuclear cross sections . . . . .	65
7.2	Lorentz transformation of photonuclear cross sections . . . . .	66

7.3	Transformation between CM or projectile frame and lab (target) frame . . .	67
7.4	Energy transformations . . . . .	68
7.5	Angle transformations . . . . .	69
7.6	Double differential cross sections . . . . .	74
<b>8</b>	<b>Results</b>	<b>76</b>
8.1	Photonuclear cross sections using energy dependent and independent branch- ing ratios compared to experiment . . . . .	76
8.2	Nucleus - nucleus cross sections using energy dependent and independent branching ratios compared to experiment . . . . .	82
8.3	Photonuclear and nucleus - nucleus differential cross sections in the projec- tile and lab frames . . . . .	86
8.4	Nucleus - nucleus spectral distributions compared to experiment . . . . .	96
<b>9</b>	<b>Conclusion</b>	<b>98</b>
<b>A</b>	<b>Tables</b>	<b>101</b>

## List of Figures

1	Energy level diagram . . . . .	23
2	Energy independent level density parameter comparison . . . . .	35
3	Myers - Swiatecki shell corrections . . . . .	38
4	Comparison of theoretical level density parameters . . . . .	38
5	Photonuclear reaction for a two - body final state . . . . .	46
6	Photonuclear reaction for a three - body final state . . . . .	47
7	Nucleus - nucleus reaction: Decay of excited parent nucleus to ground state of daughter nucleus . . . . .	57
8	Nucleus - nucleus reaction: Decay of excited parent nucleus to variety of energy levels in the excited daughter nucleus . . . . .	58
9	Relation between projectile and lab angles for an emitted photonucleon with kinetic energy $T_N = m_N$ or $\alpha = 1.15259$ . . . . .	72
10	Relation between projectile and lab angles for an emitted photonucleon with kinetic energy $T_N = 10m_N$ or $\alpha = 1.00232$ . . . . .	73
11	Relation between projectile and lab angles for an emitted photonucleon with kinetic energy $T_N = 16m_N$ or $\alpha = 0.999904$ . . . . .	73
12	Relation between projectile and lab angles for an emitted photonucleon with kinetic energy $T_N = 100m_N$ or $\alpha = 0.998222$ . . . . .	74
13	Comparison of theory, using energy dependent and independent branching ratios, to experiment for the reaction $^{14}\text{N}(\gamma, \text{n})$ . . . . .	78
14	Comparison of theory, using energy dependent and independent branching ratios, to experiment for the reaction $^{16}\text{O}(\gamma, \text{n})$ . . . . .	78

15	Comparison of theory, using energy dependent and independent branching ratios, to experiment for the reaction $^{28}\text{Si}(\gamma, n)$ . . . . .	79
16	Comparison of theory, using energy dependent and independent branching ratios, to experiment for the reaction $^{28}\text{Si}(\gamma, p)$ . . . . .	79
17	Comparison of theory, using energy dependent and independent branching ratios, to experiment for the reaction $^{88}\text{Sr}(\gamma, n)$ . . . . .	80
18	Comparison of theory, using energy dependent and independent branching ratios, to experiment for the reaction $^{91}\text{Zr}(\gamma, n)$ . . . . .	80
19	Comparison of theory, using energy dependent and independent branching ratios, to experiment for the reaction $^{208}\text{Pb}(\gamma, n)$ . . . . .	81
20	Photonuclear spectral distribution in projectile frame evaluated at a photon energy of 20 MeV . . . . .	88
21	Photonuclear angular distribution in projectile frame evaluated at a photon energy of 20 MeV . . . . .	88
22	Photonuclear double differential cross section in projectile frame evaluated at a photon energy of 20 MeV . . . . .	89
23	Photonuclear double differential cross section in lab frame evaluated at a photon energy of 20 MeV . . . . .	90
24	Photonuclear spectral distribution in lab frame evaluated at a photon energy of 20 MeV . . . . .	91
25	Photonuclear angular distribution in lab frame evaluated at a photon energy of 20 MeV . . . . .	91
26	Nucleus - nucleus spectral distribution in projectile frame . . . . .	92
27	Nucleus - nucleus angular distribution in projectile frame . . . . .	92
28	Nucleus - nucleus double differential cross section in projectile frame . . . . .	93

29	Nucleus - nucleus double differential cross section in lab frame . . . . .	94
30	Nucleus - nucleus spectral distribution in lab frame . . . . .	95
31	Nucleus - nucleus angular distribution in lab frame . . . . .	95
32	Comparison between theory and experiment [21] for the reaction $^{28}\text{Si} + \text{Pb}$ $\rightarrow 1\text{p} + ^{27}\text{Al} + \text{Pb}$ at 14.6 A GeV in the projectile frame . . . . .	97
33	Comparison between theory and experiment [21] for the reaction $^{28}\text{Si} + \text{Pb}$ $\rightarrow 1\text{n} + ^{27}\text{Si} + \text{Pb}$ at 14.6 A GeV in the projectile frame . . . . .	97

## List of Tables

2	Electromagnetic cross sections for single neutron, proton, and alpha particle removal . . . . .	84
3	Values for the width of the electric dipole Giant Dipole Resonance . . . . .	101
4	Values for the 10% charge density radius . . . . .	101
5	Values of the photoneutron cross section for $^{14}\text{N}$ calculated with energy dependent and independent branching ratios . . . . .	102
6	Values of the photoneutron cross section for $^{16}\text{O}$ calculated with energy dependent and independent branching ratios . . . . .	105
7	Values of the photoneutron cross section for $^{28}\text{Si}$ calculated with energy dependent and independent branching ratios . . . . .	109
8	Values of the photoproton cross section for $^{28}\text{Si}$ calculated with energy dependent and independent branching ratios . . . . .	112
9	Values of the photoneutron cross section for $^{88}\text{Sr}$ calculated with energy dependent and independent branching ratios . . . . .	115
10	Values of the photoneutron cross section for $^{91}\text{Zr}$ calculated with energy dependent and independent branching ratios . . . . .	118
11	Values of the photoneutron cross section for $^{208}\text{Pb}$ calculated with energy dependent and independent branching ratios . . . . .	121

# 1 Introduction

The issue of protecting astronauts from cosmic radiation is becoming increasingly important with the current plans to establish a permanent human base on the Moon with a follow - on mission to Mars. During a Mars mission, astronauts will be exposed to cosmic radiation fields for several years. When traveling into space, astronauts receive radiation from a variety of sources. Astronauts are no longer protected by Earth's magnetic field and atmosphere, so they will experience radiation from the Van Allen radiation belts, solar energetic particles, Galactic cosmic rays, and other sources. It is important that accurate estimates of crew exposure to radiation are obtained for long - term missions, since with accurate estimates, safe lunar and martian habitats will be possible. The exposure of astronauts to health risks demands attention because exploration must continue without compromising the well - being of humans in space.

To predict radiation exposure to astronauts, there currently exist a few transport codes. The Monte Carlo high energy transport code HETC [1] is commonly used to predict radiation exposure and PHITS, a general purpose Monte Carlo code, has been applied to spacecraft design [2]. Another transport code being utilized in space radiation research is MCNPX (Monte Carlo N - Particle eXtended) [3]. Two other Monte Carlo codes, FLUKA [4] and GEANT [5], which in the past have been included in particle physics experiments, are now receiving new life in calculating radiation amounts. The deterministic transport code HZETRN [6, 7] (High Z and Energy TRaNsport) is also frequently used. As input for all these transport codes, particle interaction cross sections are required.

## 1.1 Electromagnetic Dissociation Cross Sections

A relativistic nucleus - nucleus collision will result when a cosmic ray nucleus interacts with a spacecraft wall or other material. The incident projectile cosmic ray nucleus, for example, can be a proton or iron nucleus, while spacecraft have been typically designed with aluminum or light nuclei [8]. The presence of heavy nuclei ( $Z < 26$ ) with very high energy is unique to cosmic radiation fields. In calculating space radiation environments, it is therefore necessary to have an excellent knowledge of nucleus - nucleus collisions in the intermediate energy GeV region where the cosmic ray spectrum reaches a maximum. The cosmic ray's peak energy region lies around 1-10 GeV [9], which is easily accessible to particle accelerators. Therefore, experimental cross sections can be measured.

In a relativistic nucleus - nucleus collision, the nuclei may either collide or miss each other. When the nuclei come closer than approximately one femtometer to each other, they collide or undergo a strong interaction because of the small distance between them. When the distance of approach is larger, a strong interaction will not occur. The nuclei will miss each other, but they will still interact via the longer range electromagnetic (EM) force. One way to envision this process is to take the example of a virtual photon traveling from one nucleus to the other, causing a nuclear excitation [10]. There are many photons with low energy, dropping off to a few photons with high energy up to some maximum cutoff. The most important photons are those with frequencies near the resonant vibration frequency of the nucleus [10]. These result in a nuclear excitation known as the Giant Dipole Resonance (GDR), where the entire nucleus undergoes large internal vibrations, decaying with the emission of nucleons. Relativistic nucleus - nucleus reactions occurring via the EM force, with GDR excitation and subsequent particle emission, is often called ElectroMagnetic Dissociation (EMD).

A study of electromagnetic and strong interaction cross sections for single nucleon removal was conducted by Norbury and Maung [10]. Their analysis shows that for a typical space radiation reaction of an iron projectile interacting with an aluminum target, the EM cross section can be as much as 30-50% of the strong interaction cross section, for kinetic energies in the range of 1-10 GeV/A. For a kinetic energy of 50 GeV/A, the EM cross section is approximately 80% of the strong interaction cross section. The study of Norbury and Maung [10] shows the importance of including EM cross sections in space radiation transport codes, since total cross section values would be underestimated without the inclusion of EM cross sections.

## 1.2 Branching Ratios for Cross Sections

A vital component to any EMD cross section calculation is the related photonuclear cross section. The photonuclear total cross section is found by multiplying the branching ratio by the photonuclear absorption cross section. A parameterization of the absorption cross section has been well established, but the calculation of branching ratios deserves investigation. Westfall et al. [11] suggested an expression for an energy independent branching ratio, which was later improved upon by Norbury and Townsend [12]. Their combined formalism for the probability of proton and neutron emission when multiplied by experimental absorption cross sections fits experimental data for photoneutron and photoproton cross sections well, but better estimates can be achieved with a photon energy dependent branching ratio. This paper introduces energy dependent branching ratios, derived from Weisskopf - Ewing theory. With this method, branching ratios can be calculated for not only proton and neutron channels, but also for alpha particle, helion, deuteron, and triton emission.

The amount of available cross section data for the emission of particles heavier than an alpha particle is quite limited. Most experimental efforts have focused on calculating cross sections for proton or neutron emission, because proton and neutron emission is generally more probable than heavier particle emission. Consequently, only extensive comparisons to experiment calculated using both energy dependent and independent branching ratios can be made for photoneutron and photoproton cross sections. This paper examines both energy dependent and independent branching ratios and their applicability.

### 1.3 Differential Cross Sections

The transport codes HZETRN [6, 7] and FLUKA [4] include the calculation of total EMD cross sections by using currently available parameterizations of total cross sections [14, 15, 16]. HZETRN uses the nuclear fragmentation model NUCFRG2 [13] to calculate EMD cross sections. Differential EMD cross sections are necessary because fully-three dimensional transport codes require energy and angular differential cross sections. Information regarding the angle and energy in which particles emerge is lost without the inclusion of double differential cross sections.

Previous theoretical and experimental work was done on calculating EM differential cross sections [17, 18, 19, 20, 21], but what is needed is a systematic calculation of differential cross sections, such as angular distributions and spectral distributions [20]. Unfortunately, due to the limited nature of theoretical work on differential cross sections, no extensive comparisons with experiment exist. This paper discusses a theoretical program that has now been created to calculate differential EMD cross sections.

## 1.4 Cross Sections for Transport Codes

To improve run-time, transport codes often require parameterizations of cross sections. The differential cross sections developed in the present work are written in terms of the total cross section, parameterizations of which are available [14, 15, 16]. Therefore, if the parameterized form of the total cross section is used, then the differential cross sections are also parameterized.

Fully three - dimensional transport codes require cross sections in the lab frame. All the differential cross sections in this paper are evaluated in the rest frame of the compound nucleus. If the compound nucleus is the projectile, then the differential cross sections must be transformed to the lab frame for use in transport codes. If the compound nucleus is the target, then no transformation is necessary because the target is at rest in the lab frame. This paper presents Lorentz transformations for transforming between the projectile and lab frames. The formulas are such that they can be immediately used in space radiation transport codes.

## 2 Compound Nuclear Reactions

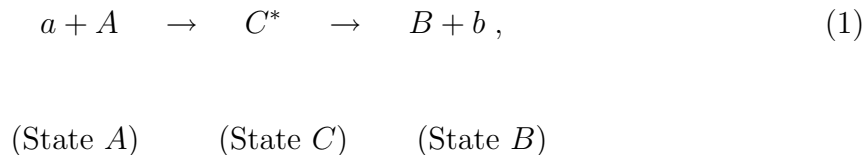
In 1936, Neils Bohr discovered that a compound nuclear reaction can be divided into two separate and independent processes. The first stage is the formation of the compound nucleus in an excited energy state. The compound nucleus reaches statistical equilibrium before the second stage, where the compound nucleus decays into the products of the reaction. The formation and decay of the compound nucleus can be considered independent processes because only the energy, angular momentum, and parity determine the disintegration of the compound system. The way in which the compound nucleus was formed will not effect the decay products. This can be tested experimentally by comparing the cross sections of identical compound nucleus decay products that are formed by two different processes. The idea that a compound nucleus' products are independent from the nuclei that formed it became known as the Bohr Independence Hypothesis [22, 23, 24]. For this hypothesis to be valid, the compound nucleus is required to reach statistical equilibrium, which takes typically  $10^{-19}$  to  $10^{-15}$  seconds [25]. Particles can then be emitted by a statistical method that resembles the evaporation of molecules from a liquid drop.

The foundation of compound nucleus reaction theory created by the Bohr Independence Hypothesis was used in 1940 by Weisskopf and Ewing [22, 23, 24, 25, 26, 27, 28, 29, 30]. They developed a theory to calculate cross sections of all the final channels in a compound nucleus reaction. The Weisskopf - Ewing theory provides a simple way of calculating compound nuclear reactions going to continuum states. The only disadvantage of this theory is that it does not consider the conservation of angular momentum. The Hauser - Feshbach theory [22, 26, 27], which was developed in 1952, is more complex since it accounts for states of different parity and angular momentum in compound nucleus formation. Here, the quantum mechanical formalism is not limited to only continuum states;

cross sections for reactions to discrete final states can also be found. Due to the large amount of computing time required to account for all the possible dynamical paths during the evaporation process [27], it was determined that this method was impracticable for space radiation calculations. This paper will no longer discuss the Hauser - Feshbach theory. To calculate the cross sections of reactions that pass through a compound nucleus state, the Weisskopf - Ewing theory will be employed.

## 2.1 Weisskopf - Ewing Theory

Consider a nuclear reaction where a particle  $a$  strikes a nucleus  $A$  to produce a residual nucleus  $B$  and an outgoing particle  $b$ . The reaction proceeds through a well - defined compound state,



where  $C$  represents the intermediate compound nucleus and the  $*$  signifies an excited state. Particles  $a$  and  $b$  may be elementary particles, such as neutrons and protons, although they could also be nuclei, such as helions, deuterons, tritons, or alpha particles. The nuclear evaporation formalism of Weisskopf and Ewing will ignore the direct reaction



Once the compound nucleus is formed, the probability of the emitted particle  $b$  can be determined. This probability is contained in the cross section formula [25, 29],

$$\sigma_{A \rightarrow B}(E_C^*, E_b) = \sigma_{A \rightarrow C}(E_C^*) \frac{\Gamma_b(E_C^*, E_b)}{\Gamma_{\text{tot}}(E_C^*, E_b)}, \quad (3)$$

where  $E_C^*$  is the excitation energy of the compound nucleus  $C$  and  $E_b$  is the kinetic energy of the emitted particle  $b$ . The cross section for this reaction can be decomposed into a cross section  $\sigma_{A \rightarrow C}(E_C^*)$  for the formation of the compound state, and the probability that the compound state will decay into the exit channel  $B$ . This probability is given by the ratio  $\Gamma_b/\Gamma_{\text{tot}}$ , where  $\Gamma_{\text{tot}}$  represents the total width of the state  $C$  and  $\Gamma_b$  is the partial width of decay into the channel  $B$ . This probability is given by  $g_b$  and is also known as the branching ratio of the reaction for the emission of particle  $b$ ,

$$g_b(E_C^*, E_b) = \frac{\Gamma_b(E_C^*, E_b)}{\Gamma_{\text{tot}}(E_C^*, E_b)}. \quad (4)$$

## 2.2 Partial Width of Decay

The partial width of decay into channel  $B$  can be found from the the probability of a transition from state  $C$  to state  $B$  [29]. Using the Fermi second Golden Rule, the probability of a transition from  $C$  to  $B$  is expressed as [29]

$$P_{C \rightarrow B} = \frac{2\pi}{\hbar} \left| \int \psi_B^* H_{C \rightarrow B} \psi_C d\tau \right|^2 \frac{dn}{dE} \quad (5)$$

$$= \frac{1}{\hbar} \Gamma_b(E_C^*, E_b), \quad (6)$$

where  $\psi_C$  and  $\psi_B^*$  are the wavefunctions of the state  $C$  and the excited state  $B$ , respectively. Also,  $H_{C \rightarrow B}$  is defined as the Hamiltonian for a transition from state  $C$  to  $B$ ,  $d\tau$  is the volume element, and  $dn/dE$  is the density of continuum states. Now, rearrange equation (6) to find the relation for the partial width of decay into channel  $B$ ,

$$\Gamma_b(E_C^*, E_b) = 2\pi \left| \int \psi_B^* H_{C \rightarrow B} \psi_C d\tau \right|^2 \frac{dn}{dE} . \quad (7)$$

The partial width of decay can also be found using the principle of detailed balance [23, 27]. Using either the second Golden Rule or the principle of detailed balance will yield the same expression for the partial width.

### 2.2.1 Density of Continuum States

In the final state  $B$ , the particle  $b$  has a momentum  $p_b$  and a spin  $s_b$ . The number of available states requires a multiplicative term, the statistical weight  $(2s_b + 1)$ , to be included. The relation for the number of accessible states becomes [29]

$$dn = \frac{4\pi p_b^2 dp_b}{(2\pi\hbar)^3} (2s_b + 1) \mathcal{V}_b , \quad (8)$$

where the volume of normalization is given by  $\mathcal{V}_b$ . Dividing each side by  $dE$  gives the relation for the density of continuum states,

$$\frac{dn}{dE} = \frac{4\pi p_b^2}{(2\pi\hbar)^3} \frac{dp_b}{dE} (2s_b + 1) \mathcal{V}_b . \quad (9)$$

The kinetic energies  $E_B$  and  $E_b$ , for the residual nucleus  $B$  and the emitted particle  $b$ , respectively, are small enough that nonrelativistic energy and momentum relations can be used. To emphasize this point, take a 20 MeV proton. The nonrelativistic limit corresponds to  $v \ll c$ , where  $v$  is the velocity and  $c$  is the speed of light. A 20 MeV proton will have a velocity of approximately  $9.69/c$ , which is much less than  $c$ .

For the reaction in equation (1), the total energy is given by

$$E = E_b + E_B \quad (10)$$

$$= \frac{p_b^2}{2M_b} + \frac{p_B^2}{2M_B}, \quad (11)$$

where  $p_b$  and  $p_B$  are the momentum for the emitted particle  $b$  and the residual nucleus  $B$ , respectively. Also,  $M_b$  is the mass for the emitted particle  $b$  and  $M_B$  is the mass for the residual nucleus  $B$ . From conservation laws, the momentum is expressed as

$$\mathbf{p}_b = -\mathbf{p}_B. \quad (12)$$

Differentiating equation (11) with respect to the momentum for particle  $b$  results in

$$\begin{aligned} \frac{dE}{dp_b} &= \frac{p_b}{M_b} + \frac{1}{M_B} \frac{d(p_B^2)}{dp_b} \\ &= p_b \left( \frac{1}{M_b} + \frac{1}{M_B} \right) \\ &= p_b \left( \frac{M_B + M_b}{M_b M_B} \right). \end{aligned} \quad (13)$$

Insert the momentum for the emitted particle  $b$ ,  $p_b = \sqrt{2M_b E_b}$ , to find

$$\frac{dE}{dp_b} = \sqrt{2M_b E_b} \left( \frac{M_B + M_b}{M_b M_B} \right). \quad (14)$$

The nonrelativistic kinetic energy for the emitted particle  $b$  is given by  $E_b = \frac{1}{2}M_b v_b^2$ , where  $v_b$  is the velocity of the emitted particle  $b$ . When inserting  $E_b$ , the statistical factor  $dE/dp_b$  reduces to

$$\begin{aligned} \frac{dE}{dp_b} &= \sqrt{2M_b \left( \frac{1}{2}M_b v_b^2 \right)} \left( \frac{M_B + M_b}{M_b M_B} \right) \\ &= M_b v_b \left( \frac{M_B + M_b}{M_b M_B} \right) \\ &= v_b \left( \frac{M_B + M_b}{M_B} \right) \\ &= v_{bB}, \end{aligned} \quad (15)$$

where  $v_{bB}$  is the relative velocity between the emitted particle  $b$  and the residual nucleus  $B$ . By inverting equation (15) the relationship for the statistical factor  $dp_b/dE$  has the form

$$\frac{dp_b}{dE} = \frac{1}{v_{bB}}. \quad (16)$$

The statistical factor above is now substituted into equation (9) to find a more usable form for the density of continuum states,

$$\frac{dn}{dE} = \frac{4\pi p_b^2}{(2\pi\hbar)^3} \frac{1}{v_{bB}} (2s_b + 1) \mathcal{V}_b . \quad (17)$$

In the final state, nucleus  $B$  has a kinetic energy and  $E_B^*$ , an excitation energy. Assume that  $E_B^*$  lies in the continuum of states; therefore the number of levels should be included as a multiplicative term,  $\rho_B(E_B^*)$ , which is the level density of the residual nucleus  $B$ . Thus, the excitation energy dependent density of continuum states is finally expressed as

$$\frac{dn}{dE} = \rho_B(E_B^*) \frac{4\pi p_b^2}{(2\pi\hbar)^3 v_{bB}} (2s_b + 1) \mathcal{V}_b . \quad (18)$$

### 2.2.2 Relative Velocity

To find the relative velocity  $v_{bB}$ , consider the cross section for the inverse reaction,



(State B)                      (State C)

In order to calculate the inverse reaction cross section from state  $B$  to state  $C$ , begin from the fundamental definition of a cross section. A cross section is defined as [29]

$$\sigma = \frac{\mathcal{N}}{\mathcal{J}} , \quad (20)$$

where  $\mathcal{N}$  is the number of events per second per nucleus and  $\mathcal{J}$  is the incident flux of particles. It is important to remember that both the numerator and denominator are proportional to the number of particles incident; as a result, this quantity cancels out [29].

For the inverse reaction cross section formula, the numerator contains the product of the number of incident particles and the reaction probability,  $P_{B \rightarrow C}$ . The denominator contains the product of the number of incident particles in the volume of normalization,  $\mathcal{V}_b$ , and the relative velocity,  $v_{bB}$ . The number of particles incident will drop out, as mentioned previously. The inverse reaction cross section reduces to

$$\sigma_{\text{inv}}(E_b) = P_{B \rightarrow C} \frac{\mathcal{V}_b}{v_{bB}} . \quad (21)$$

By rearranging it can be seen that the probability  $P_{B \rightarrow C}$  for the inverse reaction is related to the cross section  $\sigma_{\text{inv}}$  by the formula

$$P_{B \rightarrow C} = \frac{v_{bB} \sigma_{\text{inv}}(E_b)}{\mathcal{V}_b} . \quad (22)$$

Again, the probability  $P_{B \rightarrow C}$  can be expressed according to the Fermi second Golden Rule as

$$P_{B \rightarrow C} = \frac{2\pi}{\hbar} \left| \int \psi_C^* H_{B \rightarrow C} \psi_B d\tau \right|^2 \frac{dn}{dE} . \quad (23)$$

where  $\psi_B$  and  $\psi_C^*$  are the wavefunctions for the state  $B$  and excited state  $C$ , respectively. Also,  $H_{B \rightarrow C}$  is the Hamiltonian for the transition from state  $B$  to  $C$ . Only this time, the density of continuum states is given by the level density

$$\frac{dn}{dE} = \rho_C(E_C^*), \quad (24)$$

since the final state in reaction (19) is just the compound state [29].

Rearranging equation (22) to be put in terms of the relative velocity yields

$$v_{bB} = \frac{P_{B \rightarrow C} \mathcal{V}_b}{\sigma_{\text{inv}}(E_b)}. \quad (25)$$

Now, replace probability  $P_{B \rightarrow C}$  (23), expressed by the second Golden Rule, to obtain

$$v_{bB} = \frac{\frac{2\pi}{\hbar} |\int \psi_C^* H_{B \rightarrow C} \psi_B d\tau|^2 \frac{dn}{dE} \mathcal{V}_b}{\sigma_{\text{inv}}(E_b)}. \quad (26)$$

Finally, substitute in the density of continuum states (24) to achieve the relative velocity relationship,

$$v_{bB} = \frac{\frac{2\pi}{\hbar} |\int \psi_C^* H_{B \rightarrow C} \psi_B d\tau|^2 \rho_C(E_C^*) \mathcal{V}_b}{\sigma_{\text{inv}}(E_b)}. \quad (27)$$

### 2.2.3 Partial Width of Decay Formula

Putting all the derived pieces together, the final form for the partial width of decay into channel  $B$  can now be found. The probability formula, given by the second Golden Rule, once rearranged gave a starting point for the partial width relationship. Begin by substituting the density of continuum states, given by equation (18), into the partial width of decay equation (7) to obtain

$$\Gamma_b(E_C^*, E_b) = 2\pi \left| \int \psi_B^* H_{C \rightarrow B} \psi_C d\tau \right|^2 \rho_B(E_B^*) \frac{4\pi p_b^2}{(2\pi\hbar)^3} \frac{1}{v_{bB}} (2s_b + 1) \mathcal{V}_b. \quad (28)$$

Inserting the relative velocity relation (27) yields

$$\Gamma_b(E_C^*, E_b) = 2\pi \left| \int \psi_B^* H_{C \rightarrow B} \psi_C d\tau \right|^2 \rho_B(E_B^*) \frac{4\pi p_b^2}{(2\pi\hbar)^3} \quad (29)$$

$$\times \frac{\sigma_{\text{inv}}(E_B^*)}{\frac{2\pi}{\hbar} \left| \int \psi_C^* H_{B \rightarrow C} \psi_B d\tau \right|^2 \rho_C(E_C^*) \mathcal{V}_b} (2s_b + 1) \mathcal{V}_b. \quad (30)$$

Rearrange and simplify to find

$$\Gamma_b(E_C^*, E_b) = \frac{\left| \int \psi_B^* H_{C \rightarrow B} \psi_C d\tau \right|^2}{\left| \int \psi_C^* H_{B \rightarrow C} \psi_B d\tau \right|^2} \frac{1}{2\pi^2 \hbar^2} p_b^2 (2s_b + 1) \frac{\rho_B(E_B^*)}{\rho_C(E_C^*)} \sigma_{\text{inv}}(E_b). \quad (31)$$

The matrix elements in  $\Gamma_b$  will cancel giving [29]

$$\Gamma_b(E_C^*, E_b) = \frac{1}{2\pi^2 \hbar^2} p_b^2 (2s_b + 1) \frac{\rho_B(E_B^*)}{\rho_C(E_C^*)} \sigma_{\text{inv}}(E_b). \quad (32)$$

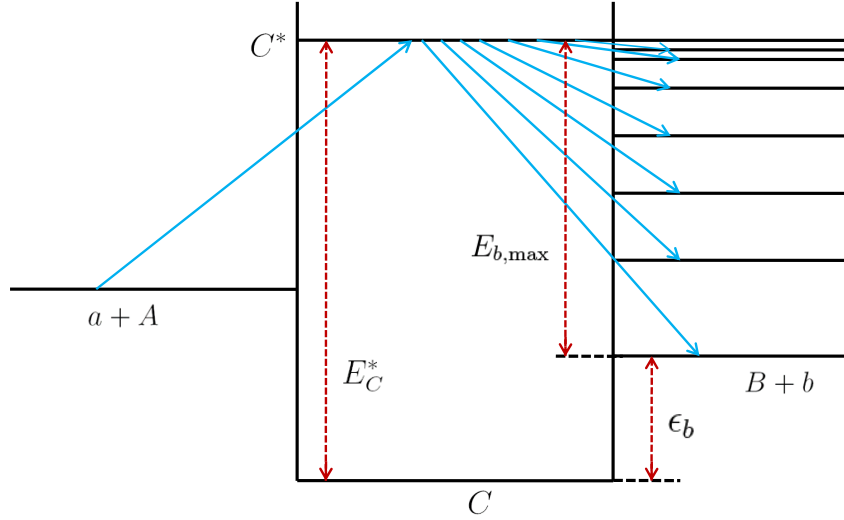


Figure 1: Schematic representation of the energy level diagram for nuclear reaction  $a + A \rightarrow C^* \rightarrow B + b$ . Diagram adapted from Figure 45.1 of reference [29].

It can be seen from the energy level diagram, Figure 1, that the excitation energy for particle  $B$  is

$$E_B^* = E_C^* - \epsilon_b - E_b \quad (33)$$

$$= E_{b,\max} - E_b, \quad (34)$$

where  $\epsilon_b$  is the binding energy of particle  $b$  and  $E_{b,\max}$  is the maximum kinetic energy of the emitted particle  $b$ , which is given by  $E_{b,\max} = E_C^* - \epsilon_b$ . Now, substitute equation (33) into the expression for the partial width. Consequently, the partial width of decay will be given in terms of  $E_C^*$  and  $E_b$ ,

$$\Gamma_b(E_C^*, E_b) = \frac{1}{2\pi^2\hbar^2} p_b^2 (2s_b + 1) \frac{\rho_B(E_C^* - \epsilon_b - E_b)}{\rho_C(E_C^*)} \sigma_{\text{inv}}(E_b) . \quad (35)$$

Inserting the momentum for particle  $b$ ,  $p_b = \sqrt{2M_b E_b}$ , the final relation for the partial width of decay into channel  $B$  is then determined,

$$\Gamma_b(E_C^*, E_b) = \frac{M_b}{\pi^2\hbar^2} (2s_b + 1) \frac{\rho_B(E_C^* - \epsilon_b - E_b)}{\rho_C(E_C^*)} E_b \sigma_{\text{inv}}(E_b) , \quad (36)$$

To find the partial width of decay that is only dependent on the excitation energy of the compound nucleus  $C$ , integrate equation (36) from the Coulomb potential barrier  $V_{\text{Coulomb},b}$  for particle  $b$ , to  $E_{b,\text{max}}$ . The maximum kinetic energy of particle  $b$  is defined in equation (33) as  $E_{b,\text{max}} = E_C^* - \epsilon_b$ . Therefore, the partial width of decay will take the form

$$\Gamma_b(E_C^*) = \frac{1}{\rho_C(E_C^*)} \frac{M_b(2s_b + 1)}{\pi^2\hbar^2} \int_{V_{\text{Coulomb},b}}^{E_C^* - \epsilon_b} \sigma_{\text{inv}}(E_b) \rho_B(E_C^* - \epsilon_b - E_b) E_b dE_b . \quad (37)$$

### 3 Components of the Partial Width of Decay

In order to use the Weisskopf - Ewing theory for the purposes of calculating emission branching ratios, three components require special consideration. The first factor is the limits of integration in equation (37). These limits depend strongly on the values of the Coulomb potential barrier and the binding energy of the emitted  $b$  particle. The second is the cross section for the inverse reaction, which is calculated with optical model potentials. Last is the nuclear level density, which is calculated using the Equidistant Model, where the single particle levels are equidistant and nondegenerate [32]. Of all of components discussed, the nuclear level density impacts the Weisskopf - Ewing calculations most critically.

#### 3.1 Limits of Integration

This section will discuss the limits of integration used in equation (37). The minimum energy required for the evaporation process will depend on the specific type of particle emitted. For charged particles, the kinetic energy of particle  $b$  cannot be smaller than the Coulomb potential barrier,  $V_{\text{Coulomb},b}$ . If the emitted particle is a neutron, the lower limit will be equal to zero, since there is no Coulomb barrier for a neutron. The form of the Coulomb barrier for charged particles will be presented in this section. The upper limit of integration in equation (37) is given by the maximum kinetic energy of the emitted particle  $b$ , which is defined as  $E_{b,\text{max}} = E_C^* - \epsilon_b$ . The excitation energy of the compound nucleus must be greater than the binding energy of the particle  $b$ . The binding energy will depend on the type of particle emitted, and will now be presented.

### 3.1.1 Binding Energy of Emitted Particles

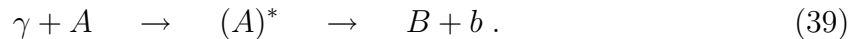
The emitted particle's binding energy is defined as the amount of energy needed to remove a particle from a nucleus. The formalism for the partial width of decay presented in Section 2.2.3 limits the emitted particle  $b$  in equation (1) to be either a neutron, proton, alpha particle, helion, deuteron, or triton. The binding energy is thus dependent on the type of particle emitted.

A photonuclear reaction will occur when the photon energy exceeds the binding energy. The binding energy, for a photonuclear reaction, corresponds to the projectile threshold kinetic energy, which is the minimum amount of kinetic energy needed for particles to react. The threshold energy for emitting a particle  $b$  is given by the relation [33],

$$E_{\text{Th},b} = c^2 \frac{[(m_B + m_b) + m_A + m_a][(m_B + m_b) - m_A - m_a]}{2m_A}, \quad (38)$$

where  $m_A$ ,  $m_a$ ,  $m_B$ , and  $m_b$  are the nuclear masses of the nucleus  $A$ , particle  $a$ , residual nucleus  $B$ , and emitted particle  $b$ , respectively. The speed of light is given by  $c$ .

The simplicity of the Weisskopf - Ewing theory is lost when using this form for the binding energy; the compound nucleus' products are no longer independent of the nuclei that formed them. However, this problem can easily be resolved. For a photonuclear reaction, equation (1) will be expressed as,



Therefore, for a photonuclear reaction such as the one above, the threshold energy will

be given by

$$E_{\text{Th},b} = c^2 \frac{[(m_B + m_b) + m_A][(m_B + m_b) - m_A]}{2m_A} . \quad (40)$$

Now, the threshold energy depends on only the residual nucleus  $B$ , emitted particle  $b$ , and compound nucleus  $A$ . Equation (40) was used to calculate the binding energies for the photonuclear reactions presented in Section 8 to follow. Mass values were taken from reference [34]. Please note that this paper restricts the emitted particle  $b$  to being a neutron, proton, alpha particle, helion, deuteron, or triton.

### 3.1.2 Coulomb Potential Barrier

The Coulomb potential barrier is an energy barrier resulting from electrostatic interactions. It is usually thought of as the classical threshold for nuclear reactions in the center - of - mass system. Calculating the reaction barrier using elementary electrostatics ignores the quantum mechanical tunneling effect, so in order to account for this phenomenon, the classical Coulomb barrier is multiplied by a penetrability coefficient,  $k_c$ , that is dependent on the particle incident [35, 36, 37, 38],

$$V_{\text{Coulomb},c} = k_c V_0 , \quad (41)$$

where  $c$  stands for a charged particle, specifically a proton, alpha particle, helion, deuteron, or triton. It is important to reiterate that since a neutron carries no charge, there is no Coulomb barrier for a neutron. Therefore, when the emitted particle  $b$  is a neutron, the lower limit in the partial width equation (37) is zero.

The classical Coulomb barrier,  $V_0$ , is given by [25]

$$V_0 = \frac{\kappa Z_b Z_B e^2}{R_{0,B}}, \quad (42)$$

where  $\kappa$  is Coulomb's constant,  $Z_b$  is the atomic number of the outgoing particle,  $Z_B$  is the atomic number of the residual nucleus  $B$ , and  $e$  is the electron charge. The nuclear radius,  $R_{0,B}$ , is expressed as

$$R_{0,B} = r_0 \mathcal{A}_B^{1/3}, \quad (43)$$

where  $\mathcal{A}_B$  is the atomic mass of the residual nucleus and the radius parameter  $r_0$  is taken to be 1.18 fm.

The value of the penetrability coefficient in equation (41) depends on the particle  $b$  as [38]

$$k_c = \begin{cases} 0.7 & \text{for } p \\ 0.83 & \text{for } \alpha \\ 0.8 & \text{for } {}^3\text{He} \\ 0.77 & \text{for } d \\ 0.8 & \text{for } t \end{cases} . \quad (44)$$

The penetrability coefficients were found as fits to the quantum mechanical barrier penetration formula for medium mass nuclei [35]. Therefore, for medium mass nuclei, the penetrability coefficients address the effects of quantum tunneling quite well. For light and heavy nuclei, the coefficients give less of an approximation. Even though the coefficients do not approximate the quantum mechanical penetration expression for every mass range, it will only introduce a small error to the total cross section for the emission of a specific particle [35]. For this reason, equation (41) was used for all mass values.

### 3.2 Cross Section of an Inverse Reaction

The inverse of the reaction given in equation (1) is shown in equation (19). The cross section for the formation of the compound nucleus  $C$  in equation (19) is otherwise known as the inverse cross section, which is dependent on the emitted particle's energy and the residual nucleus' atomic number and radius. However, it is independent of the target nucleus and the quantum state. From the method of continuum theory [24], the inverse cross section can be derived, the expression of which will depend on the type of incident particle. It is assumed the any particle that hits the nucleus is absorbed.

For charged particles, the Coulomb field has a strong influence on the inverse cross section. The incident charged particles are repelled and deflected by the Coulomb field, so charged particles must penetrate the Coulomb potential barrier,  $V_{\text{Coulomb},c}$ , which is given by equation (41). The barrier effect is considered by multiplying the geometrical cross section,  $\sigma_{\text{geo},B}$ , by the Coulomb barrier transmission probability. The charged particle inverse cross section is expressed as [27]

$$\sigma_{\text{inv},c}(E_c) = \begin{cases} \sigma_{\text{geo},B} \left(1 - \frac{V_{\text{Coulomb},c}}{E_c}\right) & \text{for } E_c > V_{\text{Coulomb},c} \\ 0 & \text{for } E_c < V_{\text{Coulomb},c} \end{cases}, \quad (45)$$

where  $c$  again stands for charged particles (p,  $\alpha$ ,  $^3\text{He}$ , d, t). For energies below the Coulomb barrier, the charged particle inverse cross section will equal zero. As the energy becomes large, the inverse cross section will approach the geometrical cross section. The nuclear surface is assumed to be a sphere of radius  $R_{0,B}$ , which is given by equation (43). Therefore, the geometrical cross section,  $\sigma_{\text{geo},B}$ , will be represented by the classical target area

$$\sigma_{\text{geo},B} = \pi R_{0,B}^2 . \quad (46)$$

The inverse cross section for neutrons was once thought to be equal to just the geometric cross section, until Dostrovsky, Fraenkel, and Friedlander [39] suggested a form that took into account the energy and mass number dependence,

$$\sigma_{\text{inv},n}(E_n) = \begin{cases} C_n \sigma_{\text{geo},B} \left(1 + \frac{\beta_n}{E_n}\right) & \text{for } E_n > \beta_n \\ 0 & \text{for } E_n < \beta_n \end{cases} , \quad (47)$$

where

$$C_n = 0.76 + 2.2\mathcal{A}^{-1/3} \quad \text{and} \quad \beta_n = (2.12\mathcal{A}^{-2/3} - 0.050)/C_n . \quad (48)$$

From equation (47) it can easily be seen that with large neutron energy values, the neutron inverse cross section will tend towards the geometric cross section. It can also be observed that as the neutron energy becomes smaller, the neutron inverse cross section will become larger.

### 3.3 Nuclear Level Density

The most important quantity describing the statistical nature of compound nucleus decay is the nuclear level density. In this section, the level density is derived for an ideal Fermi gas using a thermodynamical approach. It will be shown that the level density is a function of the excitation energy. The formulation of the level density parameter, which is a component of the nuclear level density, will be examined in detail. Also, sources of experimental information for the nuclear level density will be discussed.

### 3.3.1 Theoretical Level Density Evaluation

A nucleus can be excited into many different higher energy levels or states. At low energies, the energy levels are sufficiently separated and few in number, so that the nature of the excitations are uncomplicated. With increasing excitation energy, the spacing between these levels eventually becomes less than the experimental energy resolution. The widths begin to increase and eventually overlap. The configuration of the energy levels quickly grows in complexity. To describe this behavior, a statistical approach is required.

In compound nucleus decay, the matrix elements between the different states become averaged over a large number of levels due to their very high density, the process of which is eventually determined by the phase space of the products [32, 30, 40]. The system's statistical nuclear properties must thus be described by the level or state density. Since the nucleus is not fully equilibrated, the level or state density can be described for a fixed number of excited particles and holes.

The state density is a function of excitation energy  $E^*$  and spin  $s$ . It accounts for the  $(2s + 1)$  degeneracy of the nuclear levels and is represented as  $\omega(E^*, s)$ . The level density on the other hand is only a function of excitation energy and is expressed as  $\rho(E^*)$ . Many different expressions have been introduced to describe the level density. Initially, the nucleus was represented as a gas of noninteracting fermions confined to the nuclear volume [32], which means that the nucleons in the nucleus are treated as an ideal Fermi gas.

The state density was derived in Sections 2.2.1 and was given by equation (18). Previously, the state density was referred to as the density of states and was expressed as  $dn/dE$ . The level density has not yet been expressed, but now will be derived for an ideal

Fermi gas using a thermodynamical approach.

The thermal heat capacity is defined as the specific thermal energy per degree of temperature. Therefore, the thermal heat capacity at constant volume is given by  $\partial E/\partial\Theta$ , where  $\Theta$  is the nuclear temperature. The specific heat will disappear when  $\Theta = 0$ , due to the Nernst heat theorem. Now, when considering a power series expansion of energy  $E(\Theta)$  around  $\Theta = 0$ , the first term of the series must be proportional to  $\Theta^2$ . When neglecting terms higher than  $\Theta^2$ , the zeroth order expansion energy will be expressed as

$$E(\Theta) = a\Theta^2, \quad (49)$$

where  $a$  is the level density parameter. Rearranging (49), the nuclear temperature is expressed as a function of  $E$  by the formula

$$\Theta(E) = \left(\frac{E}{a}\right)^{1/2}. \quad (50)$$

After inserting (50) into the equation for entropy,  $S = \ln \rho(E) = \int \frac{dE}{\Theta}$ , and rearranging, the level density can be written as

$$\rho(E) = \zeta \exp \left[ 2(aE)^{1/2} \right], \quad (51)$$

where  $\zeta$  is regarded as a constant by some authors [24, 39, 27] and a function of  $E$  by others [32, 41, 42, 43, 44].

Using the zeroth order approximation to the level density of a Fermi gas corresponds to employing the equidistant model. This model is extremely popular in data analysis due to its simplicity; the energy levels are equally spaced and nondegenerate. The downfall of the model is that it contains little physical information and is quite unrealistic, but will be

used here due to its' simple formalism. A complex expression for the excited level density, discussed recently by many authors [32, 41], describes  $\zeta$  as a function of excitation energy  $E^*$ , such that the level density is expressed as

$$\rho(E^*) = \frac{\sqrt{\pi}}{12a^{1/4}E^{*5/4}} \exp \left[ 2(aE^*)^{1/2} \right]. \quad (52)$$

Integration in closed form is impossible when inserting a sophisticated level density such as (52), in which  $\zeta$  is a function of excitation energy  $E^*$ , into the partial width formula, equation (37). Series expansions can be employed, but for excitation energies below 1 MeV, the expansions diverge. Above 1 MeV, the effect of an excitation energy dependent  $\zeta$  is negligible due to the dominant nature of the exponential function. For these reasons, this paper uses an approximated definition for the level density,

$$\rho(E^*) \approx \exp \left[ 2(aE^*)^{1/2} \right]. \quad (53)$$

### 3.3.2 Level Density Experimental Sources

Information on level densities has come from numerous sources. Charged particle capture resonances can provide information on the density of levels of restricted angular momentum [32]. It is a spectroscopical approach that is usually employed for level densities that cannot be determined by neutron resonance spectroscopy, which will be subsequently discussed. Nuclear level densities can also be ascertained from Ericson fluctuation widths [45]. Level densities can even be deduced from measured spectra of evaporated particles [45]. The neutron resonance technique, however, provides the most sizable contribution of level density information used today [32, 45].

For the neutron resonance technique, the compound nuclear level density is observed

at an energy that is just above the neutron binding energy. From spectroscopic studies, the number of levels is inferred by tabulating the resonances in specific nuclear energy intervals. Neutron resonance experiments require the level spacing to be larger than the width. The advantage of this technique is its applicability to all mass number  $\mathcal{A}$  values. This allows for the analysis of how the level density changes with various  $\mathcal{A}$  values. However, the level density data obtained from neutron resonance spectroscopy also suffers from some limitations. For example, regions of high and low excitation energy are effected by experimental error. Even though the neutron resonance technique has some disadvantages, it is extremely important in providing information on the nuclear level density.

### 3.3.3 Level Density Parameter

The level density parameter,  $a$ , was once considered to be a constant independent of excitation energy. It was regarded as an adjustable parameter that was determined by comparison with experiment [35]. Several models have calculated the level density parameter using the results of low energy reactions, where values were empirically fitted to the Fermi gas model. The results of various authors show that the values obtained differ greatly [35].

In 1937, two authors reported contrasting values for the level density parameter. Bardeen [46] calculated a value of  $a = \mathcal{A}/22 \text{ MeV}^{-1}$  for the free particle model with correlation, while Bethe [36] determined  $a = \mathcal{A}/11 \text{ MeV}^{-1}$ . Weisskopf [47] in 1947 computed  $a = 0.85(\mathcal{A} - 40)^{1/2} \text{ MeV}^{-1}$  for atoms heavier than mass 60. In 1950, Le Couteur [38] using the energy spectra of Page [48] and Harding, Lattimore, and Perkins [49], found  $a = \mathcal{A}/12.4 \text{ MeV}^{-1}$ . In the same year, Fujimoto and Yamaguchi [50] suggested  $a = \mathcal{A}/10.5 \text{ MeV}^{-1}$ . Blatt and Weisskopf [24] calculated an  $a$  value for odd nuclei in the region of

mass 100-200 of  $a = \mathcal{A}/17 \text{ MeV}^{-1}$  from data on slow neutron capture in 1952. Eisberg, Igo, and Wegner [51] in 1955 suggested a constant value for the level density parameter,  $a = 8 \text{ MeV}^{-1}$ . Fong [52] in 1956 calculated a best fit of  $a = \mathcal{A}/20 \text{ MeV}^{-1}$  to data for various nuclei on fast neutron capture cross sections. In 1972, Huizenga [53] calculated a value of  $a = \mathcal{A}/8 \text{ MeV}^{-1}$ .

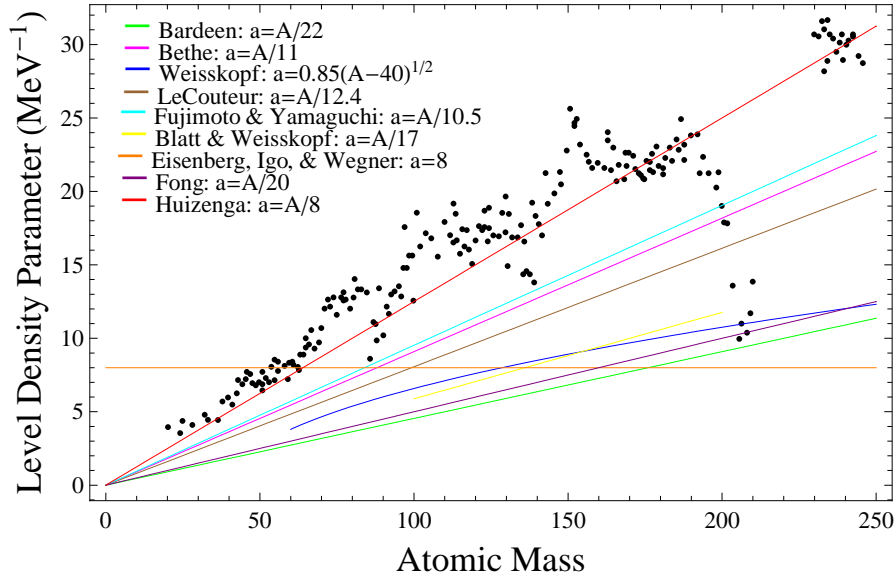


Figure 2: Energy independent level density parameters,  $a$ , of various authors compared to experimental level density parameters deduced from neutron resonance data versus atomic mass number,  $\mathcal{A}$ . Experimental data is from Figure 6 of [32].

With the exception of Eisberg, Igo, and Wegner [51], all of the authors agreed that the level density parameter  $a$  varies with the mass number  $\mathcal{A}$ . Figure 2 compares the level density parameter formulas, of the authors mentioned above, to experimental values deduced from neutron resonance data. Huizenga's formula of  $a = \mathcal{A}/8 \text{ MeV}^{-1}$  is the best fit to the experimental data from Figure 6 of [32]. Deviations from  $a = \mathcal{A}/8 \text{ MeV}^{-1}$  occur for  $\mathcal{A}$  values near closed shells. The actual values of the level density parameter

for closed shell nuclei are substantially lower than Huizenga's level density parameter of  $a = \mathcal{A}/8 \text{ MeV}^{-1}$ . This variation is due to the shell structure of the single particle spectrum near the Fermi energy. Damping of the shell effect at high energies has been observed in microscopic calculations of the nuclear level densities [54, 55, 56]. The level density parameter must become energy dependent in order to account for the damping of shell effects. The energy dependent nuclear level density parameter is given by [57],

$$a(E^*, Z, \mathcal{A}) = \tilde{a}(\mathcal{A}) \left[ 1 + \frac{\delta E_0}{E^*} [1 - \exp(-\gamma_{\text{damp}} E^*)] \right], \quad (54)$$

where  $\tilde{a}(\mathcal{A})$  is the asymptotic level density parameter,  $\delta E_0$  is the shell correction energy, and  $\gamma_{\text{damp}}$  is the damping parameter. The level density parameters for neutron binding energies are shown in Figure 4 as a function of  $\mathcal{A}$  values.

The shell correction energy, shown in Figure 3, will be found with parameters of the liquid drop model formula for spherical nuclei. The shell correction energy is determined by the formula [41]

$$\delta E_0 = E_{\text{exp}}(Z, \mathcal{A}) - E_{\text{ld}}(Z, \mathcal{A}, 0) - E_{\text{deform}}(Z, \mathcal{A}, \beta_{\text{deform}}), \quad (55)$$

where  $E_{\text{exp}}$  is the experimental atomic mass excess. Please note that when no experimental values have been calculated,  $E_{\text{exp}}$  will be taken from the Myers - Swiatecki formula [41]. Also,  $E_{\text{ld}}$  is the energy calculated with the liquid drop model. Myers - Swiatecki parameters, for spherical shaped nuclei, are used. The deformation energy,  $E_{\text{deform}}$  is also calculated with the liquid drop model and is defined as the correction for the deformed nuclear shape [41]. The deformation parameters,  $\beta_{\text{deform}}$ , determine the shape. Calculations made in this paper use the shell corrections calculated from the Myers - Swiatecki mass formula, which were compiled by Igatyuk [58] for reference [41].

When inserting shell corrections calculated from the Myers - Swiatecki mass formula, as shown in Figure 3, and the experimental level density parameters of the Fermi - gas model with normal shift for neutron binding energies, see Figure 4, into equation (54), the asymptotic level density parameter and damping parameter can be derived. The semi - classical formulas used are [41]

$$\tilde{a}(\mathcal{A}) = \alpha_v \mathcal{A} + \beta_s \mathcal{A}^{2/3} \quad (56)$$

and

$$\gamma_{\text{damp}} = \gamma_{\text{damp},0} / \mathcal{A}^{1/3} . \quad (57)$$

The coefficients  $\alpha_v$  and  $\beta_s$  correspond to the volume and surface components, which, along with  $\gamma_{\text{damp},0}$ , are taken to be phenomenological constants that are determined from a least-squares fit of the  $a$  parameters, and are given by [41]:

$$\alpha_v = 0.0959 \pm 0.0005 \text{ MeV}^{-1} \quad (58)$$

$$\beta_s = 0.1468 \pm 0.0035 \text{ MeV}^{-1} \quad (59)$$

$$\gamma_{\text{damp},0} = 0.325 \pm 0.015 \text{ MeV}^{-1} \quad (60)$$

It is important to note that for the level density values calculated with equation (53), this paper employs equation (54) for the level density parameter, equation (55) for the shell correction, equation (56) for the asymptotic level density parameter, and equation (57) for the damping parameter. Also, parameters given in equations (58), (59), and (60) are utilized.

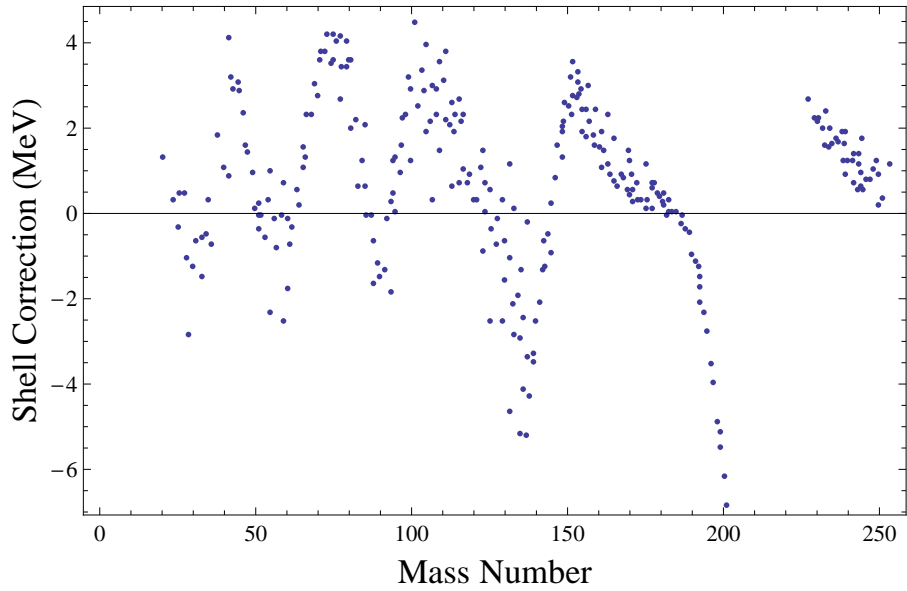


Figure 3: Myers - Swiatecki shell correction,  $\delta E_0$ , estimates to the nuclear binding energies versus the atomic mass number,  $\mathcal{A}$ . Adapted from Figure 6.3 of reference [41].

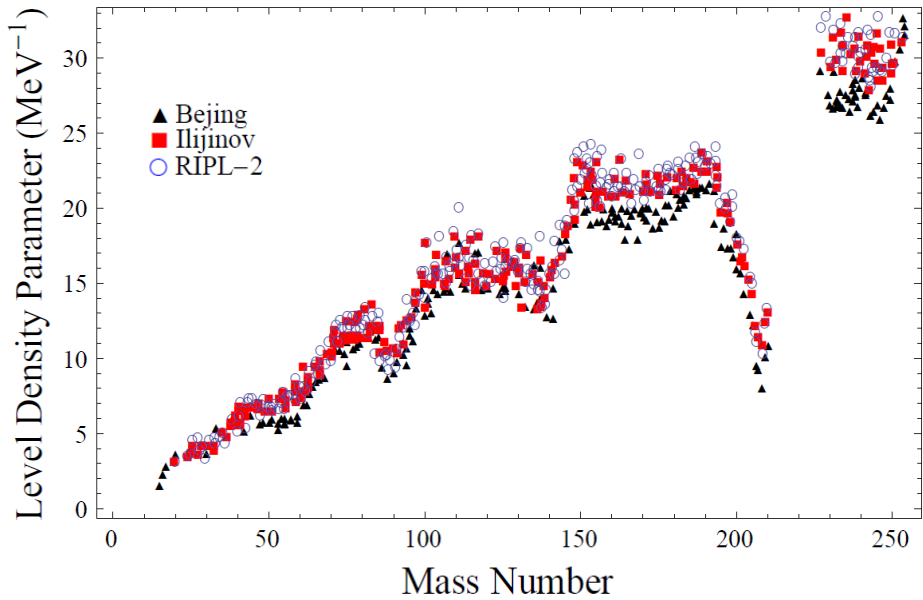


Figure 4: Theoretical level density parameters,  $a$ , of the Fermi - gas model with normal shift, from three sources, versus the atomic mass number,  $\mathcal{A}$ . Adapted from Figure 6.1 of reference [41].

## 4 Branching Ratios

A statistical approach has been presented in previous sections to calculate the relative probabilities of different decay modes for a compound nucleus reaction. These relative probabilities, otherwise known as branching ratios, have been expressed as functions of the excitation energy of the compound nucleus and the kinetic energy of the emitted particle. In this section, a form for the branching ratio, which is only excitation energy dependent, will be introduced that is calculated on the basis of the Weisskopf - Ewing evaporation model of nuclear reactions. In addition, an energy independent branching ratio will be presented that is not only restricted to compound nucleus decay, but can also be applied to direct reactions.

### 4.1 Energy Dependent Branching Ratio

A formula for an energy dependent branching ratio is given in equation (4). The branching ratio is defined as the partial width of particle  $b$  emission divided by the total width. The partial width and total width are dependent on two energies: the excitation energy of the compound nucleus and the kinetic energy of the emitted particle  $b$ . It is possible to integrate out the partial width's dependence on the kinetic energy of emitted particle  $b$ , as was shown in equation (37). Therefore, a new branching ratio relationship can now be defined

$$g_b(E_C^*) = \frac{\Gamma_b(E_C^*)}{\Gamma_{\text{tot}}(E_C^*)}. \quad (61)$$

This paper takes into account the possibility of emission for six particle types: neutron,

proton, alpha particle, helion, deuteron, and triton. This paper will assume emission of other particles as negligible. As a result, the total width is given by

$$\Gamma_{\text{tot}}(E_C^*) = \Gamma_n(E_C^*) + \Gamma_p(E_C^*) + \Gamma_\alpha(E_C^*) + \Gamma_{3He}(E_C^*) + \Gamma_d(E_C^*) + \Gamma_t(E_C^*) . \quad (62)$$

Other decay modes, like fission and gamma emission, could also be included, but the partial width for these two modes of decay would require a different formalism than the six particle types discussed above. The fission partial width will be different because particle emission is three - dimensional, whereas fission is usually referred to as a one - dimensional process [59]. This is due to the nucleus committing to fission once it passes through the saddle point. The partial width for gamma emission includes the possibility of radiating different frequencies, while neutron emission, for example, depends on only the probability of fluctuations occurring in the distribution of the excitation energy [60]. This provides the energy needed to separate from the nucleus. The partial width for fission and gamma emission lies outside of the scope of this document, but will be addressed in future articles.

#### 4.1.1 Approximate Analytic Partial Width of Decay Formula

The partial decay width formula, given in equation (37), is expressed in terms of the excitation energy of the compound nucleus  $C$ . The difficulty in utilizing this equation is due to the upper limit of the integration containing  $E_C^*$ . To achieve a more usable form, a series expansion is employed for the integrand in equation (37) near the upper limit [62, 63].

Begin by inserting the inverse cross section for either a charged particle (45) or a

neutron (47), the level density (53) for the residual nucleus  $B$ , and the level density parameter (54) for the residual nucleus  $B$  into the formula for the partial width of decay (37). Then, by employing the series expansion of Moretto [63], an approximate analytic expression can be found for the partial width of decay. Since the formula for the inverse cross section is dependent on whether the emitted particle  $b$  is charged, the approximated form of the partial width of decay is also contingent on whether particle  $b$  is charged.

For the neutron, the partial width of decay is expressed as [62, 28]

$$\begin{aligned} \Gamma_n(E_C^*) &\approx \frac{M_n C_n (2s_n + 1)}{\pi^2 \hbar^2} \sigma_{\text{geo},B} \frac{\rho_B(E_C^* - \epsilon_n)}{\rho_C(E_C^*)} \mathsf{T}_B \\ &\times \left[ (\epsilon_n - E_C^* - \mathsf{T}_B - \beta_n) \exp\left(\frac{\epsilon_n - E_C^*}{\mathsf{T}_B}\right) + \mathsf{T}_B + \beta_n \right]. \end{aligned} \quad (63)$$

The partial width for a charged particle is defined by [62, 28]

$$\begin{aligned} \Gamma_c(E_C^*) &\approx \frac{M_c (2s_c + 1)}{\pi^2 \hbar^2} \sigma_{\text{geo},B} \frac{\rho_B(E_C^* - \epsilon_c)}{\rho_C(E_C^*)} \mathsf{T}_B \\ &\times \left[ (\epsilon_c - E_C^* - \mathsf{T}_B - V_{\text{Coulomb},c}) \exp\left(\frac{\epsilon_c - E_C^*}{\mathsf{T}_B}\right) \right. \\ &\left. + \mathsf{T}_B \exp\left(\frac{-V_{\text{Coulomb},c}}{\mathsf{T}_B}\right) \right]. \end{aligned} \quad (64)$$

Both expressions contain  $\mathsf{T}_B$ , the temperature of the residual nucleus after  $b$  emission, which is calculated by [62, 28]

$$\begin{aligned}
\tau_B &= \left( \frac{d \ln \rho_B}{d E_C^*} \right)^{-1} \\
&= \left( \frac{E_C^* - \epsilon_b}{a_B (E_C^* - \epsilon_b)} \right)^{1/2} \left( 1 + \frac{\delta E_{0,B}}{E_C^* - \epsilon_b} \frac{\tilde{a}_B}{a_B (E_C^* - \epsilon_b)} \right. \\
&\quad \left. \times [\exp(-\gamma_{\text{damp},B}[E_C^* - \epsilon_b])(1 + \gamma_{\text{damp},B}[E_C^* - \epsilon_b]) - 1] \right)^{-1}. \quad (65)
\end{aligned}$$

## 4.2 Energy Independent Branching Ratio

In 1979, Westfall et al. [11] suggested a formula for the proton branching ratio, based on three pieces of information. The ratio incorporated an estimate using the enhanced production of manganese for heavy targets, a parameterization of the proton branching ratio curve of Weinstock and Halpern [61], and an assumption that the ratio would not exceed the fraction of protons in the nucleus. The relation that Westfall et al. [11] formulated is

$$g_p = \min \left[ \frac{Z_P}{A_P}, 1.95 \exp(-0.075 Z_P) \right], \quad (66)$$

where  $Z_P$  is the atomic number of the projectile nucleus and  $A_P$  is the mass number of the projectile nucleus. In equation (66), the minimum value of the two quantities is to be used. With the ratio of proton emission now formulated, the neutron branching ratio could be found easily,

$$g_n = 1 - g_p, \quad (67)$$

since only proton and neutron decay are considered. Emission of other particles was thought to compete insignificantly with proton and neutron emission, so it was neglected

for simplicity.

In 1993, Norbury and Townsend [12] suggested an improvement to the proton branching ratio for light nuclei ( $Z_P < 14$ ). The proton branching ratio that incorporates the improvements of Norbury and Townsend to the expression suggested by Westfall et al. [11] is

$$g_p = \begin{cases} 0.5 & \text{for } Z_P < 6 \\ 0.6 & \text{for } 6 \leq Z_P \leq 8 \\ 0.7 & \text{for } 8 < Z_P < 14 \\ \min \left[ \frac{Z_P}{A_P}, 1.95 \exp(-0.075 Z_P) \right] & \text{for } 14 \leq Z_P \end{cases} . \quad (68)$$

It should be noted that for the above relations, it is assumed that only single nucleon emission occurs.

## 5 Photonuclear Cross Sections

Nucleus - nucleus electromagnetic dissociation cross sections require photonuclear cross sections as input. The photonuclear process is presented in this section. Included is a discussion of the differential photonuclear cross section, which will be important when determining the nucleus - nucleus differential EMD cross section. A reminder of the total cross section parameterization is also presented because this will be used in obtaining differential cross sections.

### 5.1 Relationship of Compound Nucleus Decay and Differential Cross Sections

Consider the compound nucleus as a true intermediate resonance state, as emphasized in Section 2. The reaction proceeds through a well defined intermediate compound state, as shown in equation (1), rather than proceeding via a direct reaction, as given in equation (2). This means that the kinematics are entirely different.

For the direct reaction, described in equation (2), a double differential cross section  $\frac{d^2\sigma}{dE d\Omega}$  *cannot* be formed for the final particle  $b$  because  $\frac{d\sigma}{dE}$  and  $\frac{d\sigma}{d\Omega}$  are *not* independent. They are functions of each other. However, for the compound nucleus reaction, an essential feature is that the compound nucleus “forgets” how it was formed after reaching statistical equilibrium due to the Bohr Independence Hypothesis [22, 23, 24], which was discussed in section 2. This means that the formation and decay of the compound nucleus can be considered completely independent processes from one another. Now, focus can be placed on the compound nucleus decay



Here, the spectral and angular distributions will be *independent* of each other. Therefore, the double differential cross section  $\frac{d^2\sigma}{dE d\Omega}$  can be formed for the final particle  $b$ . In the simplest model, the angular distributions will be constant and the spectral distribution will represent the statistical thermal decay of a Boltzmann system.

## 5.2 Two - Body Final State

Now consider reactions involving two or three particles in the final state. Suppose that for a reaction with only two bodies in the final state,

$$1 + 2 \rightarrow 3 + 4 , \tag{70}$$

where the number denotes the particle. An example of such a reaction is

$$\gamma + A \rightarrow A^* \rightarrow (A - N)_0 + N , \tag{71}$$

where  $\gamma$  represents a photon,  $A$  denotes a parent nucleus,  $N$  symbolizes a particle with mass number  $N$ , and  $(A - N)_0$  denotes a daughter nucleus in its *ground state*. In this reaction, the incident photon excites the parent nucleus to a compound nucleus excited state denoted by  $A^*$ . The excited parent compound nucleus decays directly to the ground state of the daughter, with the emission of particle  $N$ , as shown in Figure 5.

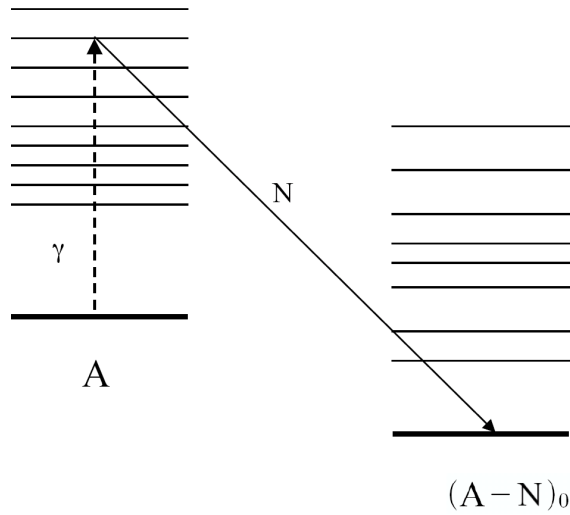


Figure 5: Photonuclear reaction with a two - body final state,  $\gamma + A \rightarrow (A - N)_0 + N$ . This shows the decay of an excited parent nucleus, with particle  $N$  emission, to the ground state of the daughter nucleus. The parent is excited to only one energy level  $E$ , which is determined by the incident photon of energy  $E_\gamma$  in the photonuclear reaction. The energy of the emitted particle is fixed.

### 5.3 Three - Body Final State

Now consider a three - body final state, such as

$$1 + 2 \rightarrow 3 + 4 + 5 , \tag{72}$$

where the number denotes the particle. An example of such a reaction is

$$\gamma + A \rightarrow A^* \rightarrow (A - N)^* + N \rightarrow (A - N)_0 + \gamma + N . \tag{73}$$

In this reaction, the parent nucleus is excited to an intermediate compound nucleus state, but now it decays to an excited state of the daughter nucleus again with the emission of

particle  $N$ . The excited daughter then decays to its ground state by emitting a photon. Please note that the excited daughter could also decay to another excited state and emit another photon. As shown in Figure 6, there will be a variety of excited daughter states that are possible to populate.

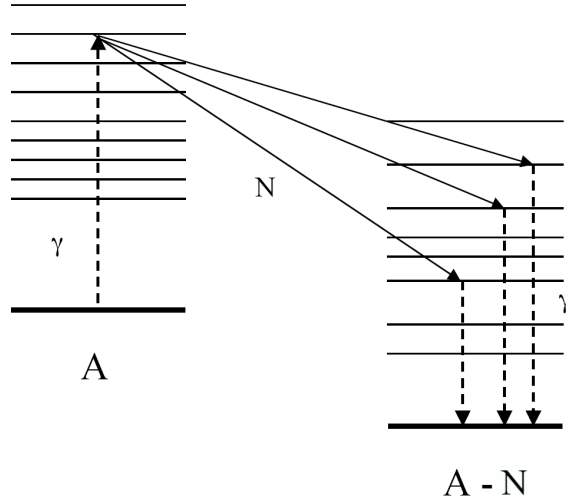


Figure 6: Photonuclear reaction with a three - body final state,  $\gamma + A \rightarrow (A - N) + \gamma + N$ . This shows the decay of an excited parent nucleus, with particle  $N$  emission, to a variety of energy levels in the excited daughter nucleus. The parent is excited to only one energy  $E$ , which is determined by the incident photon of energy  $E_\gamma$  in the photonuclear reaction. The energy level distribution  $\rho(E)$  in the daughter nucleus gives rise to the a variety of energies  $E$  for the emitted particle, which infers the Boltzmann distribution  $e^{-E/k\Theta}$ .

For photonuclear reactions, *both* the spectral  $\frac{d\sigma}{dE_N}$  and angular  $\frac{d\sigma}{d\Omega_N}$  distribution for an emitted particle  $N$  can be measured. Equivalently, the double differential cross section  $\frac{d^2\sigma}{dE_N d\Omega_N}$  can be formed. If the reaction occurred via (71), then both differential cross sections cannot be determined. It is important to realize that both angular and spectral distributions are *only* possible when the photonuclear reaction involves a three - body final state as in (73). Alternatively, this reaction could be thought of as involving a two - body final state  $\gamma + A \rightarrow (A - N)^* + N$  where the mass of the daughter nucleus  $(A - N)^*$

is not fixed but can vary, because it can exist in many different excited states or energy levels as shown in Figure 6. This effectively means that the mass of the excited daughter nucleus is not fixed. Thus, the energy of the emitted particle  $N$  can *vary* allowing the formation of  $\frac{d\sigma}{dE}$ .

## 5.4 Angular Distribution

In the simplest compound nucleus model, the photonuclear angular distribution is approximately isotropic [64, 65, 66, 67], meaning that the angular distribution is constant with respect to angle,

$$\frac{d\sigma_{\gamma A}(E_\gamma)}{d\Omega_N} = K(E_\gamma) , \quad (74)$$

where  $K(E_\gamma)$  is a constant. It is trivial to evaluate  $K(E_\gamma)$  from the total cross section because

$$\sigma_{\gamma A}(E_\gamma) = \int \frac{d\sigma_{\gamma A}(E_\gamma)}{d\Omega_N} d\Omega_N = 4\pi K(E_\gamma) . \quad (75)$$

Rearranging gives

$$K(E_\gamma) = \frac{\sigma_{\gamma A}(E_\gamma)}{4\pi} . \quad (76)$$

Now an isotropic angular distribution can be written as

$$\frac{d\sigma_{\gamma A}(E_\gamma)}{d\Omega_N} = \frac{\sigma_{\gamma A}(E_\gamma)}{4\pi} . \quad (77)$$

## 5.5 Spectral Distribution

The energy level density in Figure 6 can be approximated [68], [69] (p. 326) by a Boltzmann distribution

$$\rho(E) \sim e^{-E/k\Theta} \quad (78)$$

with the nuclear temperature given by [68, 69]

$$k\Theta = \sqrt{\frac{\mathcal{D} E_\gamma}{A_P}} , \quad (79)$$

where  $\mathcal{D}$  is a constant, sometimes taken as  $\mathcal{D} = 10$ . Here,  $\Theta$  is the nuclear temperature and  $k$  is the Boltzmann constant.

The photonuclear spectral distribution is parameterized as

$$\frac{d\sigma_{\gamma A}(E_\gamma)}{dE_N} = \mathcal{C} T_N e^{-T_N/k\Theta} , \quad (80)$$

where  $T_N$  is the kinetic energy of the emitted particle  $N$ . Two features of the spectral distribution must be pointed out. First, the spectral distribution can be written as  $\frac{d\sigma}{dE_N}$  instead of  $\frac{d\sigma}{dT_N}$ . The total energy is given by  $E_N = T_N + m_N$ , where  $m_N$  is the atomic

mass of particle  $N$ ; consequently  $dE_N = dT_N$ . Second, if the form  $E_N e^{-E_N/k\Theta}$  was used, a plot of  $E_N$  versus  $E_N e^{-E_N/k\Theta}$  would not rise smoothly from zero, but would begin at some finite value. The energy  $E_N$  begins at  $m_N$  rather than zero.

### 5.5.1 Useful Integrals

In order to evaluate the constant  $\mathcal{C}$  in the above expression for the spectral distribution, the following integrals are needed [70],

$$\int dx x e^{-ax} = -\frac{1+ax}{a^2} e^{-ax} \quad (81)$$

$$\int dE E e^{-E/k\Theta} = -k\Theta(E+k\Theta) e^{-E/k\Theta} \quad (82)$$

and [71]

$$\int_0^\infty dx x^n e^{-ax} = \frac{\Gamma(n+1)}{a^{n+1}} = \frac{n!}{a^{n+1}} \quad (83)$$

$$\int_0^\infty dx x e^{-ax} = \frac{1}{a^2} \quad (84)$$

$$\int_0^\infty dE E e^{-E/k\Theta} = (k\Theta)^2. \quad (85)$$

However, different limits are need for these integrals, such as a minimum or maximum energy of the projectile,  $E_{\min} = E_{\text{threshold}}$  or  $E_{\max}$ . Thus, the following integrals will be useful. From reference [70],

$$\int_B^C dx x e^{-ax} = \frac{1+aB}{a^2} e^{-aB} - \frac{1+aC}{a^2} e^{-aC}$$

$$= \frac{1 + aB}{a^2} e^{-aB} \quad \text{for } C = \infty \text{ and } \text{Re}[a] > 0. \quad (86)$$

This reduces to the above result for  $B = 0$  and  $C = \infty$ ,

$$\begin{aligned} \int_{E_{\min}}^{E_{\max}} dE E e^{-E/k\Theta} &= k\Theta(E_{\min} + k\Theta)e^{-E_{\min}/k\Theta} - k\Theta(E_{\max} + k\Theta)e^{-E_{\max}/k\Theta} \\ &= k\Theta(E_{\min} + k\Theta)e^{-E_{\min}/k\Theta} \quad \text{for } E_{\max} = \infty. \end{aligned} \quad (87)$$

### 5.5.2 Spectral Distribution in terms of Total Cross Section

The photonuclear spectral distribution is written in equation (80), where  $T_N$  is the kinetic energy of the emitted particle  $N$  and  $\mathcal{C}$  is some constant determined by the requirement

$$\sigma_{\text{tot}}(E_\gamma) = \int dE_N \frac{d\sigma_{\gamma A}(E_\gamma)}{dE_N}, \quad (88)$$

where  $\sigma_{\text{tot}}(E_\gamma)$  is the photonuclear total cross section. Assume that the limits of integration are 0 and  $\infty$ . Then

$$\sigma_{\text{tot}}(E_\gamma) = \int_0^\infty dE_N \frac{d\sigma_{\gamma A}(E_\gamma)}{dE_N} = \mathcal{C} \int_0^\infty dT_N T_N e^{-T_N/k\Theta} = \mathcal{C}(k\Theta)^2 \quad (89)$$

giving

$$\mathcal{C} = \frac{\sigma_{\text{tot}}(E_\gamma)}{(k\Theta)^2} \quad (90)$$

or

$$\frac{d\sigma_{\gamma A}(E_\gamma)}{dE_N} = \frac{\sigma_{\text{tot}}(E_\gamma)}{(k\Theta)^2} T_N e^{-T_N/k\Theta}, \quad (91)$$

which is the photonuclear spectral distribution.

This result maintains the correct units, since the units of  $k\Theta$  are MeV (in units where  $k \equiv 1$  and  $\Theta$  is in MeV, which is used in the computer codes for this work). Equation (91) is reasonable because the differential cross section is just the total cross section times the probability of decay,  $\frac{d\sigma}{dE_N} \sim \sigma e^{-T_N/k\Theta}$ . See Figures 2 and 3 of reference [72]. The more general calculation with arbitrary limits  $T_{\min}$  and  $T_{\max}$ , yields

$$\begin{aligned} \sigma_{\text{tot}}(E_\gamma) &= \int_{T_{\min}}^{T_{\max}} dE_N \frac{d\sigma}{dE_N} = \mathcal{C} \int_{T_{\min}}^{T_{\max}} dT_N T_N e^{-T_N/k\Theta} \\ &= \mathcal{C} \left[ k\Theta(T_{\min} + k\Theta)e^{-T_{\min}/k\Theta} - k\Theta(T_{\max} + k\Theta)e^{-T_{\max}/k\Theta} \right]. \end{aligned} \quad (92)$$

Rearranging gives

$$\mathcal{C} = \frac{\sigma_{\text{tot}}(E_\gamma)}{k\Theta(T_{\min} + k\Theta)e^{-T_{\min}/k\Theta} - k\Theta(T_{\max} + k\Theta)e^{-T_{\max}/k\Theta}}. \quad (93)$$

Substituting this value of  $\mathcal{C}$  into equation (80) yields

$$\begin{aligned}
\frac{d\sigma}{dE_N} &= \frac{\sigma_{\text{tot}}(E_\gamma)}{k\Theta(T_{\text{min}} + k\Theta)e^{-T_{\text{min}}/k\Theta} - k\Theta(T_{\text{max}} + k\Theta)e^{-T_{\text{max}}/k\Theta}} T_N e^{-T_N/k\Theta} \\
&= \frac{\sigma_{\text{tot}}(E_\gamma)}{k\Theta(T_{\text{min}} + k\Theta)e^{-T_{\text{min}}/k\Theta}} T_N e^{-T_N/k\Theta} \quad \text{for } T_{\text{max}} = \infty .
\end{aligned} \tag{94}$$

This reduces to equation (91) when  $T_{\text{min}} = 0$  and  $T_{\text{max}} = \infty$ .

## 5.6 Double Differential Cross Section

From reference [67] (pp. 27, 40)(with  $f = 0$ ), the photonuclear double differential cross section can be expressed as

$$\frac{d^2\sigma_{\gamma A}(E_\gamma)}{dE_N d\Omega_N} = \frac{1}{4\pi} \frac{d\sigma_{\gamma A}(E_\gamma)}{dE_n}, \tag{95}$$

which corresponds to an isotropic angular distribution.

## 5.7 Lorentz Invariant Differential Cross Section

The Lorentz invariant differential cross section  $E \frac{d^3\sigma}{d^3p}$  is related to the non - invariant double differential cross section via

$$E_N \frac{d^3\sigma_{\gamma A}(E_\gamma)}{d^3p_N} = \frac{1}{p_N} \frac{d^2\sigma_{\gamma A}(E_\gamma)}{dE_N d\Omega_N}, \tag{96}$$

where  $p_N \equiv |\mathbf{p}_N|$ . Note that the entire right - hand side is to be evaluated in the *same* frame. For example, if the double differential cross section  $\frac{d^2\sigma}{dE_N d\Omega_N}$  is evaluated in the

projectile frame, then the term  $\frac{1}{p_N}$  also refers to the projectile frame.

If the angular distribution is isotropic, the Lorentz invariant differential cross section will reduce to

$$E_N \frac{d^3 \sigma_{\gamma A}(E_\gamma)}{d^3 p_N} = \frac{1}{4\pi p_N} \frac{d\sigma_{\gamma A}(E_\gamma)}{dE_N} . \quad (97)$$

## 5.8 Total Cross Section

The above equations for the photonuclear differential cross sections (77), (91), (95), and (97) were all written in terms of the photonuclear total cross section. Relevant equations to calculate the photonuclear total cross section will now be presented. The photonuclear total cross section for producing particle X is [68, 73]

$$\sigma(E_\gamma, X) = g_X \sigma_{\text{abs}}(E_\gamma) , \quad (98)$$

where  $g_X$  is the branching ratio and  $\sigma_{\text{abs}}(E_\gamma)$  is the photonuclear absorption cross section, which is parameterized in the region near the giant dipole resonance as

$$\sigma_{\text{abs}}(E_\gamma) = \frac{\sigma_m}{1 + [(E_\gamma^2 - E_{\text{GDR}}^2)^2 / E_\gamma^2 \Gamma^2]} . \quad (99)$$

The abbreviation, GDR, stands for the giant dipole resonance. Here,  $E_{\text{GDR}}$  is the energy at which the photonuclear cross section has its peak value and  $\Gamma$  is the width of the electric dipole (E1) giant dipole resonance. Values of  $\Gamma$  used in this paper can be found in Table

3 in Appendix A. Also,

$$\sigma_m = \frac{\sigma_{\text{TRK}}}{\pi\Gamma/2}, \quad (100)$$

with the Thomas - Reiche - Kuhn cross section given by [73]

$$\sigma_{\text{TRK}} = \frac{60N_P Z_P}{A_P} \text{ MeV mb} \quad (101)$$

with the subscript P referring to excitation of the projectile. (In reference [73] a typing error had this referring to the target.) The GDR energy is [73]

$$E_{\text{GDR}} = \frac{\hbar c}{\left[ \frac{m^* c^2 R_0^2}{8J} \left( 1 + u - \frac{1+\epsilon+3u}{1+\epsilon+u} \epsilon \right) \right]^{1/2}} \quad (102)$$

with

$$u = \frac{3J}{Q'} A_P^{-1/3} \quad (103)$$

and

$$R_0 = r_0 A_P^{1/3}. \quad (104)$$

(In reference [73] a typing error had this referring to the target.) The parameters are:

$$\epsilon = 0.0768 \quad (105)$$

$$Q' = 17 \text{ MeV} \quad (106)$$

$$J = 36.8 \text{ MeV} \quad (107)$$

$$r_0 = 1.18 \text{ fm} \quad (108)$$

$$m^* = 0.7 m_{\text{nucleon}} , \quad (109)$$

where  $m_{\text{nucleon}}$  is the nucleon mass, taken as 938.95 MeV/c.

## 6 Nucleus - Nucleus Cross Sections

In a nucleus - nucleus collision mediated by the EM force, the target (or projectile) represents a source of virtual photons, which impinge upon the projectile (or target). The spectrum of virtual photons contains a variety of energies, in contrast to a photonuclear reaction where the incoming photon possesses only a single energy. For a nucleus - nucleus collision, Figures 5 and 6 get replaced by Figures 7 and 8, which show a variety of energy levels being excited in the parent nucleus.

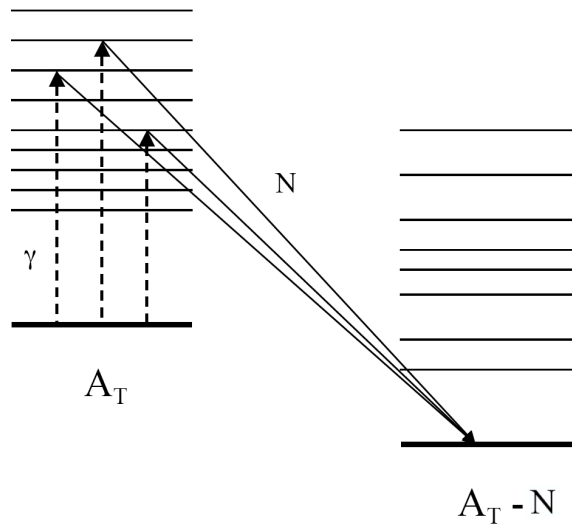


Figure 7: Nucleus - Nucleus Reaction,  $A_P + A_T \rightarrow A_P + (A_T - N) + N$ . This shows the decay of an excited parent target nucleus, with particle  $N$  emission, to the ground state of the daughter nucleus. The parent can be excited to a variety of energies because the projectile nucleus  $A_P$  brings in a variety of incident photon energies. The energy of the emitted particle  $N$  can vary.

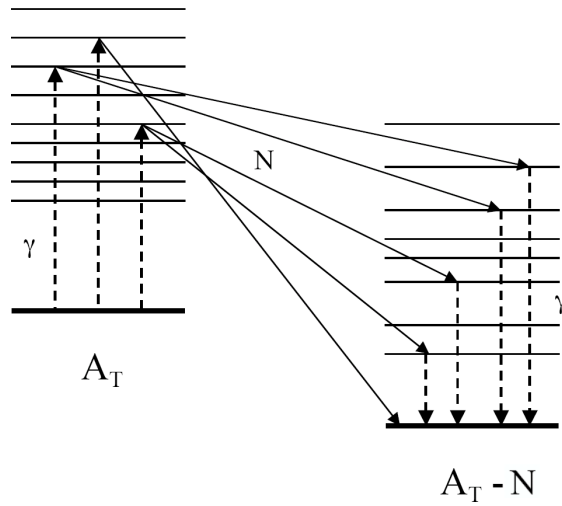


Figure 8: Nucleus - Nucleus Reaction,  $A_P + A_T \rightarrow A_P + (A_T - N) + N$ . This shows the decay of an excited parent nucleus, with particle  $N$  emission, to a variety of energy levels in the excited daughter nucleus. The parent can be excited to a variety of energies because the projectile nucleus brings in a variety of incident photon energies. The energy of the emitted particle  $N$  can vary.

## 6.1 Total Cross Section

The total cross section for electromagnetic nucleus - nucleus reactions can be written in the form

$$\sigma_{AA} = \int dE_\gamma N(E_\gamma) \sigma_{\gamma A}(E_\gamma), \quad (110)$$

where  $N(E_\gamma)$  is the Weizsacker - Williams virtual photon spectrum and  $\sigma_{\gamma A}(E_\gamma)$  is the photonuclear total cross section.

Equation (98) expresses  $\sigma_{\gamma A}(E_\gamma)$  as the branching ratio,  $g_X$ , multiplied by the absorption cross section,  $\sigma_{\text{abs}}(E_\gamma)$ . When replacing the photonuclear total cross section in equation (110) with equation (98), the form of the total cross section for electromagnetic

nucleus - nucleus reaction will depend on whether the branching ratio is energy dependent or independent. For the case of an energy dependent branching ratio,

$$\sigma_{AA} = \int dE_\gamma N(E_\gamma) g_X(E_\gamma) \sigma_{\text{abs}}(E_\gamma) , \quad (111)$$

whereas an energy independent branching ratio can be pulled outside the integral,

$$\sigma_{AA} = g_X \int dE_\gamma N(E_\gamma) \sigma_{\text{abs}}(E_\gamma) , \quad (112)$$

which allows for faster computation.

### 6.1.1 Weizsacker - Williams Virtual Photon Spectrum

A relativistic electromagnetic interaction can be described by the method of virtual quanta. This method relates the field of a relativistic particle to that of a plane wave. Consequently, the perturbing fields of a particle are replaced by an equivalent pulse of radiation [74]. It is this pulse or wave that is analyzed into a frequency spectrum of virtual quanta [74]. The basis for the equivalent photon method came from Enrico Fermi, who in 1924 related the energy loss by ionization to the absorption of X-rays by atoms. Ten years later, C. F. Weizsacker and E. J. Williams independently developed what became to be known as the Weizsacker-Williams method.

Equation (110) requires the Weizsacker - Williams virtual photon spectrum. The virtual photon spectrum describes the number of photons the target contributes at a specific energy. This number spectrum,  $N(E_\gamma, \mathfrak{b})$ , is linked to the frequency spectrum of

virtual quanta,  $d\mathcal{I}(E_\gamma, \mathfrak{b})/dE_\gamma$ , by the relation [74, 73]

$$N(E_\gamma, \mathfrak{b}) = \frac{1}{E_\gamma} \frac{d\mathcal{I}(E_\gamma, \mathfrak{b})}{dE_\gamma}, \quad (113)$$

where  $\mathfrak{b}$  is the impact parameter.

After some calculations, see [74, 75], the number of equivalent photons incident per unit area and per unit energy is given by

$$N(E_\gamma, \mathfrak{b}) = \frac{1}{E_\gamma} \frac{Z_T^2 \alpha_{\text{fsc}}}{\pi^2} \left( \frac{E_\gamma}{\gamma' \beta \hbar c} \right)^2 \frac{1}{\beta^2} \left[ K_1^2(x) + \frac{1}{\gamma'^2} K_0^2(x) \right], \quad (114)$$

where  $Z_T$  is the nuclear charge of the target nucleus,  $c$  is the speed of light, and  $\alpha_{\text{fsc}}$  is the EM fine structure constant given by  $\alpha_{\text{fsc}} = e^2/\hbar c$ . The relativistic beta factor is expressed as

$$\beta = \sqrt{1 - \frac{1}{\gamma'^2}} \quad (115)$$

and the relativistic gamma factor of the projectile is given by

$$\gamma' = \frac{1 + T_{\text{lab}}}{m_N}, \quad (116)$$

where  $T_{\text{lab}}$  is the kinetic energy per particle  $N$  of the projectile. The modified Bessel functions  $K_0(x)$  and  $K_1(x)$  are functions of the parameter  $x$ . The parameter  $x$  is given

by

$$x = \frac{E_\gamma \mathfrak{b}}{\gamma \beta (\hbar c)} . \quad (117)$$

For a relativistic nuclear collision, the number of virtual photons per unit energy for an EM process is acquired by integrating out the impact parameter  $\mathfrak{b}$  in equation (114). The minimum impact parameter,  $\mathfrak{b}_{\min}$ , and  $\infty$  are the lower and upper limits of integration, respectively. Therefore [75, 73],

$$\begin{aligned} N(E_\gamma) &= \int_{\mathfrak{b}_{\min}}^{\infty} 2\pi \mathfrak{b} N(E_\gamma, \mathfrak{b}) d\mathfrak{b} \\ &= \frac{1}{E_\gamma} \frac{2}{\pi} Z_T^2 \alpha_{\text{fsc}} \frac{1}{\beta^2} \left[ \xi K_0(\xi) K_1(\xi) - \frac{1}{2} \xi^2 \beta^2 (K_1^2(\xi) - K_0^2(\xi)) \right] . \end{aligned} \quad (118)$$

Now, the modified Bessel functions,  $K_0(\xi)$  and  $K_1(\xi)$ , are functions of the adiabacity parameter  $\xi$ ,

$$\xi = \frac{E_\gamma \mathfrak{b}_{\min}}{\gamma \beta (\hbar c)} . \quad (119)$$

The minimum impact parameter,  $\mathfrak{b}_{\min}$ , is the value below which the strong force is assumed to dominate [76] and is found from the relation [73]

$$\mathfrak{b}_{\min} = R_{0.1,P} + R_{0.1,T} - d_{\text{overlap}} , \quad (120)$$

where  $R_{0.1,P}$  and  $R_{0.1,T}$  are the 10% charge density radii for the projectile and target nuclei, respectively. Values of the 10% charge density radii used in this paper can be found in Table 4 in Appendix A. The overlap distance is expressed as  $d_{\text{overlap}}$  and is treated as an arbitrary parameter.

By substituting the Weizsacker - Williams virtual photon spectrum, given in equation (118), into equation (110), the total cross section for an electromagnetic nucleus - nucleus reaction can be found. This now allows for the formation of differential cross sections.

## 6.2 Angular Distribution

From the perspective of EMD reactions, the spectator nucleus is nothing more than a source of virtual photons. Therefore, the angular and spectral distributions may also be written in the form of equation (110). Now, the angular distribution, for emission of a particle  $N$  in the direction  $\Omega_N$ , is given by

$$\frac{d\sigma_{AA}}{d\Omega_N} = \int dE_\gamma N(E_\gamma) \frac{d\sigma_{\gamma A}(E_\gamma)}{d\Omega_N}, \quad (121)$$

where  $\frac{d\sigma_{\gamma A}(E_\gamma)}{d\Omega_N}$  is the photonuclear angular distribution for emission of particle  $N$  in the direction  $\Omega_N$ . If the photonuclear angular distribution is approximately isotropic, then use of equations (77) and (121) gives

$$\frac{d\sigma_{AA}}{d\Omega_N} = \frac{\sigma_{AA}}{4\pi}. \quad (122)$$

It must be emphasized that this is the angular distribution in the *rest frame of the*

*excited (compound) nucleus.* If the excited (compound) nucleus is the projectile, then this must be transformed to the lab frame for use in transport codes. If the excited (compound) nucleus is the target, then no transformation is necessary because the target is at rest in the lab frame.

### 6.3 Spectral Distribution

The spectral distribution, for emission of particle  $N$  with energy  $E_N$ , may also be written in the form of equation (110), namely

$$\frac{d\sigma_{AA}}{dE_N} = \int dE_\gamma N(E_\gamma) \frac{d\sigma_{\gamma A}(E_\gamma)}{dE_N}, \quad (123)$$

where  $\frac{d\sigma_{\gamma A}(E_\gamma)}{dE_N}$  is the photonuclear spectral distribution for emission of particle  $N$  with energy  $E_N$ . *Note that the spectral distribution cannot be taken outside the integral because the nuclear temperature  $\Theta$  depends on the photon excitation energy  $E_\gamma$ .*

### 6.4 Double Differential Cross Section

The double differential cross section, for emission of particle  $N$  with energy  $E_N$  in the direction  $\Omega_N$ , may also be written in the form of equation (110), namely

$$\frac{d^2\sigma_{AA}}{d\Omega_N dE_N} = \int dE_\gamma N(E_\gamma) \frac{d^2\sigma_{\gamma A}(E_\gamma)}{d\Omega_N dE_N}, \quad (124)$$

where  $\frac{d^2\sigma_{\gamma A}(E_\gamma)}{d\Omega_N dE_N}$  is the photonuclear double differential cross section for emission of particle  $N$  with energy  $E_N$  in the direction  $\Omega_N$ . If the photonuclear angular distribution is

isotropic, use (95) to give

$$\begin{aligned}\frac{d^2\sigma_{AA}}{d\Omega_N dE_N} &= \frac{1}{4\pi} \int dE_\gamma N(E_\gamma) \frac{d\sigma_{\gamma A}(E_\gamma)}{dE_N} \\ &= \frac{1}{4\pi} \frac{d\sigma_{AA}}{dE_N},\end{aligned}\tag{125}$$

which is analogous to equation (95).

## 6.5 Lorentz Invariant Differential Cross Section

The Lorentz invariant differential cross section is related to the non - invariant double differential cross section as before, namely

$$E_N \frac{d^3\sigma_{AA}}{d^3p_N} = \frac{1}{p_N} \frac{d^2\sigma_{AA}}{dE_N d\Omega_N}.\tag{126}$$

An isotropic distribution will be completely analogous to equation (97). Thus,

$$E_N \frac{d^3\sigma_{AA}}{d^3p_N} = \frac{1}{4\pi p_N} \frac{d\sigma_{AA}}{dE_N}.\tag{127}$$

## 7 Lorentz Transformation of Cross Sections

The nucleus - nucleus differential cross sections (121), (123), and (124) all involve a photonuclear differential cross section or a total cross section. The photonuclear differential cross sections are all evaluated in the rest frame of the excited nucleus. Differential cross sections in radiation transport codes are required in the lab frame (spacecraft rest frame). If the projectile nucleus is undergoing photodisintegration, then the nucleus - nucleus differential cross sections (121), (123), and (124) are first evaluated in the projectile frame, at which point they must be Lorentz transformed to the lab frame. The technique for doing this is the subject of the present section.

### 7.1 Discussion of Photonuclear Cross Sections

For a two - body final state, such as the reaction in equation (71), *either* the angular *or* spectral distribution can be formed, but not both. A double differential cross section or Lorentz invariant differential cross section cannot be formed in this case. For a three - body final state, such as the reaction in equation (73), both the spectral and angular distributions can be formed independently, as well as the double and Lorentz invariant differential cross sections. This can be seen in the literature for photonuclear reactions.

For general photonuclear reactions, numerous discussions of double differential cross sections [72, 77, 78, 79, 80, 81, 82, 83, 84] can be found; however, for photonuclear reactions to the ground state, information regarding only angular distributions [85, 86, 87, 88] can be found. This result is expected because when making a transition to the ground state, as shown in Figure 5, there will be no energy distribution for the emitted particle when assuming the incident photon is monoenergetic. This is true for *any* transition to a *particular* energy state in the daughter nucleus. Although, when transitions to a variety

of energy states in the daughter is allowed, as shown in Figure 6, there will then be a variety of possible emitted particle energies whose spectral distribution will reflect the energy level density of the daughter nucleus. A transition to the ground state of the daughter nucleus is distinctive because no photon is emitted. Therefore, the final state will be a two - body state. Consequently, the angular distribution calculated in the projectile frame will need to be transformed into the lab frame, which is a complicated task.

From the viewpoint of statistical compound nucleus decay, there is nothing special about the ground state. It is just one of a continuum of possible final states, which is given by the continuous energy level distribution  $\rho(E)$ . In this general case, the final state is three - body. This enables the formation of a Lorentz invariant differential cross section, which is easily transformed from the projectile to the lab frame. (Even though  $E \frac{d^3\sigma}{d\beta p}$  is invariant, it must be transformed when plotting it as a function of energy or angle.)

## 7.2 Lorentz Transformation of Photonuclear Cross Sections

A Lorentz transformation of a photonuclear differential cross section is almost never considered because it is usually defined in the rest frame of the nucleus, which undergoes the reaction. The projectile is a photon, the target is a nucleus, and a Lorentz transformation is not necessary. When considering *nucleus - nucleus* collisions, Lorentz transformations are needed. Assume that the projectile nucleus is undergoing the excitation. Now the projectile photonuclear differential cross section *must* be transformed into the target nucleus frame.

In this section, when a Lorentz transformation of a differential photonuclear cross section is discussed, the different frames available to the nucleus - nucleus reaction is

considered, not the photonuclear reaction. This is admittedly a confusing point. It is important to realize that the photonuclear reaction is still occurring to the projectile nucleus. Normally, the projectile photonuclear cross section is integrated over the virtual photon spectrum coming from the target nucleus. This operation is still performed, but the projectile photonuclear cross section is first transformed to the lab (target) frame. It should be noted that although the photonuclear cross sections are transformed to the lab frame and written in terms of lab variables, they are still photonuclear cross sections for projectile fragmentation.

### 7.3 Transformation between CM or Projectile Frame and Lab (Target) Frame

Suppose quantities in the center of momentum (cm) or projectile frames need to be transformed to the lab frame. *The cm frame moves at speed  $\beta_{cl}$  relative to the lab frame.* The corresponding  $\gamma$  factor is labeled as  $\gamma_{cl}$ . *The projectile frame moves at speed  $\beta_{pl}$  relative to the lab frame.* The corresponding  $\gamma$  factor is labeled as  $\gamma_{pl}$ . The Lorentz transformations are

$$\begin{pmatrix} E_* \\ p_{||*} \end{pmatrix} = \begin{pmatrix} \gamma_{*l} & -\gamma_{*l}\beta_{*l} \\ -\gamma_{*l}\beta_{*l} & \gamma_{*l} \end{pmatrix} \begin{pmatrix} E_l \\ p_{||l} \end{pmatrix}, \quad p_{T*} = p_{Tl} \quad (128)$$

and inverse transformations are

$$\begin{pmatrix} E_l \\ p_{||l} \end{pmatrix} = \begin{pmatrix} \gamma_{*l} & \gamma_{*l}\beta_{*l} \\ \gamma_{*l}\beta_{*l} & \gamma_{*l} \end{pmatrix} \begin{pmatrix} E_* \\ p_{||*} \end{pmatrix}, \quad p_{Tl} = p_{T*}, \quad (129)$$

where

$$p_{||} \equiv p_z = |\mathbf{p}| \cos \theta \quad (130)$$

$$p_T = |\mathbf{p}| \sin \theta . \quad (131)$$

With this notation, both cm and projectile frames are included. The notation means that a quantity  $x_*$  is the value of the quantity  $x$  *evaluated in that particular frame* with

$$* = c \quad \text{or} \quad * = p , \quad (132)$$

where the  $c$  or  $p$  subscript refers to the cm or projectile frame, respectively, and  $\beta_{*l}$  is the speed of that frame *with respect to the lab frame* with

$$\beta_{*l} = \beta_{cl} \quad \text{or} \quad \beta_{*l} = \beta_{pl} . \quad (133)$$

## 7.4 Energy Transformations

The energy Lorentz transformation from the lab ( $l$ ) frame to the starred ( $*$ ) frame is

$$\begin{aligned} E_{j*} &= \gamma_{*l}(E_{jl} - \beta_{*l}p_{||jl}) \\ &= \gamma_{*l}(E_{jl} - \beta_{*l}|\mathbf{p}_{jl}| \cos \theta_{jl}) \\ &= \gamma_{*l} \left( E_{jl} - \beta_{*l} \sqrt{E_{jl}^2 - m^2} \cos \theta_{jl} \right) . \end{aligned} \quad (134)$$

The inverse transformation is

$$E_{jl} = \gamma_{*l} \left( E_{j*} + \beta_{*l} \sqrt{E_{j*}^2 - m^2} \cos \theta_{j*} \right) . \quad (135)$$

## 7.5 Angle Transformations

The angle is obtained from

$$\tan \theta = \frac{p_T}{p_z} . \quad (136)$$

Thus, the angle of particle  $j$  is

$$\begin{aligned} \tan \theta_{jl} = \frac{p_{Tjl}}{p_{zjl}} &= \frac{p_{Tj*}}{\gamma_{*l} \beta_{*l} E_{j*} + \gamma_{*l} p_{zj*}} \\ &= \frac{|\mathbf{p}_{j*}| \sin \theta_{j*}}{\gamma_{*l} (\beta_{*l} E_{j*} + |\mathbf{p}_{j*}| \cos \theta_{j*})} . \end{aligned} \quad (137)$$

Defining  $\alpha_{j*}$  as the speed of the cm or projectile frame relative to the lab frame divided by the speed of particle  $j$  in the cm or projectile frame

$$\alpha_{j*} \equiv \frac{\beta_{*l}}{\beta_{j*}} \quad (138)$$

and using

$$\beta_{j^*} = \frac{|\mathbf{P}_{j^*}|}{E_{j^*}} \quad (139)$$

obtains

$$\tan \theta_{jl} = \frac{\sin \theta_{j^*}}{\gamma_{*l} (\cos \theta_{j^*} + \alpha_{j^*})} . \quad (140)$$

See references [89] (p. 402), [90] (p. 42), [91] (p. 17), and [92] (p. 26). This is a complicated function of  $\theta$  because, in general,

$$\alpha_{j^*} = \alpha_{j^*}(E_{j^*}) = \alpha_{j^*}(\theta_{j^*}) . \quad (141)$$

*Usually,  $\alpha_{j^*}$  is a function of  $\theta_{j^*}$ , making  $\tan \theta_{jl}$  a complicated function of  $\theta_{j^*}$ . For the cm frame and for three - body states, however,  $E_{j_c}$  is not a function of  $\theta_{j_c}$ . This means that  $\alpha_{j_c}$  is not a function of  $\theta_{j_c}$  [90] (pp. 42, 58). Three - body states are considered in the present work so that the aforementioned complications are avoided.*

The angle transformation for  $* = c$  is plotted in references [89](p. 403), [90](p. 43), and [93]. When  $\alpha_{j^*} > 1$ , the function is double - valued. This results from the two different angles in the cm or projectile frame giving rise to the same angle in the lab frame for  $\alpha_{j^*} > 1$ . The two angles can be distinguished by their energies, labeled in the cm frame as  $E_{j_c}^{\pm}$  [89] (p. 402). This is true for a two - body final state.

To show that the cm or projectile angle is double - valued, specify the  $*$  frame in equation (140) to be the projectile frame. Then,

$$\tan \theta_{jl} = \frac{\sin \theta_{jp}}{\gamma_{pl} (\cos \theta_{jp} + \alpha_{jp})}, \quad (142)$$

where  $\alpha_{jp}$  is defined as the ratio of the projectile velocity to the velocity of particle  $j$  in the projectile system. It is dependent on the lab kinetic energy  $T_N$ , as in  $\alpha_{jp}(T_N)$ . When  $\alpha_{jp} > 1$ , particles are emitted forwards and backwards in the projectile system, but appear at the same lab angle.

To examine the relationship between projectile and lab angles, take the case of an emitted photonucleon. Figures 9 - 12 are evaluated at the lab kinetic energy of  $m_N$ ,  $10m_N$ ,  $16m_N$ , and  $100m_N$ , respectively. Where in this case,  $m_N$  is the nucleon mass. Figures 9 and 10 are examples of what happens when  $\alpha_{jp} > 1$ . It can be seen that the range of the lab angle,  $0 \leq \theta_{lab} \leq \theta_{max}$ , is dependent on  $\alpha_{jp}$ . The lab angle is confined to a forward cone, as the projectile angle ranges from 0 to  $\pi$ . This means that the projectile angle will be double - valued for every lab angle. Figures 11 and 12, however, illustrate the relationship between the projectile angle and the lab angle when  $\alpha_{jp} < 1$ . Notice that the lab angle range is now between 0 and  $\pi$ . The lab angle is now a single-valued function of the projectile angle.

In the present work, three - body final states are considered. The curves plotted in [89](p. 403) correspond to a particular value of the particle energy, or in other words, to a particular value of  $\alpha_{j*}$ . For a three - body reaction, the energy of the emitted particle is *not* related to the angle. Thus, for a particular lab angle, there is a continuous range of lab energies corresponding to a *family* of curves. This is plotted in reference [89](p. 403). The family of curves will be for both  $\alpha > 1$  and  $\alpha < 1$ .

The inverse transformation is

$$\tan \theta_{j^*}^{\pm} = \frac{\sin \theta_{jl}}{\gamma_{*l}(\cos \theta_{jl} - \alpha_{jl}^{\pm})}, \quad (143)$$

where

$$\beta_{jl}^{\pm} = \frac{|\mathbf{p}_{jl}^{\pm}|}{E_{jl}^{\pm}} \quad (144)$$

$$\alpha_{jl}^{\pm} \equiv \frac{\beta_{*l}}{\beta_{jl}^{\pm}}. \quad (145)$$

The  $\pm$  notation is emphasizing that, in general, two different angles in the cm or projectile frames can correspond to a single angle in the lab frame.

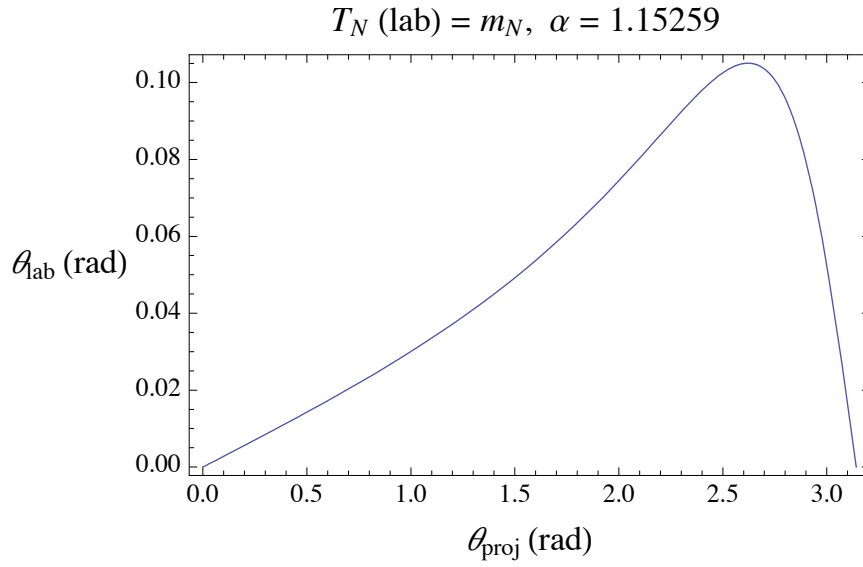


Figure 9: Relation between projectile and lab angles for an emitted photonucleon with kinetic energy  $T_N = m_N$  or  $\alpha = 1.15259$ . The calculation used equation (143).

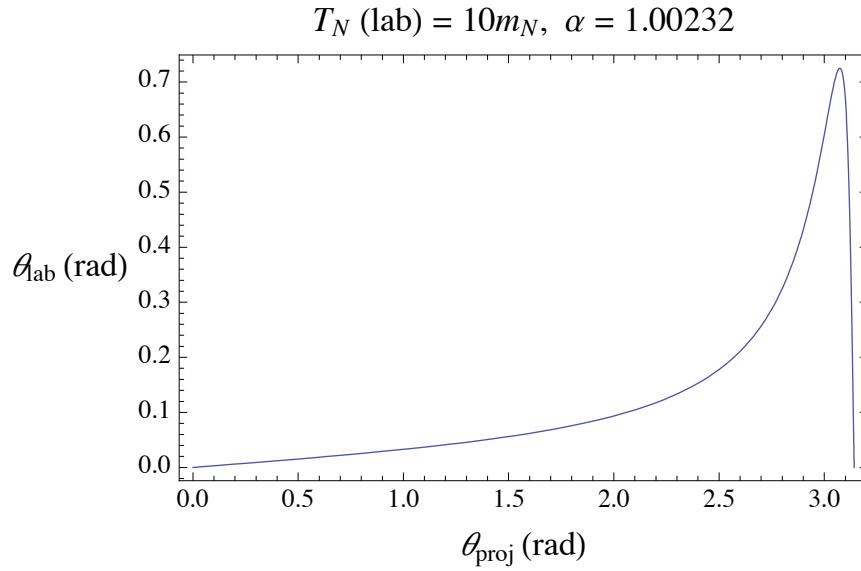


Figure 10: Relation between projectile and lab angles for an emitted photonucleon with kinetic energy  $T_N = 10m_N$  or  $\alpha = 1.00232$ . The calculation used equation (143).

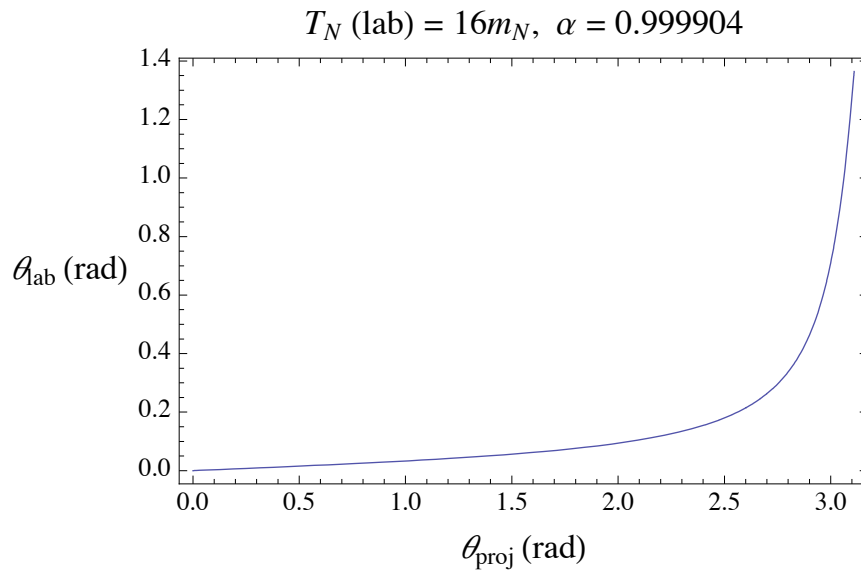


Figure 11: Relation between projectile and lab angles for an emitted photonucleon with kinetic energy  $T_N = 16m_N$  or  $\alpha = 0.999904$ . The calculation used equation (143).

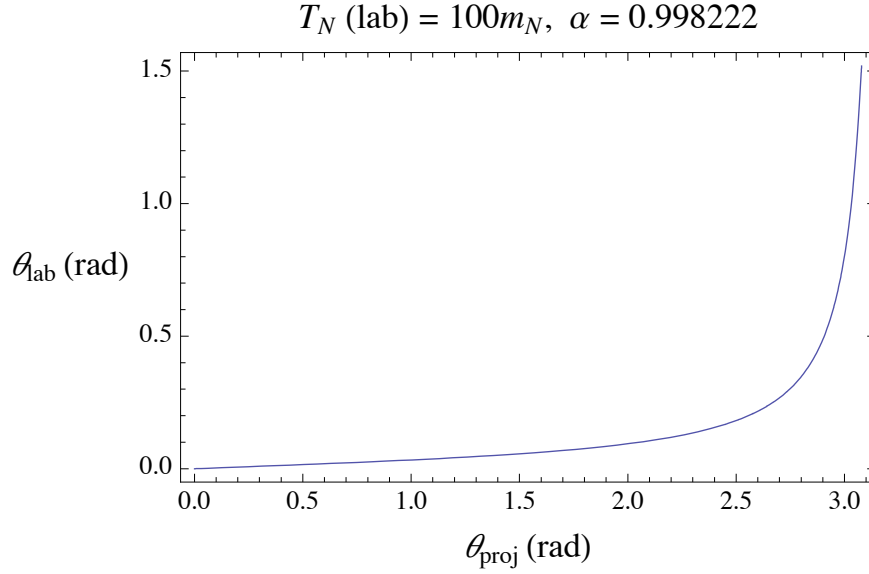


Figure 12: Relation between projectile and lab angles for an emitted photonucleon with kinetic energy  $T_N = 100m_N$  or  $\alpha = 0.998222$ . The calculation used equation (143).

## 7.6 Double Differential Cross Sections

The transformation of a double differential cross section is described in reference [94].

The cross sections are related by the Jacobian

$$\frac{d^2\sigma}{dE_{jl}d\Omega_{jl}} = \frac{d^2\sigma}{dE_{j*}d\Omega_{j*}} \frac{\partial(E_{j*}, \Omega_{j*})}{\partial(E_{jl}, \Omega_{jl})}, \quad (146)$$

which is evaluated as

$$\frac{\partial(E_*, \Omega_*)}{\partial(E_l, \Omega_l)} = \frac{|\mathbf{p}_l|}{|\mathbf{p}_*|} = \frac{\sin \theta_*}{\sin \theta_l}, \quad (147)$$

to give

$$\frac{d^2\sigma}{dE_{jl}d\Omega_{jl}} = \frac{|\mathbf{p}_l|}{|\mathbf{p}_*|} \frac{d^2\sigma}{dE_{j*}d\Omega_{j*}} = \frac{\sin \theta_{j*}}{\sin \theta_{jl}} \frac{d^2\sigma}{dE_{j*}d\Omega_{j*}}. \quad (148)$$

The left - hand side is a function of  $E_{jl}$  and  $\theta_{jl}$ , so the right - hand side should also be a function of  $E_{jl}$  and  $\theta_{jl}$ . This is accomplished by replacing  $E_{j*}$  and  $\theta_{j*}$  on the right - hand side with equations (134) and (143). *Thus, the entire right - hand side is written as an explicit function of lab variables.* Two versions of the right - hand side are given, either of which can be used. The one involving the sine functions will be a good test of the correctness of the angle transformations.

*Equation (148) is the equation used for obtaining all cross sections in the lab frame. The method is to use (148) to obtain the photonuclear double differential cross section in the lab frame. Then, integrate the lab frame double differential cross section (148) to get the photonuclear spectral and angular differential cross sections in the lab frame. To obtain any nucleus - nucleus differential cross section in the lab frame, take the lab frame photonuclear cross sections and integrate over the virtual photon spectrum.*

## 8 Results

The formalism for the photonuclear and nucleus - nucleus cross sections will be contingent on whether energy dependent or independent branching ratios are used. An extensive comparison of photonuclear and nucleus - nucleus cross sections, calculated with both energy dependent and independent branching ratios, to experiment will be presented in this section. The applicability of both energy dependent and independent branching ratios will be examined. This section will also present graphical representations of differential cross sections in both the projectile and laboratory frame. Lastly, the formalism for differential cross sections will be tested by comparisons to experiment. Due to the limited amount of data for differential cross sections, only spectral distributions will be compared to experiment.

### 8.1 Photonuclear Cross Sections using Energy Dependent and Independent Branching Ratios Compared to Experiment

Photonuclear cross sections, calculated with equation (98), are presented in this section. Energy dependent and independent branching ratios are used and their corresponding photonuclear cross sections are compared to experiment for a variety of nuclei, as shown in Figures 13 - 19. A true comparison between the energy dependent and independent branching ratios can be made, since the branching ratios are multiplied by experimental absorption cross sections, from reference [67], at various photon energies. The experimental values used are presented in Tables 5 - 11 of Appendix A.

Please note that comparisons of theoretical photonuclear cross sections, calculated with both energy dependent and independent branching ratios, to experiment are limited to reactions where experimental data is available for *both* the absorption cross section and photonuclear cross section. *By using both the experimental absorption and photonuclear*

*cross section, the validity of using energy dependent and independent branching ratios can be tested and their regions of applicability can be examined.* In future papers, the parameterized absorption cross section, given in equation (99), will be used and comparisons to many other experimental photonuclear cross sections can be made.

The energy *dependent* branching ratios are determined from equation (61). Since, this section discusses photonuclear reactions, the excitation energy of the compound nucleus, found in equation (61), will be equal to the virtual photon energy. For equation (61), the partial decay width in the numerator is replaced by equation (37) and the total width in the denominator is substituted with (62). This energy dependent branching ratio formalism allows for the emission of a proton, neutron, alpha particle, helion, deuteron, or triton. The contribution from other particles is assumed to be negligible, as mentioned previously. For the energy *independent* branching ratios, equations (67) and (68) are used. Since the energy independent branching ratios were formulated for only proton and neutron emission, only photoneutron and photoproton cross sections can be calculated. Due to this fact, comparisons between using energy dependent and independent branching ratios to calculate photonuclear cross sections, can be tested for only photoneutron and photoproton cross sections.

It is important to reiterate that the theoretical photonuclear cross sections, seen in Figures 13 - 19, are calculated with equation (98). In this equation, the branching ratio is multiplied by the absorption cross section. Experimental values, given in reference [67], are used for the absorption cross section, as mentioned previously. Equation (61) is used for an energy dependent branching ratio, while equations (67) and (68) are utilized for an energy independent branching ratio.

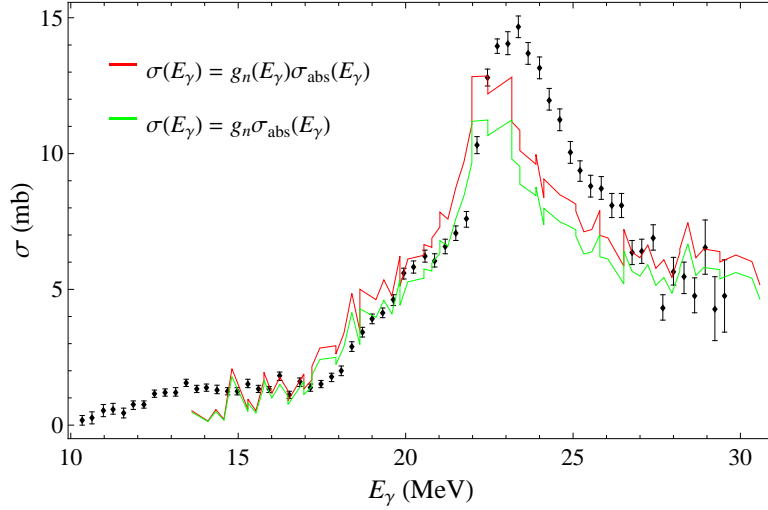


Figure 13: Theoretical, using energy dependent [displayed in red, calculated with equations (61), (37), and (62)] and independent [displayed in green, calculated with equations (67) and (68)] branching ratios, and experimental photoneutron cross sections for  $^{14}\text{N}$ . Experimental data is from Figure 14(b) of reference [95].

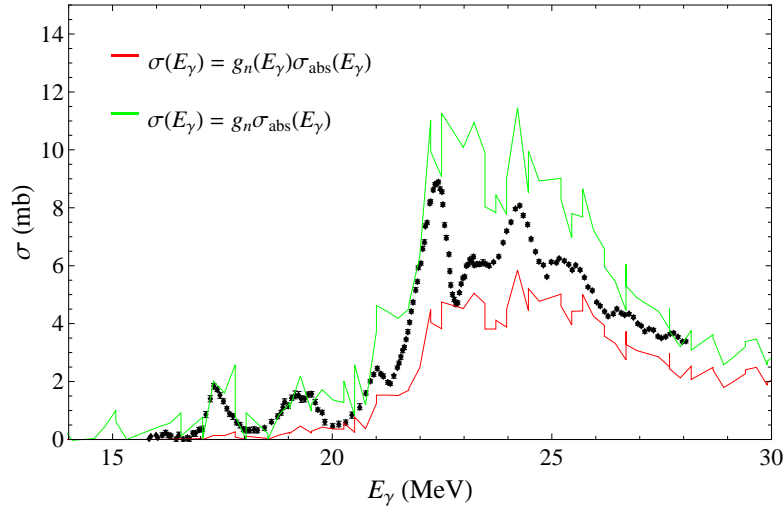


Figure 14: Theoretical, using energy dependent [displayed in red, calculated with equations (61), (37), and (62)] and independent [displayed in green, calculated with equations (67) and (68)] branching ratios, and experimental photoneutron cross sections for  $^{16}\text{O}$ . Experimental data is from Figure 14(c) of reference [95].

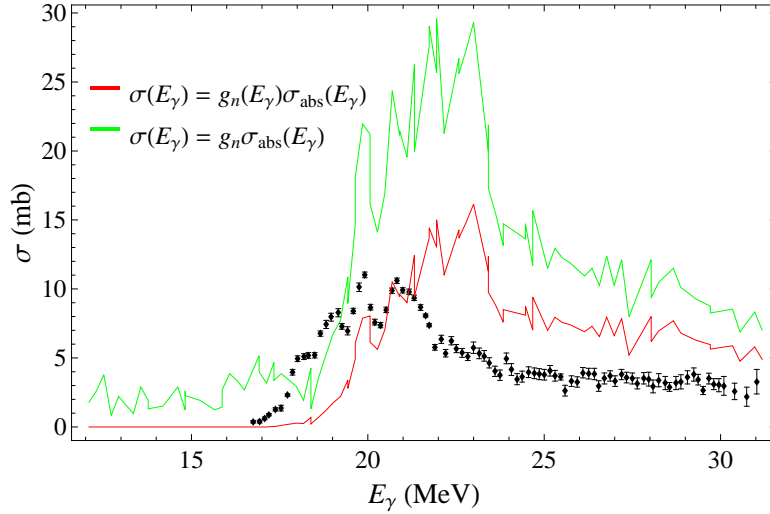


Figure 15: Theoretical, using energy dependent [displayed in red, calculated with equations (61), (37), and (62)] and independent [displayed in green, calculated with equations (67) and (68)] branching ratios, and experimental photoneutron cross sections for  $^{28}\text{Si}$ . Experimental data is from Figure 15(b) of reference [95].

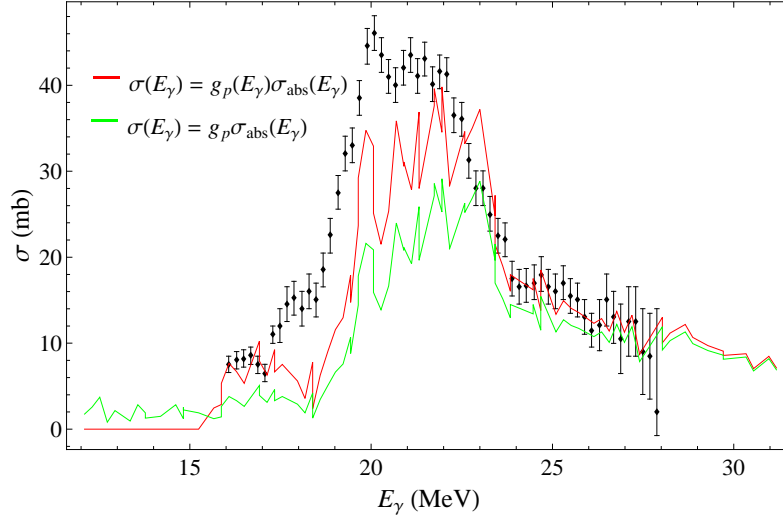


Figure 16: Theoretical, using energy dependent [displayed in red, calculated with equations (61), (37), and (62)] and independent [displayed in green, calculated with equation (68)] branching ratios, and experimental photoproton cross sections for  $^{28}\text{Si}$ . Experimental data is from reference [67] (p. 110).

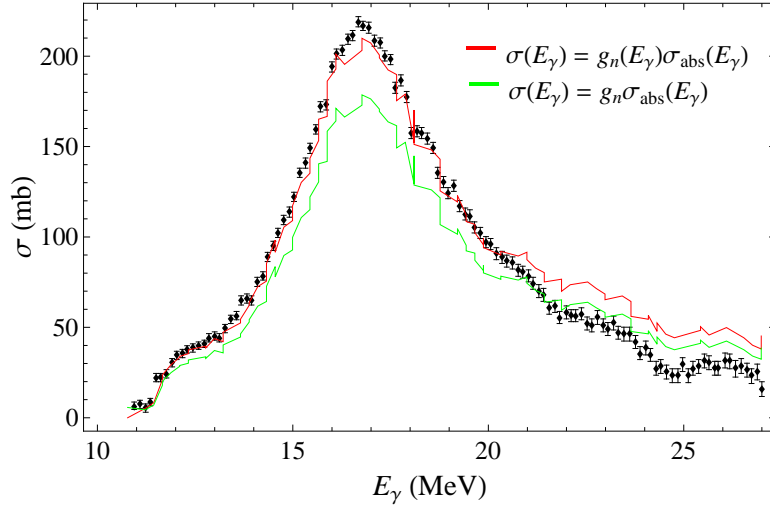


Figure 17: Theoretical, using energy dependent [displayed in red, calculated with equations (61), (37), and (62)] and independent [displayed in green, calculated with equations (67) and (68)] branching ratios, and experimental photoneutron cross sections for  $^{88}\text{Sr}$ . Experimental data is from reference [67] (p. 168).

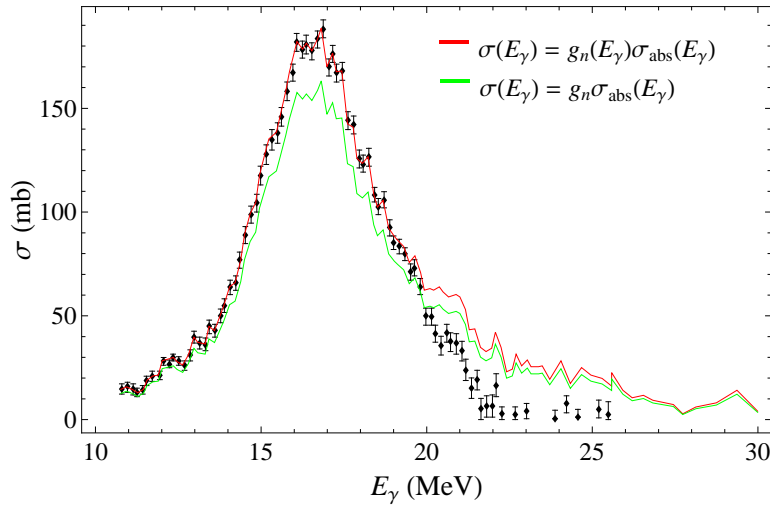


Figure 18: Theoretical, using energy dependent [displayed in red, calculated with equations (61), (37), and (62)] and independent [displayed in green, calculated with equations (67) and (68)] branching ratios, and experimental photoneutron cross sections for  $^{91}\text{Zr}$ . Experimental data is from reference [67] (p. 171).

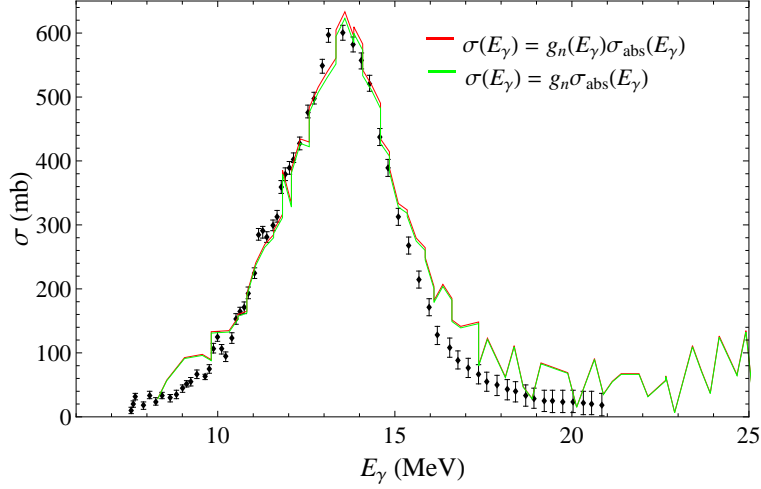


Figure 19: Theoretical, using energy dependent [displayed in red, calculated with equations (61), (37), and (62)] and independent [displayed in green, calculated with equations (67) and (68)] branching ratios, and experimental photoneutron cross sections for  $^{208}\text{Pb}$ . Experimental data is from reference [67] (p. 251).

It can be seen in Figures 13 - 19 that the theoretical photonuclear cross sections, calculated with energy dependent and independent branching ratios, adequately agree with experiment. *For most of the reactions, the theoretical photonuclear cross section, calculated with an energy dependent branching ratio, provides a better fit to experiment.* This can be observed for the reactions  $^{14}\text{N}(\gamma, n)$ ,  $^{28}\text{Si}(\gamma, n)$ ,  $^{28}\text{Si}(\gamma, p)$ ,  $^{88}\text{Sr}(\gamma, n)$ , and  $^{91}\text{Zr}(\gamma, n)$ , as shown in Figures 13, 15 16, 17, and 18, respectively. It should be noted that for Figures 17 and 18, the energy dependent branching ratio provides a much better fit to the experimental values around the peak of the photonuclear cross section. Differences between the values of the energy dependent and independent branching ratio at a specific photon energy can be observed in Tables 5 - 11 of Appendix A.

It is also important to mention that agreement between theory and experiment seems to improve with increasing target mass, as can be observed in the photonuclear cross section graphs for  $^{88}\text{Sr}(\gamma, n)$ ,  $^{91}\text{Zr}(\gamma, n)$ , and  $^{208}\text{Pb}(\gamma, n)$ . Improvement is seen for theoretical

cross sections calculated with both energy dependent and independent branching ratios. This is due to the strong dependence of the neutron channel. For these three cases, the energy independent branching ratio is approximately equal to 1 and the energy dependent branching ratio is in the range of 0.85 to 1, which can be seen in Tables 9 - 11 of Appendix A.

As previously stated, mostly all the photonuclear cross sections calculated with energy dependent branching ratios compare more accurately to experiment. However, for Figure 14, the theoretical photoneutron cross section for  $^{16}\text{O}$ , calculated with an energy *independent* branching ratio, provides a better fit to the experimental results. This is due to a significant contribution of the photonuclear reaction for oxygen coming from direct reactions [67]. Therefore, calculating photonuclear reactions for oxygen using energy dependent branching ratios, determined from the Weisskopf - Ewing statistical theory for compound nucleus decay, is inappropriate. Comparisons between energy dependent branching ratios, calculated using the Weisskopf - Ewing theory, and energy independent branching ratios should not be made for the case of oxygen. *In fact, any reaction that proceeds mainly through a direct reaction should not use the Weisskopf - Ewing method.* Another theory for calculating energy dependent branching ratios for reactions that proceed mainly through direct channels will need to be developed before comparisons can be made.

## **8.2 Nucleus - Nucleus Cross Sections using Energy Dependent and Independent Branching Ratios Compared to Experiment**

In this section, EMD cross sections for single neutron, proton, and alpha particle removal are calculated using energy dependent and independent branching ratios and then

compared to experiment, as shown in Table 2. To calculate the nucleus - nucleus cross section using an energy *independent* branching ratio, equation (112) is employed, where the proton and neutron branching ratios are given by equations (68) and (67), respectively. It is important to reiterate that for the case of energy independent branching ratios, the formulation was based on the assumption that only neutron and proton emission occurred. For a nucleus - nucleus cross section that utilizes an energy *dependent* branching ratio, equation (111) is used. The energy dependent branching ratio is given by equation (61), with the total width given by equation (62) and the partial width given by equations (63) and (64) for a neutron and charged particle, respectively.

Electromagnetic dissociation cross sections for single neutron and proton removal, calculated using energy dependent and independent branching ratios, are compared with nucleus - nucleus experimental data in Table 2. EMD cross sections for single alpha particle removal were also calculated using energy dependent branching ratios and compared to experiment in Table 2. An energy independent branching ratio equation for alpha particle emission was not formulated; therefore, single alpha particle removal EMD cross sections, calculated using energy independent branching ratios, could not be determined.

It can be seen that the calculated EM cross sections for  $^{12}\text{C}$  and  $^{16}\text{O}$  projectiles, using both energy dependent and independent branching ratios, are within the experimental error estimates for mostly all target and energy combinations. It is surprising that the EMD cross sections calculated with energy *dependent* branching ratios agree so well with the experimental data because  $^{12}\text{C}$  and  $^{16}\text{O}$  reactions proceed mainly through a direct reaction. The energy dependent branching ratios for  $^{12}\text{C}$  and  $^{16}\text{O}$  are calculated using the Weisskopf - Ewing theory, which is specifically designed for compound nucleus decay. It is therefore recommended that the energy independent branching ratios be used for  $^{12}\text{C}$  and  $^{16}\text{O}$  reactions.

Table 2: Electromagnetic Cross Sections for Single Neutron, Proton, and Alpha Particle Removal.

Projectile	Target	$T_{\text{lab}}$ (GeV/N)	Decay Channel	$\sigma_{\text{expt}}^{\text{EMD}}$ (mb) *	$\sigma_{(112)}^{\text{EMD}}$ (mb) †	$\sigma_{(111)}^{\text{EMD}}$ (mb) ‡
$^{12}\text{C}$	$^{208}\text{Pb}$	2.1	$^{11}\text{C} + 1\text{n}$	$51 \pm 18$	42.9964	35.2666
$^{12}\text{C}$	$^{208}\text{Pb}$	2.1	$^{11}\text{B} + 1\text{p}$	$50 \pm 25$	70.2699	38.6367
$^{12}\text{C}$	$^{208}\text{Pb}$	1.05	$^{11}\text{C} + 1\text{n}$	$39 \pm 24$	25.2166	19.8329
$^{12}\text{C}$	$^{208}\text{Pb}$	1.05	$^{11}\text{B} + 1\text{p}$	$50 \pm 25$	41.8808	22.1407
$^{16}\text{O}$	$^{208}\text{Pb}$	2.1	$^{15}\text{O} + 1\text{n}$	$50 \pm 24$	62.051	50.2401
$^{16}\text{O}$	$^{208}\text{Pb}$	2.1	$^{15}\text{N} + 1\text{p}$	$96 \pm 26$	102.91	83.5714
$^{12}\text{C}$	$^{108}\text{Ag}$	2.1	$^{11}\text{C} + 1\text{n}$	$21 \pm 10$	16.7542	13.8676
$^{12}\text{C}$	$^{108}\text{Ag}$	2.1	$^{11}\text{B} + 1\text{p}$	$18 \pm 13$	27.2921	15.1292
$^{12}\text{C}$	$^{108}\text{Ag}$	1.05	$^{11}\text{C} + 1\text{n}$	$21 \pm 10$	10.5761	8.44344
$^{12}\text{C}$	$^{108}\text{Ag}$	1.05	$^{11}\text{B} + 1\text{p}$	$25 \pm 19$	17.4608	9.36414
$^{16}\text{O}$	$^{108}\text{Ag}$	2.1	$^{15}\text{O} + 1\text{n}$	$26 \pm 13$	23.9174	19.532
$^{16}\text{O}$	$^{108}\text{Ag}$	2.1	$^{15}\text{N} + 1\text{p}$	$30 \pm 16$	39.4881	32.1429
$^{12}\text{C}$	$^{64}\text{Cu}$	2.1	$^{12}\text{C} + 1\text{n}$	$10 \pm 7$	7.06394	5.87764
$^{12}\text{C}$	$^{64}\text{Cu}$	2.1	$^{11}\text{B} + 1\text{p}$	$4 \pm 8$	11.4855	6.39671
$^{12}\text{C}$	$^{64}\text{Cu}$	1.05	$^{11}\text{C} + 1\text{n}$	$9 \pm 8$	4.65276	3.74663
$^{12}\text{C}$	$^{64}\text{Cu}$	1.05	$^{11}\text{B} + 1\text{p}$	$5 \pm 8$	7.65609	4.13926
$^{16}\text{O}$	$^{64}\text{Cu}$	2.1	$^{15}\text{O} + 1\text{n}$	$9 \pm 8$	10.0187	8.2224
$^{16}\text{O}$	$^{64}\text{Cu}$	2.1	$^{15}\text{N} + 1\text{p}$	$15 \pm 8$	16.499	13.4477
$^{12}\text{C}$	$^{27}\text{Al}$	2.1	$^{11}\text{C} + 1\text{n}$	$0 \pm 5$	1.6516	1.3846
$^{12}\text{C}$	$^{27}\text{Al}$	2.1	$^{11}\text{B} + 1\text{p}$	$0 \pm 5$	2.67839	1.50157
$^{12}\text{C}$	$^{27}\text{Al}$	1.05	$^{11}\text{C} + 1\text{n}$	$1 \pm 6$	1.15605	0.942364
$^{12}\text{C}$	$^{27}\text{Al}$	1.05	$^{11}\text{B} + 1\text{p}$	$1 \pm 7$	1.89353	1.03538
$^{16}\text{O}$	$^{27}\text{Al}$	2.1	$^{15}\text{O} + 1\text{n}$	$0 \pm 5$	2.31977	1.91739
$^{16}\text{O}$	$^{27}\text{Al}$	2.1	$^{15}\text{N} + 1\text{p}$	$-1 \pm 9$	3.80662	3.10831
$^{12}\text{C}$	$^{12}\text{C}$	2.1	$^{11}\text{C} + 1\text{n}$	$-2 \pm 5$	0.393841	0.331945
$^{12}\text{C}$	$^{12}\text{C}$	2.1	$^{11}\text{B} + 1\text{p}$	$-1 \pm 4$	0.637513	0.359076
$^{12}\text{C}$	$^{12}\text{C}$	1.05	$^{11}\text{C} + 1\text{n}$	$-2 \pm 5$	0.287878	0.236711
$^{12}\text{C}$	$^{12}\text{C}$	1.05	$^{11}\text{B} + 1\text{p}$	$-2 \pm 5$	0.470029	0.259044
$^{16}\text{O}$	$^{12}\text{C}$	2.1	$^{15}\text{O} + 1\text{n}$	$-1 \pm 4$	0.549095	0.456151
$^{16}\text{O}$	$^{12}\text{C}$	2.1	$^{15}\text{N} + 1\text{p}$	$-1 \pm 4$	0.898782	0.734837
$^{18}\text{O}$	$^{238}\text{U}$	1.7	$^{17}\text{O} + 1\text{n}$	$140.8 \pm 4.1$	87.5476	211.602
$^{18}\text{O}$	$^{238}\text{U}$	1.7	$^{17}\text{N} + 1\text{p}$	$25.1 \pm 1.6$	101.782	0.419803
$^{18}\text{O}$	$^{208}\text{Pb}$	1.7	$^{17}\text{O} + 1\text{n}$	$136 \pm 2.9$	71.7717	173.512
$^{18}\text{O}$	$^{208}\text{Pb}$	1.7	$^{17}\text{N} + 1\text{p}$	$20.2 \pm 1.8$	83.6706	0.34833
$^{18}\text{O}$	$^{48}\text{Ti}$	1.7	$^{17}\text{O} + 1\text{n}$	$8.7 \pm 2.7$	7.05503	17.0903
$^{18}\text{O}$	$^{48}\text{Ti}$	1.7	$^{17}\text{N} + 1\text{p}$	$-0.5 \pm 1.0$	8.43365	0.0383709
$^{28}\text{Si}$	$^{208}\text{Pb}$	13.7	$^{27}\text{Si} + 1\text{n}$	$347 \pm 18$	397.914	149.051
$^{28}\text{Si}$	$^{208}\text{Pb}$	13.7	$^{27}\text{Al} + 1\text{p}$	$743 \pm 27$	503.048	629.371
$^{28}\text{Si}$	$^{208}\text{Pb}$	14.6	$^{27}\text{Si} + 1\text{n}$	$241.0 \pm 4.2$	409.25	153.513
$^{28}\text{Si}$	$^{208}\text{Pb}$	14.6	$^{27}\text{Al} + 1\text{p}$	$676.4 \pm 7.6$	516.844	646.874
$^{28}\text{Si}$	$^{208}\text{Pb}$	14.6	$^{24}\text{Mg} + 1\alpha$	$72 \pm 32$	N/A	264.33
$^{28}\text{Si}$	$^{120}\text{Sn}$	13.7	$^{27}\text{Si} + 1\text{n}$	$136 \pm 6$	156.115	58.631
$^{28}\text{Si}$	$^{120}\text{Sn}$	13.7	$^{27}\text{Al} + 1\text{p}$	$313 \pm 4$	196.982	246.619
$^{28}\text{Si}$	$^{120}\text{Sn}$	14.6	$^{27}\text{Si} + 1\text{n}$	$100.0 \pm 2.0$	160.345	60.2976
$^{28}\text{Si}$	$^{120}\text{Sn}$	14.6	$^{27}\text{Al} + 1\text{p}$	$274.0 \pm 4.4$	202.128	253.148
$^{28}\text{Si}$	$^{120}\text{Sn}$	14.6	$^{24}\text{Mg} + 1\alpha$	$58 \pm 30$	N/A	102.795

Continued on Next Page...

Table 2 – Continued

Projectile	Target	T <sub>lab</sub> (GeV/N)	Decay Channel	$\sigma_{\text{expt}}^{\text{EMD}}$ (mb) *	$\sigma_{(112)}^{\text{EMD}}$ (mb) †	$\sigma_{(111)}^{\text{EMD}}$ (mb) ‡
<sup>28</sup> Si	<sup>64</sup> Cu	14.6	<sup>27</sup> Si + 1n	40.4 ± 1.7	56.5488	21.3114
<sup>28</sup> Si	<sup>64</sup> Cu	14.6	<sup>27</sup> Al + 1p	111.0 ± 3.3	71.17	89.1858
<sup>28</sup> Si	<sup>64</sup> Cu	14.6	<sup>24</sup> Mg + 1 $\alpha$	17 ± 19	N/A	36.0171
<sup>28</sup> Si	<sup>27</sup> Al	13.7	<sup>27</sup> Si + 1n	15 ± 4	11.7522	4.43562
<sup>28</sup> Si	<sup>27</sup> Al	13.7	<sup>27</sup> Al + 1p	37 ± 5	14.7747	18.522
<sup>28</sup> Si	<sup>27</sup> Al	14.6	<sup>27</sup> Si + 1n	13.11 ± 0.59	12.0398	4.54909
<sup>28</sup> Si	<sup>27</sup> Al	14.6	<sup>27</sup> Al + 1p	31.6 ± 1.2	15.1243	18.9656
<sup>28</sup> Si	<sup>27</sup> Al	14.6	<sup>24</sup> Mg + 1 $\alpha$	21 ± 16	N/A	7.6096

\*  $\sigma_{\text{expt}}^{\text{EMD}}$  are the experimental EMD cross sections from references [21, 96, 97, 98, 99].

†  $\sigma_{(112)}^{\text{EMD}}$  are the theoretical EMD cross sections using equation (112).

‡  $\sigma_{(111)}^{\text{EMD}}$  are the theoretical EMD cross sections using equation (111).

It is obvious that discrepancies exist between the calculated EMD cross sections and experimental data for <sup>18</sup>O projectiles. The EMD cross sections calculated with energy dependent and independent branching ratios will show disagreement because the parameterization of the absorption cross section, equation (99), was designed for only stable nuclei. Before comparisons can be made for <sup>18</sup>O projectiles, a parameterization for the absorption cross section for unstable nuclei will need to be developed. Nevertheless, energy dependent branching ratios should not be used for <sup>18</sup>O projectiles, since reactions with oxygen proceed mainly through direct channels.

Problems can also be observed for the <sup>28</sup>Si projectile. Disparities are prevalent for the EM cross sections calculated with energy *dependent* branching ratios. Compound nucleus decay is found for the neutron and alpha particle channels in <sup>28</sup>Si, but different behavior is observed for the proton decay. Predominately direct GDR decay occurs for the proton channel of <sup>28</sup>Si [100]. Mostly all of the partial (ground state, first excited state, etc.) proton cross sections demonstrate different intermediate structures [100]. This behavior is contradictory to the statistical particle emission of the Weisskopf - Ewing theory. Con-

sequently, the energy dependent branching ratios calculated using the Weisskopf - Ewing statistical theory will not be representative of the proton decay channel. The erroneously calculated proton branching ratios will also have an effect on the values of the neutron and alpha particle branching ratios. Remember that in the denominator of the energy dependent branching ratio formula (111) is the total width (62), which is given by the sum of all the decay channels. Therefore, if one channel is calculated incorrectly, it will ultimately effect all of the channels. Here is another case where the energy dependent branching ratio should not be employed.

### 8.3 Photonuclear and Nucleus - Nucleus Differential Cross Sections in the Projectile and Lab Frames

Photonuclear differential cross sections are presented in Figures 20 - 25, which are evaluated at a photon value of 20 MeV near the peak of the giant dipole resonance. Nucleus - nucleus differential cross sections are presented in Figures 26 - 31. The cross sections in Figures 20 - 31 are for the reaction



at 14.6 A GeV. Since the projectile is  $^{28}\text{Si}$ , energy independent branching ratios will be used as discussed previously.

Figure 20 shows the application of equation (91) to calculate the photonuclear spectral distribution in the projectile frame. Equation (77) was used to calculate an isotropic photonuclear angular distribution in the projectile frame, as seen in Figure 21. The photonuclear double differential cross section in the projectile frame is given by equation (95) and is shown in Figure 22.

These photonuclear cross sections are transformed to the lab frame and are shown in Figures 23 - 25. The photonuclear double differential cross section in the lab frame, as shown in Figure 23, displays the double peak feature discussed by Hagedorn [101] (pp. 47-49). This double peak occurs because there is a single peak in the spectral distribution in the projectile frame (Figure 20), which gets boosted both forward and backward in the lab frame depending on kinematic conditions. Figure 24 displays the photonuclear spectral distribution in the lab frame, which results from integrating the photonuclear double differential cross section in the lab frame over all lab angles. Compared to Figure 20, it can be seen that the nucleon kinetic energies receive a large boost because of the high energy of the projectile. The angular distribution in the lab frame is obtained by integrating the photonuclear double differential cross section in the lab frame over all lab energies. In the projectile frame, the photonuclear angular distribution is isotropic, while in the lab frame, it becomes non - isotropic and is peaked strongly in the forward direction. These features of the photonuclear angular distribution in the lab frame can be observed in Figure 25.

The nucleus - nucleus differential cross sections are obtained by taking the corresponding photonuclear cross section and integrating over the virtual photon spectrum, as discussed previously. It can be seen that all the nucleus - nucleus differential cross sections, in both the projectile and lab frames, follow the shapes of the corresponding photonuclear differential cross sections, as shown in Figures 26 - 31. This makes sense because the photonuclear differential cross sections are just integrated over the virtual photon spectrum. In the lab frame, the nucleus - nucleus differential cross sections, just like for the photonuclear differential cross sections, have nucleon kinetic energies that receive a large boost and angles that strongly peak in the forward direction. This can be seen in Figures 29 - 31.

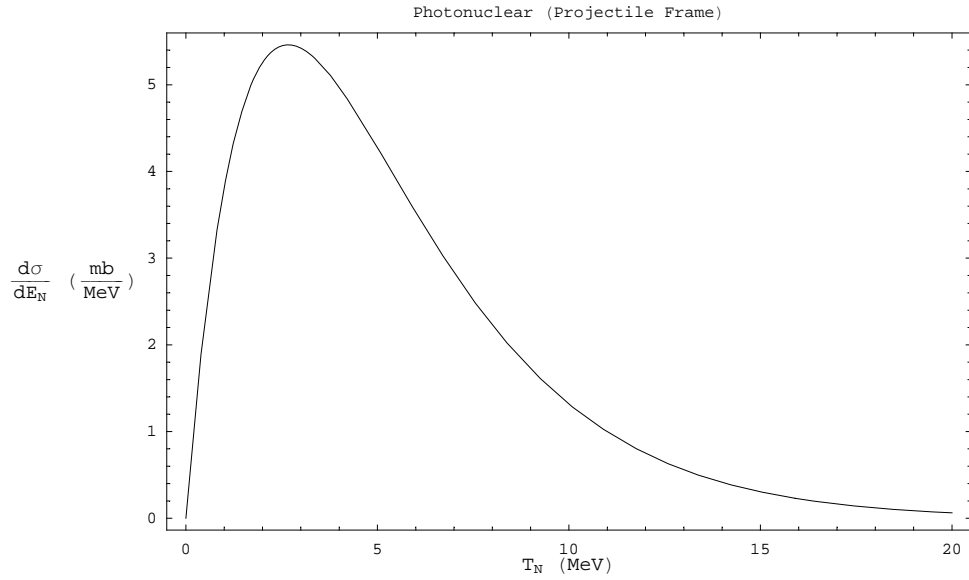


Figure 20: Photonuclear spectral distribution in the projectile frame evaluated at a photon energy of 20 MeV. The calculation was done using equation (91).

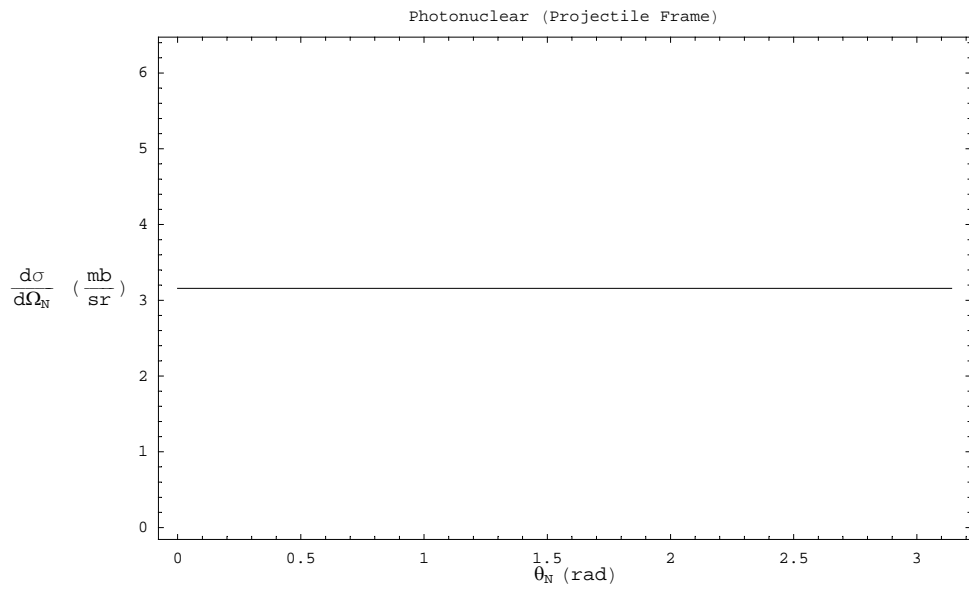


Figure 21: Photonuclear angular distribution in the projectile frame evaluated at a photon energy of 20 MeV. The calculation was done using equation (77).

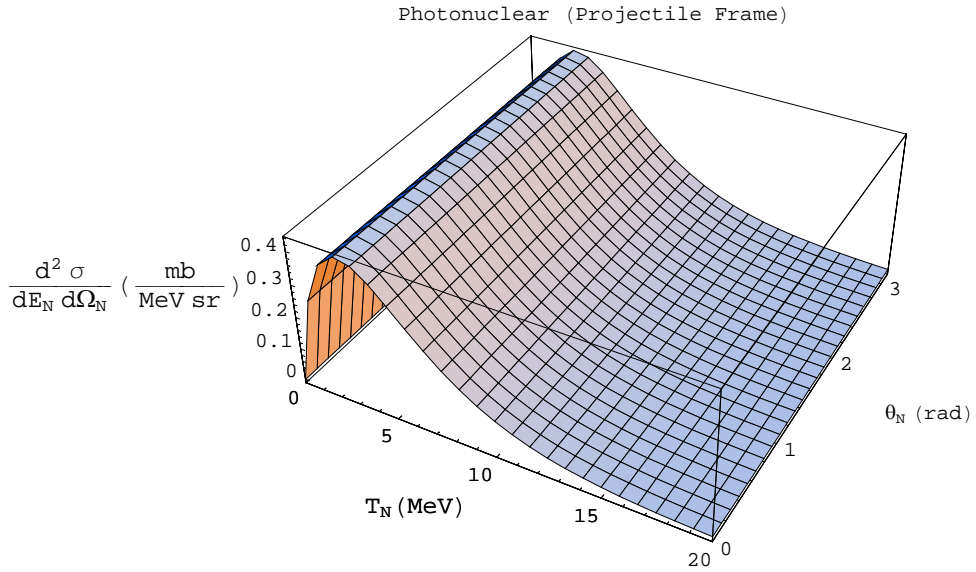


Figure 22: Photonuclear double differential cross section in the projectile frame evaluated at a photon energy of 20 MeV. (Bottom figure is same as top figure, except rotated.) The calculation was done using equation (95).

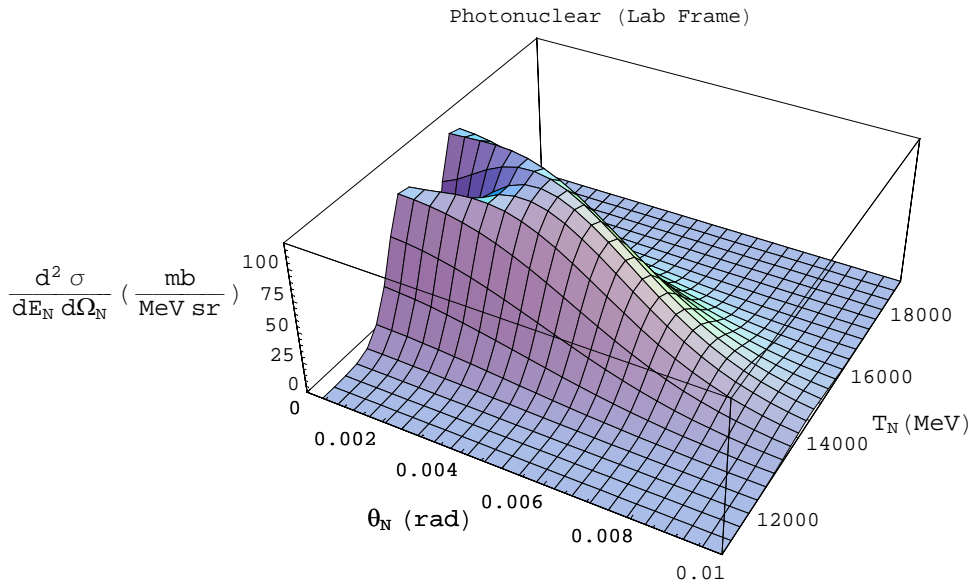
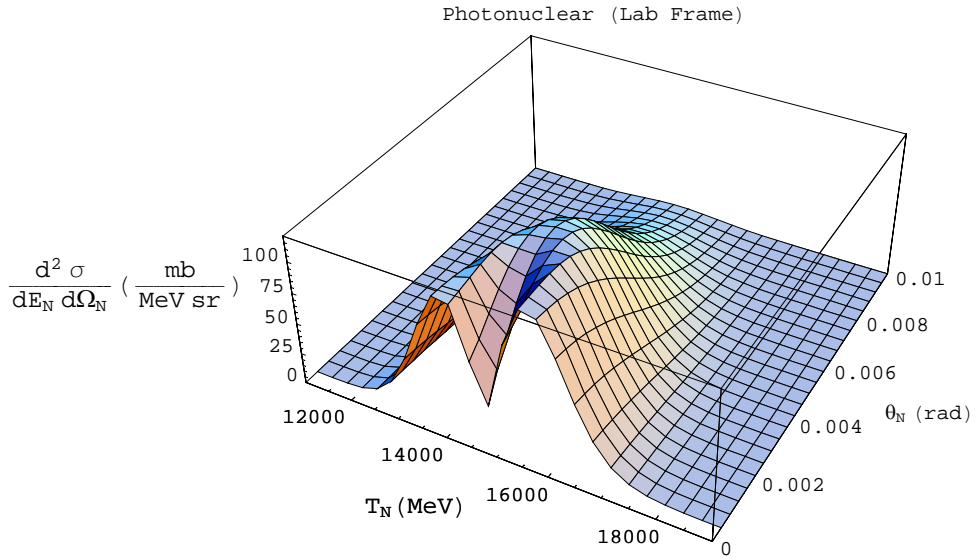


Figure 23: Photonuclear double differential cross section in the lab frame evaluated at a photon energy of 20 MeV. (Bottom figure is same as top figure, except rotated.) The calculation was done using equation (148).

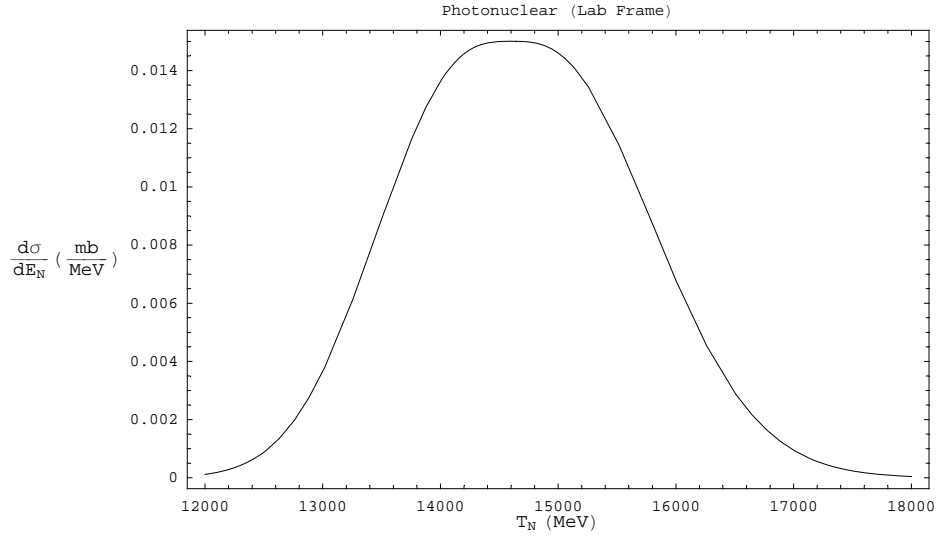


Figure 24: Photonuclear spectral distribution in the lab frame evaluated at a photon energy of 20 MeV. The calculation was done using equation (148) and integrating over angle.

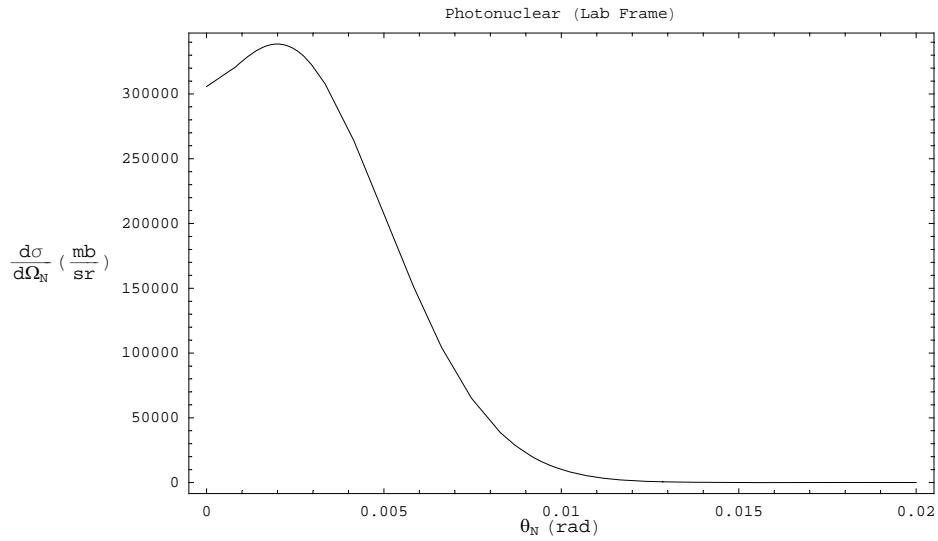


Figure 25: Photonuclear angular distribution in the lab frame evaluated at a photon energy of 20 MeV. The calculation was done using equation (148) and integrating over energy.

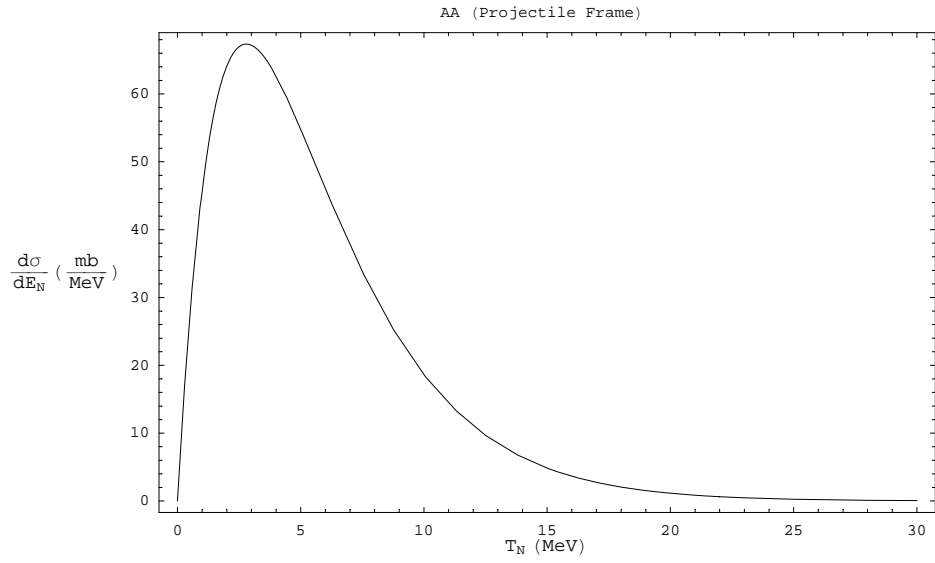


Figure 26: Nucleus - nucleus spectral distribution in the projectile frame. The calculation was done using equation (123).

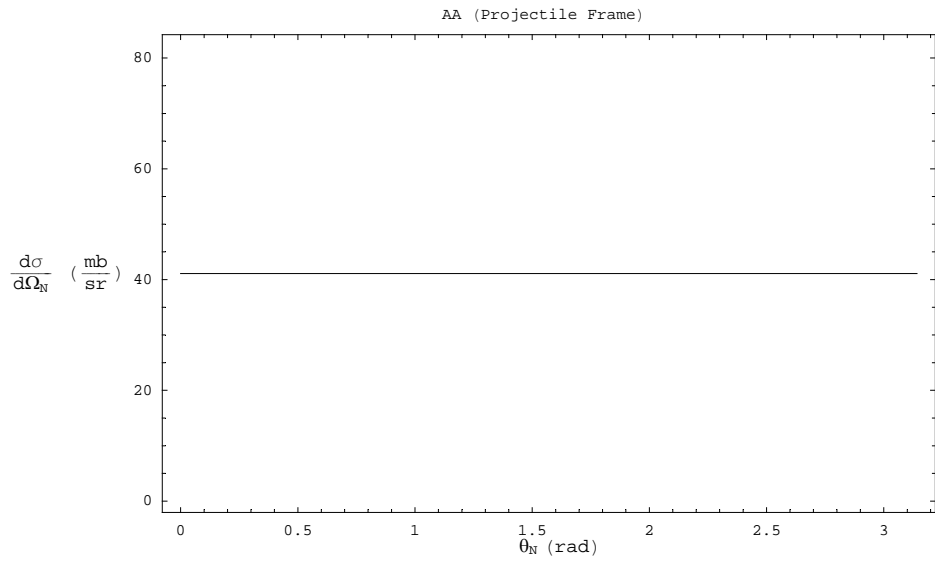


Figure 27: Nucleus - nucleus angular distribution in the projectile frame. The calculation was done using equation (121).

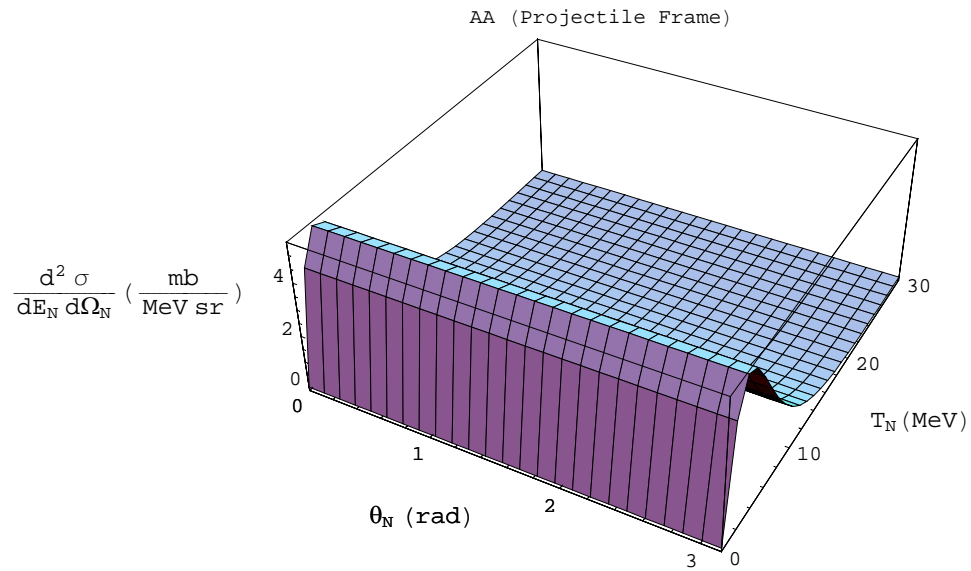
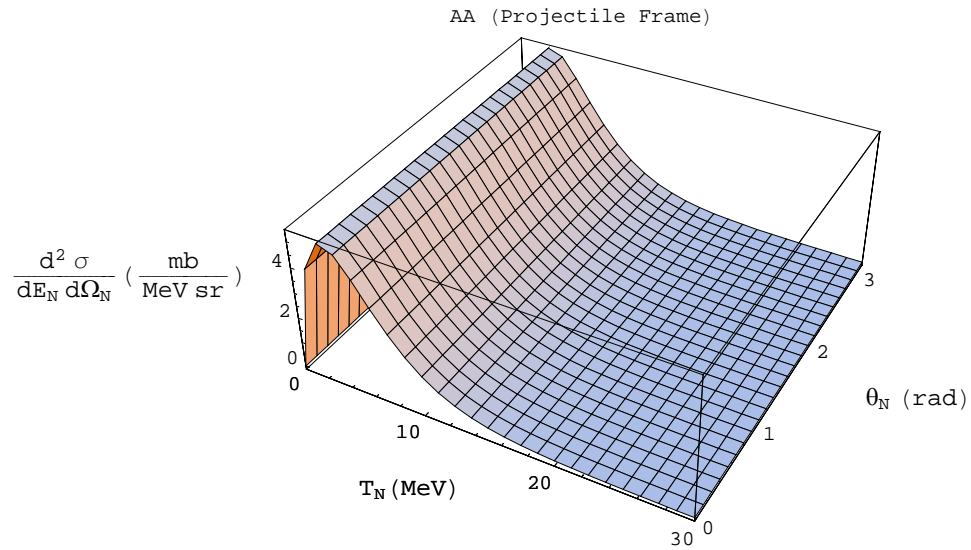


Figure 28: Nucleus - nucleus double differential cross section in the projectile frame. (Bottom figure is same as top figure, except rotated.) The calculation was done using equation (124).

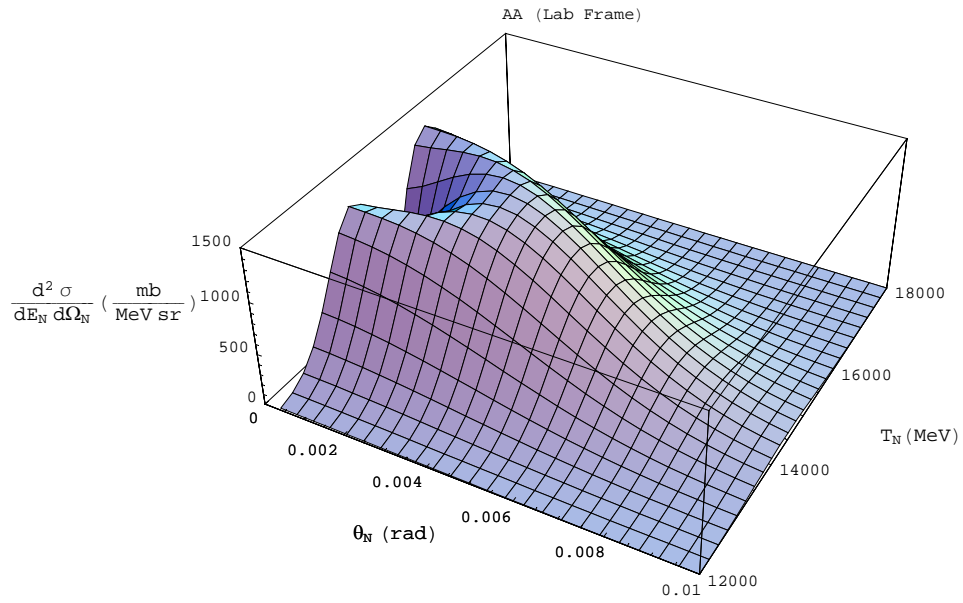
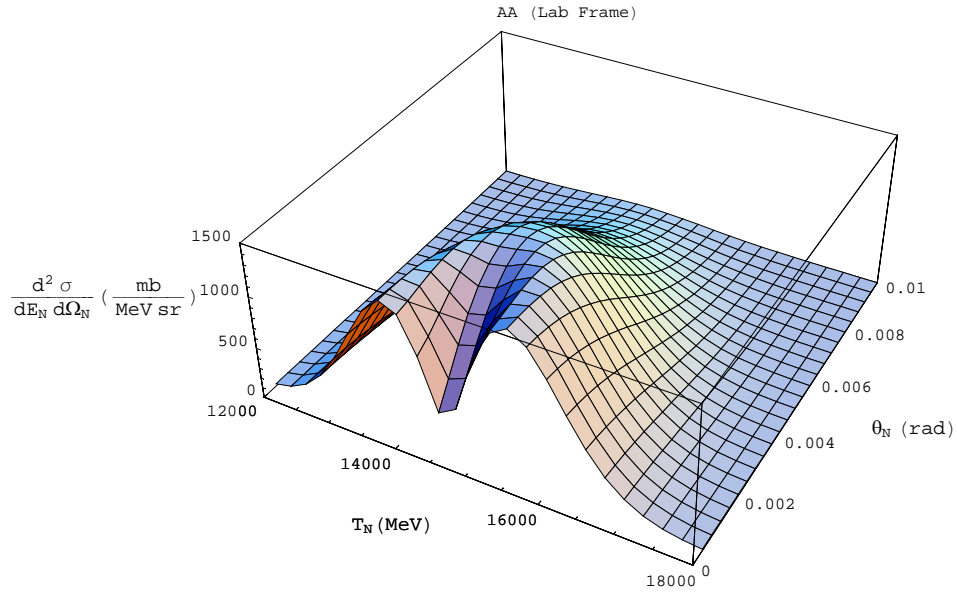


Figure 29: Nucleus - nucleus double differential cross section in the lab frame. (Bottom figure is same as top figure, except rotated.) The calculation was done using equation (124) and by transforming to the lab frame.

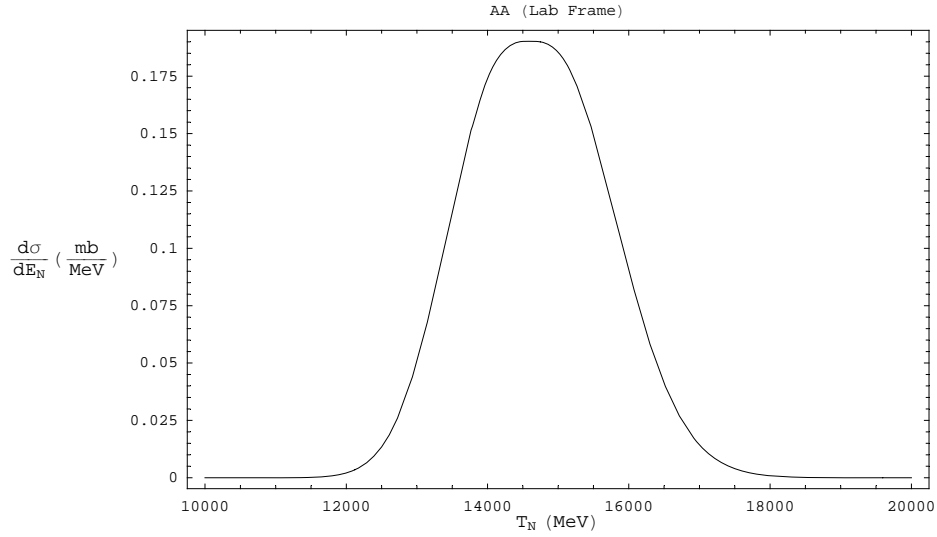


Figure 30: Nucleus - nucleus spectral distribution in the lab frame. The calculation was done using equation (124), then transforming to the lab frame, and finally integrating over angle.

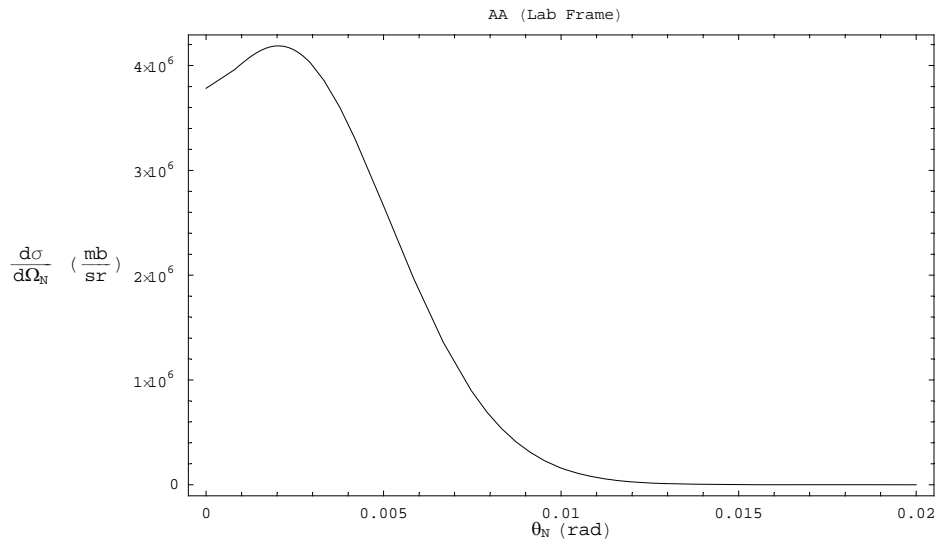


Figure 31: Nucleus - nucleus angular distribution in the lab frame. The calculation was done using equation (124), then transforming to the lab frame, and finally integrating over energy.

## 8.4 Nucleus - Nucleus Spectral Distributions Compared to Experiment

There is very little experimental data concerning differential cross sections for electromagnetic dissociation. The best data available has been measured by Barrette et al. [20, 21], but much of their data involved spectral distributions of excitation energy. This will be analyzed in future work; however, a notable feature of their measurements is that *all of their angular distributions are approximately isotropic in the projectile frame, which agrees with the assumption of the present work.* Some kinetic energy distributions have been measured for outgoing neutrons and protons: see Figure 13 of Barrette et al. [21]. Figures 32 and 33 compare the theory presented in this paper to the data of Barrette et al. [21]. There are two points to note about these Figures. Firstly, the experimental work quoted arbitrary units, so it was necessary to fit the absolute value (peak cross section) to the experiment. Secondly, the best fit is obtained by choosing the nuclear temperature constant in equation (79) as  $\mathcal{D} = 20$ . The comparison between theory and the limited experimental data is good. A better fit can probably be obtained with a more sophisticated approach to calculating the nuclear temperature and the spectral distribution (91).

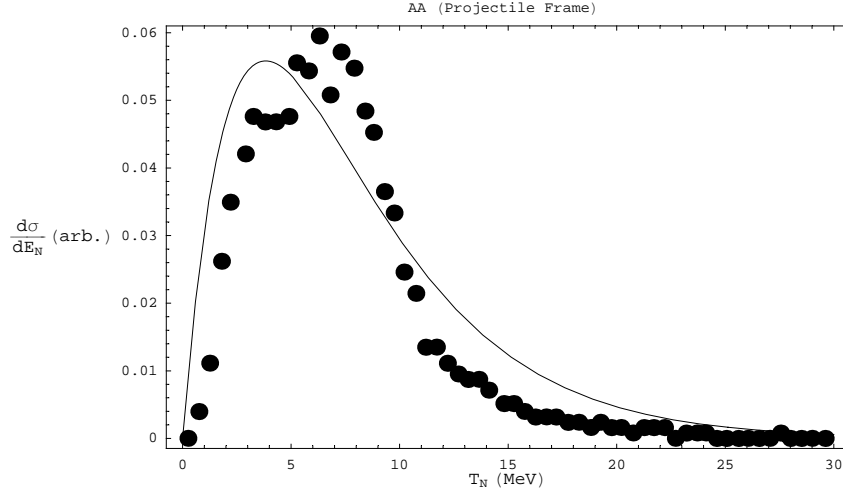


Figure 32: Comparison between theory and experiment for the proton kinetic energy distribution in the projectile frame. The reaction is  $^{28}\text{Si} + \text{Pb} \rightarrow 1\text{p} + ^{27}\text{Al} + \text{Pb}$  at 14.6 A GeV. Experimental data is from Figure 13(b) of reference [21]. Cross section units are arbitrary. Error bars are smaller than symbol sizes.

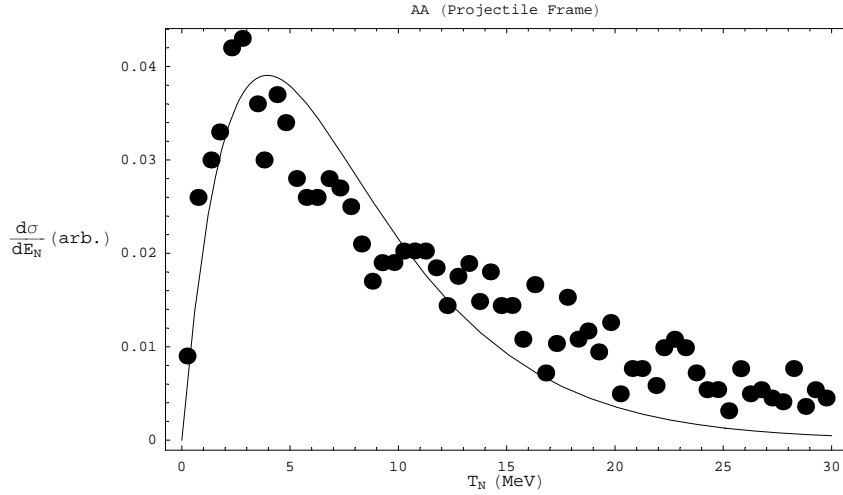


Figure 33: Comparison between theory and experiment for the neutron kinetic energy distribution in the projectile frame. The reaction is  $^{28}\text{Si} + \text{Pb} \rightarrow 1\text{n} + ^{27}\text{Si} + \text{Pb}$  at 14.6 A GeV. Experimental data is from Figure 13(c) of reference [21]. Cross section units are arbitrary. Error bars are smaller than symbol sizes.

## 9 Conclusion

This paper compares energy dependent and independent branching ratios used in calculating photonuclear and nucleus - nucleus cross sections. To determine the validity of energy dependent and independent branching ratios, comparisons between theoretical and experimental photonuclear cross sections were made. Theoretical photonuclear cross sections were found by multiplying the energy dependent or independent branching ratio by an experimental absorption cross section. Only by using experimental absorption cross sections could the energy dependent and independent branching ratio formalisms be truly compared. Since both experimental absorption cross sections and experimental photonuclear cross sections were used, comparisons were limited to the availability of both data sets. Comparisons of photonuclear cross sections, calculated with both energy dependent and independent branching ratios, were made for photoneutron and photoproton reactions. The energy independent branching ratio formalism assumes that only neutron and proton emission occurs; therefore, only photoneutron and photoproton reactions can be calculated with energy independent branching ratios. The benefit of using energy dependent branching ratios, determined by the Weisskopf - Ewing method, is that it can be used to calculate the emission of a neutron, proton, alpha particle, helion, deuteron, or triton.

The theoretical photonuclear cross sections, calculated with energy dependent and independent branching ratios, both gave reasonable fits to experiment. For mostly all of the reactions examined, the energy dependent branching ratio provided the best fit. Only in cases where the reaction proceeded through mainly direct channels, for example  $^{16}\text{O}$ , did the energy independent branching ratio provide a better fit. This is the only disadvantage of the Weisskopf - Ewing theory. The method is intended for reactions that

occur primarily through a compound nucleus state.

Nucleus - nucleus EMD cross sections for single neutron, proton, and alpha particle removal were calculated using energy dependent branching ratios and then compared to experiment, while only single neutron and proton EMD cross sections could be calculated using energy independent branching ratios, for reasons discussed previously. It was surprising that the nucleus - nucleus EMD cross sections, calculated using energy dependent branching ratios, were within experimental error for mostly all energy and target combinations for  $^{12}\text{C}$  and  $^{16}\text{O}$  projectiles. Both  $^{12}\text{C}$  and  $^{16}\text{O}$  proceed through mainly direct channels. Therefore, it is recommended that energy independent branching ratios be employed for  $^{12}\text{C}$  and  $^{16}\text{O}$  reactions. For the case of  $^{18}\text{O}$  projectiles, the theoretical photonuclear cross sections, calculated with energy dependent and independent branching ratios, both showed disagreement to experiment. The parameterized absorption cross section used is only applicable to stable nuclei, so disagreement is expected. Problems could also be observed for nucleus - nucleus EMD cross sections, calculated with energy dependent branching ratios, for  $^{28}\text{Si}$  projectiles. The Weisskopf - Ewing theory should not be employed for the case of silicon because predominately direct GDR decay occurs for proton emission. It is important to remember that if just one of the decay channels in a reaction proceeds directly, it will ultimately effect the branching ratio of all of the channels.

This paper examines when energy dependent and independent branching ratios should be used. From comparisons of experiment to theoretical photonuclear cross sections and theoretical nucleus - nucleus EMD cross sections, the regions of applicability for both energy dependent and independent branching ratios can be determined. For reactions that proceed through a well - defined compound nucleus state, the energy dependent branching ratio, given by the Weisskopf - Ewing method, should be utilized. Energy

dependent branching ratios should be used when one or more of the decay channels proceeds directly. With the regions of applicability now determined, future work can focus on calculating cross sections, using Weisskopf - Ewing theory, for emissions of particles heavier than protons and neutrons. Future work will also show that the Weisskopf - Ewing formalism developed in this paper can also be used to determine energy dependent branching ratios for multiple particle emission.

The first calculations of differential cross sections for electromagnetic dissociation in nucleus - nucleus collisions are presented in this paper. These cross sections will be used in three - dimensional transport codes to improve estimates of radiation dose inside the spacecraft. The results are given in a form in which they can be immediately used in fully three - dimensional space radiation transport codes that require differential cross sections in the lab frame. Cross sections are isotropic in the projectile frame and are in agreement with experiment. Spectral distributions in the projectile frame are compared to experimental results and are found to be in excellent agreement. However, the amount of data available is very limited. The acquisition of more data would be very useful. Future work will involve a more sophisticated approach to calculating the spectral distribution and the nuclear temperature.

## A Tables

Table 3: Values for the width of the electric dipole giant dipole resonance, from [73].

Nucleus	$\Gamma$ (MeV)
$^{12}\text{C}$	8.0
$^{16}\text{O}$	10.0
$^{19}\text{O}$	12.0
$^{28}\text{Si}$	10.0

Table 4: Values for the 10% Charge Density Radius found from various models.

Nucleus	10% Chage Radius (fm)	Reference
$^{12}\text{C}$	3.33	[73]
$^{16}\text{O}$	3.77	[73]
$^{18}\text{O}$	3.88	[73]
$^{27}\text{Al}$	4.21	[73]
$^{28}\text{Si}$	4.18	[73]
$^{32}\text{S}$	4.53	[73]
$^{48}\text{Ti}$	5.00	[73]
$^{64}\text{Cu}$	5.45	[73]
$^{107}\text{Ag}$ and $^{108}\text{Ag}$	6.32	[73]
$^{124}\text{Sn}$	6.54	[102]
$^{197}\text{Au}$	7.56	[73]
$^{208}\text{Pb}$	7.83	[73]
$^{238}\text{U}$	8.13	[73]

Table 5: Cross section values for the reaction  $^{14}\text{N}(\gamma, n)$ .

$E_\gamma$ (MeV)	$\sigma_{\text{abs}}$ (mb)	$g_n$	$g_n(E_\gamma)$	$\sigma_n = g_n\sigma_{\text{abs}}(\text{mb})$	$\sigma_n = g_n(E_\gamma)\sigma_{\text{abs}}$ (mb)
13.618	1.182	0.4	0.445883	0.4728	0.527033706
14.096	0.328	0.4	0.45645	0.1312	0.149715600
14.334	1.247	0.4	0.460124	0.4988	0.573774628
14.573	0.460	0.4	0.463016	0.1840	0.212987360
14.812	4.464	0.4	0.465261	1.7856	2.076925104
15.290	1.247	0.4	0.468276	0.4988	0.583940172
15.290	2.035	0.4	0.468276	0.8140	0.952941660
15.529	1.116	0.4	0.469223	0.4464	0.523652868
15.768	3.545	0.4	0.469888	1.4180	1.665752960
15.768	4.136	0.4	0.469888	1.6544	1.943456768
16.007	2.495	0.4	0.470322	0.9980	1.173453390
16.246	3.742	0.4	0.470569	1.4968	1.760869198
16.485	2.691	0.4	0.47066	1.0764	1.266546060
16.485	1.904	0.4	0.47066	0.7616	0.896136640
16.962	4.004	0.4	0.470454	1.6016	1.883697816
16.962	2.823	0.4	0.470454	1.1292	1.328091642
17.201	3.545	0.4	0.470196	1.4180	1.666844820
17.201	4.595	0.4	0.470196	1.8380	2.160550620
17.440	6.039	0.4	0.469857	2.4156	2.837466423
17.918	6.236	0.4	0.46899	2.4944	2.924621640
17.918	5.580	0.4	0.46899	2.2320	2.616964200
18.157	7.221	0.4	0.468485	2.8884	3.382930185
18.396	10.372	0.4	0.467945	4.1488	4.853525540
18.635	7.418	0.4	0.467376	2.9672	3.466995168
18.635	10.700	0.4	0.467376	4.2800	5.000923200
19.113	9.912	0.4	0.46618	3.9648	4.620776160
19.352	11.488	0.4	0.465562	4.5952	5.348376256
19.590	10.241	0.4	0.46494	4.0964	4.761450540
19.829	13.392	0.4	0.464311	5.3568	6.218052912
19.829	11.028	0.4	0.464311	4.4112	5.120421708
20.068	13.195	0.4	0.463681	5.2780	6.118270795
20.546	13.523	0.4	0.462427	5.4092	6.253400321
20.546	14.376	0.4	0.462427	5.7504	6.647850552

Continued on Next Page...

Table 5 – Continued

$E_\gamma$ (MeV)	$\sigma_{\text{abs}}$ (mb)	$g_n$	$g_n(E_\gamma)$	$\sigma_n = g_n\sigma_{\text{abs}}(mb)$	$\sigma_n = g_n(E_\gamma)\sigma_{\text{abs}}$ (mb)
20.785	14.179	0.4	0.461806	5.6716	6.547947274
20.785	14.902	0.4	0.461806	5.9608	6.881833012
21.024	15.821	0.4	0.461192	6.3284	7.296518632
21.024	17.002	0.4	0.461192	6.8008	7.841186384
21.263	16.477	0.4	0.460586	6.5908	7.589075522
21.502	19.037	0.4	0.459988	7.6148	8.756791556
21.741	21.072	0.4	0.4594	8.4288	9.680476800
21.980	24.158	0.4	0.458822	9.6632	11.084221876
21.980	27.965	0.4	0.458822	11.1860	12.830957230
22.457	28.096	0.4	0.4577	11.2384	12.859539200
22.457	26.652	0.4	0.4577	10.6608	12.198620400
23.174	28.096	0.4	0.4561	11.2384	12.814585600
23.174	24.486	0.4	0.4561	9.7944	11.168064600
23.413	23.829	0.4	0.455591	9.5316	10.856277939
23.413	22.188	0.4	0.455591	8.8752	10.108653108
23.891	21.138	0.4	0.454607	8.4552	9.609482766
23.891	21.926	0.4	0.454607	8.7704	9.967713082
24.130	18.446	0.4	0.454133	7.3784	8.376937318
24.130	19.956	0.4	0.454133	7.9824	9.062678148
24.608	18.709	0.4	0.453221	7.4836	8.479311689
24.846	18.381	0.4	0.452785	7.3524	8.322641085
25.085	17.987	0.4	0.452358	7.1948	8.136563346
25.085	17.724	0.4	0.452358	7.0896	8.017593192
25.085	17.396	0.4	0.452358	6.9584	7.869219768
25.324	15.755	0.4	0.451942	6.3020	7.120346210
25.563	15.952	0.4	0.451538	6.3808	7.202934176
25.802	17.527	0.4	0.451144	7.0108	7.907200888
25.802	15.492	0.4	0.451144	6.1968	6.989122848
26.041	15.295	0.4	0.450761	6.1180	6.894389495
26.519	12.998	0.4	0.450026	5.1992	5.849437948
26.519	16.018	0.4	0.450026	6.4072	7.208516468
26.758	14.179	0.4	0.449673	5.6716	6.375913467
26.997	13.720	0.4	0.449331	5.4880	6.164821320
27.235	14.770	0.4	0.448998	5.9080	6.631700460

Continued on Next Page...

Table 5 – Continued

$E_\gamma$ (MeV)	$\sigma_{\text{abs}}$ (mb)	$g_n$	$g_n(E_\gamma)$	$\sigma_n = g_n\sigma_{\text{abs}}(mb)$	$\sigma_n = g_n(E_\gamma)\sigma_{\text{abs}}$ (mb)
27.474	12.867	0.4	0.448674	5.1468	5.773088358
27.713	13.589	0.4	0.448359	5.4356	6.092750451
27.952	12.144	0.4	0.448053	4.8576	5.441155632
28.191	14.179	0.4	0.447755	5.6716	6.348718145
28.191	14.508	0.4	0.447755	5.8032	6.496029540
28.430	16.674	0.4	0.447465	6.6696	7.461031410
28.669	13.786	0.4	0.447184	5.5144	6.164878624
28.908	14.508	0.4	0.446911	5.8032	6.483784788
29.386	14.311	0.4	0.446388	5.7244	6.388258668
29.386	13.457	0.4	0.446388	5.3828	6.007043316
29.863	14.048	0.4	0.445896	5.6192	6.263947008
30.341	13.523	0.4	0.445432	5.4092	6.023576936
30.580	11.619	0.4	0.445209	4.6476	5.172883371

Table 6: Cross section values for the reaction  $^{16}\text{O}(\gamma, n)$ .

$E_\gamma$ (MeV)	$\sigma_{\text{abs}}$ (mb)	$g_n$	$g_n(E_\gamma)$	$\sigma_n = g_n\sigma_{\text{abs}}(mb)$	$\sigma_n = g_n(E_\gamma)\sigma_{\text{abs}}$ (mb)
0.000	0.000	0.4	0	0	0
10.132	0.000	0.4	0	0	0
10.873	0.000	0.4	0	0	0
11.367	0.074	0.4	0	0.0296	0
11.614	1.928	0.4	0	0.7712	0
12.109	2.225	0.4	0	0.8900	0
12.356	0.000	0.4	0	0	0
12.356	1.038	0.4	0	0.4152	0
12.603	0.667	0.4	0	0.2668	0
12.850	1.112	0.4	0	0.4448	0
12.850	1.780	0.4	0	0.7120	0
13.097	0.742	0.4	0	0.2968	0
13.097	3.708	0.4	0	1.4832	0
13.344	5.117	0.4	0	2.0468	0
13.591	1.409	0.4	0	0.5636	0
13.839	1.112	0.4	0	0.4448	0
14.086	-0.074	0.4	0	-0.0296	0
14.580	0.074	0.4	0	0.0296	0
14.827	1.112	0.4	0	0.4448	0
15.074	2.521	0.4	0	1.0084	0
15.074	1.557	0.4	0	0.6228	0
15.321	0.000	0.4	0	0	0
16.063	1.112	0.4	0.0024527	0.4448	0.002727369
16.310	1.409	0.4	0.0056316	0.5636	0.007934924
16.557	2.299	0.4	0.0098627	0.9196	0.022674324
16.557	1.780	0.4	0.0098627	0.7120	0.017555588
16.557	0.297	0.4	0.0098627	0.1188	0.002929219
17.051	1.928	0.4	0.0207337	0.7712	0.039974574
17.051	0.000	0.4	0.0207337	0	0
17.298	5.042	0.4	0.0270387	2.0168	0.136329125
17.545	4.004	0.4	0.0337372	1.6016	0.135083749
17.792	6.451	0.4	0.0407180	2.5804	0.262671818
17.792	2.002	0.4	0.0407180	0.8008	0.081517436

Continued on Next Page...

Table 6 – Continued

$E_\gamma$ (MeV)	$\sigma_{\text{abs}}$ (mb)	$g_n$	$g_n(E_\gamma)$	$\sigma_n = g_n \sigma_{\text{abs}}(mb)$	$\sigma_n = g_n(E_\gamma) \sigma_{\text{abs}}$ (mb)
18.040	0.000	0.4	0.0479191	0	0
18.040	2.299	0.4	0.0479191	0.9196	0.110166011
18.534	0.519	0.4	0.0625538	0.2076	0.032465422
18.534	0.000	0.4	0.0625538	0	0
18.781	2.076	0.4	0.0699090	0.8304	0.145131084
19.028	3.114	0.4	0.0772359	1.2456	0.240512593
19.028	2.669	0.4	0.0772359	1.0676	0.206142617
19.275	5.487	0.4	0.0845051	2.1948	0.463679484
19.522	2.447	0.4	0.0916935	0.9788	0.224373995
19.522	3.040	0.4	0.0916935	1.2160	0.278748240
19.769	4.301	0.4	0.0987838	1.7204	0.424869124
20.264	3.189	0.4	0.1126480	1.2756	0.359234472
20.264	5.042	0.4	0.1126480	2.0168	0.567971216
20.511	2.076	0.4	0.1193770	0.8304	0.247826652
20.511	6.451	0.4	0.1193770	2.5804	0.770101027
20.758	2.966	0.4	0.1259730	1.1864	0.373635918
21.005	9.343	0.4	0.1324330	3.7372	1.237321519
21.005	11.568	0.4	0.1324330	4.6272	1.531984944
21.252	11.049	0.4	0.1387570	4.4196	1.533126093
21.499	10.456	0.4	0.1449430	4.1824	1.515524008
21.746	11.271	0.4	0.1509920	4.5084	1.701830832
21.746	11.716	0.4	0.1509920	4.6864	1.769022272
21.993	15.794	0.4	0.1569060	6.3176	2.478173364
22.241	27.585	0.4	0.1627090	11.0340	4.488327765
22.241	24.841	0.4	0.1627090	9.9364	4.041854269
22.488	22.691	0.4	0.1683580	9.0764	3.820211378
22.488	28.178	0.4	0.1683580	11.2712	4.743991724
22.982	25.212	0.4	0.1792720	10.0848	4.519805664
23.229	27.362	0.4	0.1845430	10.9448	5.049465566
23.476	24.767	0.4	0.1896940	9.9068	4.698151298
23.476	20.095	0.4	0.1896940	8.0380	3.811900930
23.723	19.576	0.4	0.1947280	7.8304	3.811995328
23.723	21.133	0.4	0.1947280	8.4532	4.115186824
23.970	19.428	0.4	0.1996480	7.7712	3.878761344

Continued on Next Page. . .

Table 6 – Continued

$E_\gamma$ (MeV)	$\sigma_{\text{abs}}$ (mb)	$g_n$	$g_n(E_\gamma)$	$\sigma_n = g_n \sigma_{\text{abs}}(mb)$	$\sigma_n = g_n(E_\gamma) \sigma_{\text{abs}}$ (mb)
23.970	22.542	0.4	0.1996480	9.0168	4.500465216
24.217	28.623	0.4	0.2044570	11.4492	5.852172711
24.465	21.282	0.4	0.2091750	8.5128	4.451662350
24.465	24.915	0.4	0.2091750	9.9660	5.211595125
24.712	22.320	0.4	0.2137680	8.9280	4.771301760
25.206	22.542	0.4	0.2226470	9.0168	5.018908674
25.206	20.689	0.4	0.2226470	8.2756	4.606343783
25.453	17.426	0.4	0.2269380	6.9704	3.954621588
25.453	19.502	0.4	0.2269380	7.8008	4.425744876
25.700	19.206	0.4	0.2311340	7.6824	4.439159604
25.700	21.653	0.4	0.2311340	8.6612	5.004744502
25.947	18.093	0.4	0.2352370	7.2372	4.256143041
26.194	16.462	0.4	0.2392500	6.5848	3.938533500
26.194	14.905	0.4	0.2392500	5.9620	3.566021250
26.442	13.644	0.4	0.2431910	5.4576	3.318098004
26.689	11.123	0.4	0.2470300	4.4492	2.747714690
26.689	15.127	0.4	0.2470300	6.0508	3.736822810
26.689	13.273	0.4	0.2470300	5.3092	3.278829190
26.936	12.235	0.4	0.2507870	4.8940	3.068378945
27.430	11.049	0.4	0.2580590	4.4196	2.851293891
27.677	9.566	0.4	0.2615800	3.8264	2.502274280
27.677	11.345	0.4	0.2615800	4.5380	2.967625100
27.677	9.343	0.4	0.2615800	3.7372	2.443941940
27.924	8.008	0.4	0.2650260	3.2032	2.122328208
28.171	9.417	0.4	0.2684000	3.7668	2.527522800
28.171	7.712	0.4	0.2684000	3.0848	2.069900800
28.666	9.047	0.4	0.2749500	3.6188	2.487472650
28.666	8.750	0.4	0.2749500	3.5000	2.405812500
28.913	6.451	0.4	0.2781170	2.5804	1.794132767
29.160	7.193	0.4	0.2812190	2.8772	2.022808267
29.407	8.008	0.4	0.2842570	3.2032	2.276330056
29.407	8.453	0.4	0.2842570	3.3812	2.402824421
29.654	8.676	0.4	0.2872330	3.4704	2.492033508
29.901	6.451	0.4	0.2901490	2.5804	1.871751199

Continued on Next Page...

Table 6 – Continued

$E_\gamma$ (MeV)	$\sigma_{\text{abs}}$ (mb)	$g_n$	$g_n(E_\gamma)$	$\sigma_n = g_n \sigma_{\text{abs}}(mb)$	$\sigma_n = g_n(E_\gamma) \sigma_{\text{abs}}$ (mb)
29.901	6.748	0.4	0.2901490	2.6992	1.957925452
30.148	7.489	0.4	0.2930070	2.9956	2.194329423

Table 7: Cross section values for the reaction  $^{28}\text{Si}(\gamma, n)$ .

$E_\gamma$ (MeV)	$\sigma_{\text{abs}}$ (mb)	$g_n$	$g_n(E_\gamma)$	$\sigma_n = g_n\sigma_{\text{abs}}(mb)$	$\sigma_n = g_n(E_\gamma)\sigma_{\text{abs}}$ (mb)
12.097	3.550	0.5040205781	0	1.789273052	0
12.306	5.189	0.5040205781	0	2.61536278	0
12.516	7.511	0.5040205781	0	3.785698562	0
12.726	1.639	0.5040205781	0	0.826089728	0
12.935	4.370	0.5040205781	0	2.202569926	0
13.355	1.912	0.5040205781	0	0.963687345	0
13.565	5.735	0.5040205781	0	2.890558015	0
13.774	3.824	0.5040205781	0	1.927374691	0
13.774	2.595	0.5040205781	0	1.3079334	0
14.194	3.004	0.5040205781	0	1.514077817	0
14.613	5.735	0.5040205781	0	2.890558015	0
14.823	2.458	0.5040205781	0	1.238882581	0
14.823	5.189	0.5040205781	0	2.61536278	0
14.823	4.506	0.5040205781	0	2.271116725	0
15.242	3.824	0.5040205781	0	1.927374691	0
15.661	2.458	0.5040205781	0	1.238882581	0
15.871	2.868	0.5040205781	0	1.445531018	0
15.871	5.326	0.5040205781	0	2.684413599	0
16.081	7.647	0.5040205781	0	3.854245361	0
16.290	6.691	0.5040205781	0	3.372401688	0
16.500	5.326	0.5040205781	0	2.684413599	0
16.919	10.242	0.5040205781	0	5.162178761	0
16.919	7.920	0.5040205781	0	3.991842979	0
17.129	6.282	0.5040205781	0	3.166257272	0
17.339	9.286	0.5040205781	0.00414483	4.680335088	0.038488891
17.339	6.691	0.5040205781	0.00414483	3.372401688	0.027733058
17.548	7.647	0.5040205781	0.0149189	3.854245361	0.114084828
17.968	5.872	0.5040205781	0.0461685	2.959608835	0.271101432
18.177	3.824	0.5040205781	0.0635767	1.927374691	0.243117301
18.387	8.466	0.5040205781	0.0811502	4.267038214	0.687017593
18.387	2.595	0.5040205781	0.0811502	1.3079334	0.210584769
18.597	6.964	0.5040205781	0.0982976	3.509999306	0.684544486
18.806	10.242	0.5040205781	0.114567	5.162178761	1.173395214

Continued on Next Page...

Table 7 – Continued

$E_\gamma$ (MeV)	$\sigma_{\text{abs}}$ (mb)	$g_n$	$g_n(E_\gamma)$	$\sigma_n = g_n\sigma_{\text{abs}}(mb)$	$\sigma_n = g_n(E_\gamma)\sigma_{\text{abs}}$ (mb)
19.016	13.382	0.5040205781	0.129931	6.744803376	1.738736642
19.226	15.294	0.5040205781	0.14424	7.708490721	2.20600656
19.435	21.576	0.5040205781	0.157428	10.87474799	3.396666528
19.435	17.752	0.5040205781	0.157428	8.947373302	2.794661856
19.645	29.086	0.5040205781	0.169659	14.65994253	4.934701674
19.645	35.914	0.5040205781	0.169659	18.10139504	6.093133326
19.855	43.561	0.5040205781	0.180927	21.9556404	7.881361047
20.065	42.059	0.5040205781	0.191304	21.19860149	8.046054936
20.065	32.090	0.5040205781	0.191304	16.17402035	6.13894536
20.274	27.994	0.5040205781	0.20082	14.10955206	5.62175508
20.484	33.592	0.5040205781	0.209637	16.93105926	7.042126104
20.694	48.340	0.5040205781	0.21778	24.36435475	10.5274852
20.903	41.922	0.5040205781	0.225276	21.12955068	9.444020472
20.903	42.605	0.5040205781	0.225276	21.47379673	9.59788398
21.113	38.782	0.5040205781	0.232258	19.54692606	9.007429756
21.323	52.164	0.5040205781	0.238742	26.29172944	12.45373769
21.323	39.601	0.5040205781	0.238742	19.95971891	9.454421942
21.742	54.758	0.5040205781	0.250376	27.59915882	13.71008901
21.742	57.626	0.5040205781	0.250376	29.04468983	14.42816738
21.952	50.935	0.5040205781	0.255636	25.67228815	13.02081966
21.952	58.718	0.5040205781	0.255636	29.5950803	15.01043465
22.161	43.015	0.5040205781	0.260541	21.68044517	11.20717112
22.161	42.195	0.5040205781	0.260541	21.26714829	10.9935275
22.581	52.983	0.5040205781	0.269517	26.70452229	14.27981921
22.581	50.798	0.5040205781	0.269517	25.60323733	13.69092457
22.790	54.212	0.5040205781	0.273598	27.32396358	14.83229478
23.000	58.172	0.5040205781	0.277471	29.31988507	16.14104301
23.419	39.601	0.5040205781	0.284593	19.95971891	11.27016739
23.419	43.424	0.5040205781	0.284593	21.88658958	12.35816643
23.419	34.275	0.5040205781	0.284593	17.27530531	9.754425075
23.629	30.588	0.5040205781	0.287893	15.41698144	8.806071084
23.839	26.082	0.5040205781	0.291031	13.14586472	7.590670542
23.839	29.223	0.5040205781	0.291031	14.72899335	8.504798913
24.468	27.038	0.5040205781	0.29959	13.62770839	8.10031442

Continued on Next Page...

Table 7 – Continued

$E_\gamma$ (MeV)	$\sigma_{\text{abs}}$ (mb)	$g_n$	$g_n(E_\gamma)$	$\sigma_n = g_n \sigma_{\text{abs}}(\text{mb})$	$\sigma_n = g_n(E_\gamma) \sigma_{\text{abs}}$ (mb)
24.468	29.223	0.5040205781	0.29959	14.72899335	8.75491857
24.677	23.214	0.5040205781	0.30219	11.7003337	7.01503866
24.677	31.134	0.5040205781	0.30219	15.69217668	9.40838346
25.097	22.805	0.5040205781	0.307099	11.49418928	7.003392695
25.306	25.672	0.5040205781	0.309399	12.93921628	7.942891128
25.516	24.307	0.5040205781	0.311623	12.25122819	7.574620261
25.726	23.624	0.5040205781	0.313767	11.90698214	7.412431608
26.145	21.712	0.5040205781	0.317822	10.94329479	6.900551264
26.355	22.805	0.5040205781	0.319754	11.49418928	7.29198997
26.565	20.347	0.5040205781	0.321623	10.2553067	6.544063181
26.774	24.580	0.5040205781	0.323425	12.38882581	7.9497865
26.984	20.347	0.5040205781	0.325181	10.2553067	6.616457807
27.194	24.034	0.5040205781	0.326884	12.11363057	7.856330056
27.403	15.840	0.5040205781	0.32853	7.983685957	5.2039152
28.032	24.034	0.5040205781	0.33321	12.11363057	8.00836914
28.032	18.571	0.5040205781	0.33321	9.360166156	6.18804291
28.242	20.756	0.5040205781	0.334689	10.46145112	6.946804884
28.661	22.805	0.5040205781	0.337528	11.49418928	7.69732604
28.871	20.074	0.5040205781	0.338898	10.11770908	6.803038452
29.290	18.435	0.5040205781	0.341532	9.291619357	6.29614242
29.710	17.342	0.5040205781	0.344051	8.740724865	5.966532442
29.710	16.387	0.5040205781	0.344051	8.259385213	5.637963737
30.339	16.933	0.5040205781	0.347619	8.534580449	5.886232527
30.548	13.655	0.5040205781	0.348754	6.882400994	4.76223587
30.968	16.523	0.5040205781	0.350965	8.327932012	5.798994695
31.177	13.929	0.5040205781	0.352032	7.020502632	4.903453728

Table 8: Cross section values for the reaction  $^{28}\text{Si}(\gamma,p)$ .

$E_\gamma$ (MeV)	$\sigma_{\text{abs}}$ (mb)	$g_p$	$g_p(E_\gamma)$	$\sigma_p = g_p\sigma_{\text{abs}}(\text{mb})$	$\sigma_p = g_p(E_\gamma)\sigma_{\text{abs}}$ (mb)
12.097	3.550	0.4959794219	0	1.760726948	0
12.306	5.189	0.4959794219	0	2.573637220	0
12.516	7.511	0.4959794219	0	3.725301438	0
12.726	1.639	0.4959794219	0	0.812910272	0
12.935	4.370	0.4959794219	0	2.167430074	0
13.355	1.912	0.4959794219	0	0.948312655	0
13.565	5.735	0.4959794219	0	2.844441985	0
13.774	3.824	0.4959794219	0	1.896625309	0
13.774	2.595	0.4959794219	0	1.287066600	0
14.194	3.004	0.4959794219	0	1.489922183	0
14.613	5.735	0.4959794219	0	2.844441985	0
14.823	2.458	0.4959794219	0	1.219117419	0
14.823	5.189	0.4959794219	0	2.573637220	0
14.823	4.506	0.4959794219	0	2.234883275	0
15.242	3.824	0.4959794219	0	1.896625309	0
15.661	2.458	0.4959794219	1	1.219117419	2.458
15.871	2.868	0.4959794219	1	1.422468982	2.868
15.871	5.326	0.4959794219	1	2.641586401	5.326
16.081	7.647	0.4959794219	1	3.792754639	7.647
16.290	6.691	0.4959794219	1	3.318598312	6.691
16.500	5.326	0.4959794219	1	2.641586401	5.326
16.919	10.242	0.4959794219	1	5.079821239	10.242
16.919	7.920	0.4959794219	1	3.928157021	7.92
17.129	6.282	0.4959794219	1	3.115742728	6.282
17.339	9.286	0.4959794219	0.995855	4.605664912	9.24750953
17.339	6.691	0.4959794219	0.995855	3.318598312	6.663265805
17.548	7.647	0.4959794219	0.985081	3.792754639	7.532914407
17.968	5.872	0.4959794219	0.953832	2.912391165	5.600901504
18.177	3.824	0.4959794219	0.936423	1.896625309	3.580881552
18.387	8.466	0.4959794219	0.918850	4.198961786	7.7789841
18.387	2.595	0.4959794219	0.918850	1.287066600	2.38441575
18.597	6.964	0.4959794219	0.901298	3.454000694	6.276639272
18.806	10.242	0.4959794219	0.883485	5.079821239	9.04865337

Continued on Next Page...

Table 8 – Continued

$E_\gamma$ (MeV)	$\sigma_{\text{abs}}$ (mb)	$g_p$	$g_p(E_\gamma)$	$\sigma_p = g_p\sigma_{\text{abs}}$ (mb)	$\sigma_p = g_p(E_\gamma)\sigma_{\text{abs}}$ (mb)
19.016	13.382	0.4959794219	0.865522	6.637196624	11.5824154
19.226	15.294	0.4959794219	0.847785	7.585509279	12.96602379
19.435	21.576	0.4959794219	0.830580	10.701252007	17.92059408
19.435	17.752	0.4959794219	0.830580	8.804626698	14.74445616
19.645	29.086	0.4959794219	0.813897	14.426057465	23.67300814
19.645	35.914	0.4959794219	0.813897	17.812604958	29.23029686
19.855	43.561	0.4959794219	0.797916	21.605359597	34.75801888
20.065	42.059	0.4959794219	0.782689	20.860398506	32.91911665
20.065	32.090	0.4959794219	0.782689	15.915979649	25.11649001
20.274	27.994	0.4959794219	0.768302	13.884447937	21.50784619
20.484	33.592	0.4959794219	0.754615	16.660940740	25.34902708
20.694	48.340	0.4959794219	0.741680	23.975645255	35.8528112
20.903	41.922	0.4959794219	0.729525	20.792449325	30.58314705
20.903	42.605	0.4959794219	0.729525	21.131203270	31.08141263
21.113	38.782	0.4959794219	0.718001	19.235073940	27.84551478
21.323	52.164	0.4959794219	0.707130	25.872270564	36.88672932
21.323	39.601	0.4959794219	0.707130	19.641281087	28.00305513
21.742	54.758	0.4959794219	0.687238	27.158841184	37.6317784
21.742	57.626	0.4959794219	0.687238	28.581310166	39.60277699
21.952	50.935	0.4959794219	0.678095	25.262711854	34.53876883
21.952	58.718	0.4959794219	0.678095	29.122919695	39.81638221
22.161	43.015	0.4959794219	0.669495	21.334554833	28.79832743
22.161	42.195	0.4959794219	0.669495	20.927851707	28.24934153
22.581	52.983	0.4959794219	0.653589	26.278477711	34.62910599
22.581	50.798	0.4959794219	0.653589	25.194762674	33.20101402
22.790	54.212	0.4959794219	0.646297	26.888036420	35.03705296
23.000	58.172	0.4959794219	0.639349	28.852114931	37.19221003
23.419	39.601	0.4959794219	0.626523	19.641281087	24.81093732
23.419	43.424	0.4959794219	0.626523	21.537410417	27.20613475
23.419	34.275	0.4959794219	0.626523	16.999694686	21.47407583
23.629	30.588	0.4959794219	0.620567	15.171018557	18.9819034
23.839	26.082	0.4959794219	0.614899	12.936135282	16.03779572
23.839	29.223	0.4959794219	0.614899	14.494006646	17.96919348
24.468	27.038	0.4959794219	0.599463	13.410291609	16.20828059

Continued on Next Page...

Table 8 – Continued

$E_\gamma$ (MeV)	$\sigma_{\text{abs}}$ (mb)	$g_p$	$g_p(E_\gamma)$	$\sigma_p = g_p\sigma_{\text{abs}}$ (mb)	$\sigma_p = g_p(E_\gamma)\sigma_{\text{abs}}$ (mb)
24.468	29.223	0.4959794219	0.599463	14.494006646	17.51810725
24.677	23.214	0.4959794219	0.594792	11.513666300	13.80750149
24.677	31.134	0.4959794219	0.594792	15.441823321	18.51825413
25.097	22.805	0.4959794219	0.586010	11.310810716	13.36395805
25.306	25.672	0.4959794219	0.581918	12.732783719	14.9389989
25.516	24.307	0.4959794219	0.577976	12.055771808	14.04886263
25.726	23.624	0.4959794219	0.574195	11.717017863	13.56478268
26.145	21.712	0.4959794219	0.567097	10.768705208	12.31281006
26.355	22.805	0.4959794219	0.563745	11.310810716	12.85620473
26.565	20.347	0.4959794219	0.560520	10.091693297	11.40490044
26.774	24.580	0.4959794219	0.557430	12.191174190	13.7016294
26.984	20.347	0.4959794219	0.554438	10.091693297	11.28114999
27.194	24.034	0.4959794219	0.551552	11.920369426	13.25600077
27.403	15.840	0.4959794219	0.548779	7.856314043	8.69265936
28.032	24.034	0.4959794219	0.540985	11.920369426	13.00203349
28.032	18.571	0.4959794219	0.540985	9.210833844	10.04663244
28.242	20.756	0.4959794219	0.538550	10.294548881	11.1781438
28.661	22.805	0.4959794219	0.533918	11.310810716	12.17599999
28.871	20.074	0.4959794219	0.531702	9.956290915	10.67338595
29.290	18.435	0.4959794219	0.527476	9.143380643	9.72402006
29.710	17.342	0.4959794219	0.523480	8.601275135	9.07819016
29.710	16.387	0.4959794219	0.523480	8.127614787	8.57826676
30.339	16.933	0.4959794219	0.517900	8.398419551	8.7696007
30.548	13.655	0.4959794219	0.516144	6.772599006	7.04794632
30.968	16.523	0.4959794219	0.512751	8.195067988	8.472184773
31.177	13.929	0.4959794219	0.511127	6.908497368	7.119487983

Table 9: Cross section values for the reaction  $^{88}\text{Sr}(\gamma, n)$ .

$E_\gamma$ (MeV)	$\sigma_{\text{abs}}$ (mb)	$g_n$	$g_n(E_\gamma)$	$\sigma_n = g_n\sigma_{\text{abs}}(\text{mb})$	$\sigma_n = g_n(E_\gamma)\sigma_{\text{abs}}$ (mb)
10.773	6.687	0.8509261878	0	5.690143418	0
11.217	5.144	0.8509261878	1	4.377164310	5.1440000
11.439	8.230	0.8509261878	1	7.003122526	8.2300000
11.661	21.091	0.8509261878	1	17.946884227	21.0910000
11.661	23.663	0.8509261878	1	20.135466382	23.6630000
11.883	29.321	0.8509261878	1	24.950006752	29.3210000
12.105	33.436	0.8509261878	1	28.451568015	33.4360000
12.105	33.951	0.8509261878	1	28.889795002	33.9510000
12.327	35.494	0.8509261878	1	30.202774110	35.4940000
12.327	37.551	0.8509261878	1	31.953129278	37.5510000
12.771	39.609	0.8509261878	1	33.704335373	39.6090000
12.771	38.580	0.8509261878	1	32.828732325	38.5800000
12.993	43.724	0.8509261878	1	37.205896635	43.7240000
13.215	42.181	0.8509261878	1	35.892917528	42.1810000
13.215	47.325	0.8509261878	1	40.270081838	47.3250000
13.660	52.469	0.8509261878	1	44.647246148	52.4690000
13.660	54.527	0.8509261878	1	46.398452242	54.5270000
13.882	62.243	0.8509261878	1	52.964198707	62.2430000
13.882	63.786	0.8509261878	1	54.277177815	63.7860000
14.104	72.531	0.8509261878	1	61.718527327	72.5310000
14.326	75.617	0.8509261878	1	64.344485543	75.6170000
14.326	85.391	0.8509261878	1	72.661438102	85.3910000
14.548	98.251	0.8509261878	1	83.604348878	98.2510000
14.548	91.564	0.8509261878	1	77.914205460	91.5640000
14.770	105.453	0.8509261878	1	89.732719282	105.4530000
14.992	109.054	0.8509261878	1	92.796904484	109.0540000
14.992	117.284	0.8509261878	1	99.800027010	117.2840000
15.214	130.144	0.8509261878	1	110.742937785	130.1440000
15.436	135.288	0.8509261878	1	115.120102095	135.2880000
15.436	143.519	0.8509261878	1	122.124075547	143.5190000
15.658	153.292	0.8509261878	1	130.440177180	153.2920000
15.658	165.123	0.8509261878	1	140.507484908	165.1230000
15.880	166.667	0.8509261878	1	141.821314942	166.6670000

Continued on Next Page...

Table 9 – Continued

$E_\gamma$ (MeV)	$\sigma_{\text{abs}}$ (mb)	$g_n$	$g_n(E_\gamma)$	$\sigma_n = g_n\sigma_{\text{abs}}(\text{mb})$	$\sigma_n = g_n(E_\gamma)\sigma_{\text{abs}}$ (mb)
15.880	186.214	0.8509261878	1	158.454369135	186.2140000
16.102	192.901	0.8509261878	1	164.144512553	192.9010000
16.102	201.132	0.8509261878	1	171.148486005	201.1320000
16.324	195.473	0.8509261878	1	166.333094708	195.4730000
16.768	203.189	0.8509261878	1	172.898841173	203.1890000
16.768	209.877	0.8509261878	1	178.589835517	209.8770000
16.990	207.305	0.8509261878	1	176.401253362	207.3050000
17.212	200.617	0.8509261878	1	170.710259018	200.6170000
17.212	199.074	0.8509261878	1	169.397279910	199.0740000
17.434	192.387	0.8509261878	1	163.707136492	192.3870000
17.656	189.815	0.8509261878	1	161.518554337	189.8150000
17.656	175.412	0.8509261878	1	149.262664454	175.4120000
17.878	179.012	0.8509261878	1	152.325998730	179.0120000
18.100	152.263	0.8509261878	1	129.564574133	152.2630000
18.100	170.267	0.8509261878	1	144.884649218	170.2670000
18.100	151.235	0.8509261878	1	128.689822012	151.2350000
18.544	148.148	0.8509261878	1	126.063012870	148.1480000
18.766	143.004	0.8509261878	1	121.685848560	143.0040000
18.766	130.144	0.8509261878	1	110.742937785	130.1440000
18.766	125.514	0.8509261878	1	106.803149536	125.5140000
19.211	119.342	0.8509261878	0.999999	101.551233104	119.3418807
19.211	122.942	0.8509261878	0.999999	104.614567381	122.9418771
19.433	112.140	0.8509261878	0.999998	95.422862700	112.1397757
19.433	108.539	0.8509261878	0.999998	92.358677498	108.5387829
19.655	106.996	0.8509261878	0.999996	91.045698390	106.9955720
19.655	102.366	0.8509261878	0.999996	87.105910140	102.3655905
19.877	95.679	0.8509261878	0.999995	81.415766723	95.6785216
19.877	99.280	0.8509261878	0.999995	84.479951925	99.2795036
19.877	94.136	0.8509261878	0.999995	80.102787615	94.1355293
20.321	90.021	0.8509261878	0.999991	76.601226352	90.0201898
20.321	92.078	0.8509261878	0.999991	78.351581520	92.0771713
20.765	89.506	0.8509261878	0.999984	76.162999365	89.5045679
20.987	91.564	0.8509261878	0.999980	77.914205460	91.5621687
20.987	87.449	0.8509261878	0.999980	74.412644197	87.4472510

Continued on Next Page...

Table 9 – Continued

$E_\gamma$ (MeV)	$\sigma_{\text{abs}}$ (mb)	$g_n$	$g_n(E_\gamma)$	$\sigma_n = g_n\sigma_{\text{abs}}(mb)$	$\sigma_n = g_n(E_\gamma)\sigma_{\text{abs}}$ (mb)
21.209	82.819	0.8509261878	0.999975	70.472855947	82.8169295
21.431	80.247	0.8509261878	0.999970	68.284273792	80.2445926
21.431	75.103	0.8509261878	0.999970	63.907109482	75.1007469
21.875	76.646	0.8509261878	0.999957	65.220088590	76.6427042
21.875	69.959	0.8509261878	0.999957	59.529945172	69.9559918
22.097	73.560	0.8509261878	0.999949	62.594130375	73.5562484
22.541	75.103	0.8509261878	0.999930	63.907109482	75.0977428
22.763	71.502	0.8509261878	0.999920	60.842924280	71.4962798
22.985	68.416	0.8509261878	0.999909	58.216966065	68.4097741
22.985	65.329	0.8509261878	0.999909	55.590156923	65.3230551
23.429	67.387	0.8509261878	0.999883	57.341363017	67.3791157
23.651	64.300	0.8509261878	0.999868	54.714553876	64.2915124
23.651	62.243	0.8509261878	0.999868	52.964198707	62.2347839
23.651	56.070	0.8509261878	0.999868	47.711431350	56.0625988
24.095	54.527	0.8509261878	0.999836	46.398452242	54.5180576
24.095	56.584	0.8509261878	0.999836	48.148807410	56.5747202
24.317	47.840	0.8509261878	0.999818	40.708308824	47.8312931
24.317	52.469	0.8509261878	0.999818	44.647246148	52.4594506
24.539	46.296	0.8509261878	0.999800	39.394478790	46.2867408
24.762	44.239	0.8509261878	0.999780	37.644123622	44.2292674
25.428	48.354	0.8509261878	0.999713	41.145684885	48.3401224
25.428	50.412	0.8509261878	0.999713	42.896890979	50.3975318
25.650	45.782	0.8509261878	0.999688	38.957102730	45.7677160
26.094	49.897	0.8509261878	0.999636	42.458663993	49.8788375
26.538	44.239	0.8509261878	0.999579	37.644123622	44.2203754
26.760	40.123	0.8509261878	0.999548	34.141711433	40.1048644
26.982	38.066	0.8509261878	0.999517	32.391356265	38.0476141
26.982	45.267	0.8509261878	0.999517	38.518875743	45.2451360

Table 10: Cross section values for the reaction  $^{91}\text{Zr}(\gamma, n)$ .

$E_\gamma$ (MeV)	$\sigma_{\text{abs}}$ (mb)	$g_n$	$g_n(E_\gamma)$	$\sigma_n = g_n \sigma_{\text{abs}}(mb)$	$\sigma_n = g_n(E_\gamma) \sigma_{\text{abs}}$ (mb)
10.767	14.575	0.865136	1	12.60935661	14.57500000
10.937	15.789	0.865136	1	13.65963167	15.78900000
11.107	14.575	0.865136	1	12.60935661	14.57500000
11.276	12.955	0.865136	1	11.20783636	12.95500000
11.446	14.575	0.865136	1	12.60935661	14.57500000
11.559	19.028	0.865136	1	16.46180704	19.02800000
11.729	21.053	0.865136	1	18.21370736	21.05300000
11.898	21.457	0.865136	1	18.56322229	21.45700000
12.011	28.340	0.865136	1	24.51795310	28.34000000
12.351	29.960	0.865136	1	25.91947336	29.96000000
12.464	27.935	0.865136	1	24.16757304	27.93500000
12.633	26.316	0.865136	1	22.76691792	26.31600000
12.803	31.174	0.865136	1	26.96974841	31.17400000
12.973	39.676	0.865136	1	34.32513434	39.67600000
13.086	37.247	0.865136	1	32.22371909	37.24700000
13.312	36.437	0.865136	1	31.52295897	36.43700000
13.425	44.939	0.865136	1	38.87834490	44.93900000
13.595	42.915	0.865136	1	37.12730971	42.91500000
13.764	50.202	0.865136	1	43.43155545	50.20200000
13.877	55.061	0.865136	1	47.63525108	55.06100000
14.047	63.968	0.865136	1	55.34101708	63.96800000
14.216	65.992	0.865136	1	57.09205226	65.99200000
14.386	76.923	0.865136	1	66.54885344	76.92300000
14.499	89.069	0.865136	1	77.05679480	89.06900000
14.669	99.190	0.865136	1	85.81283585	99.19000000
14.838	104.453	0.865136	1	90.36604641	104.45300000
14.952	117.814	0.865136	1	101.92512797	117.81400000
15.121	128.340	0.865136	1	111.03154908	128.34000000
15.234	135.223	0.865136	1	116.98627989	135.22300000
15.460	138.462	0.865136	1	119.78845527	138.46200000
15.574	146.154	0.865136	1	126.44308107	146.15400000
15.743	158.300	0.865136	1	136.95102244	158.30000000
15.856	167.611	0.865136	1	145.00630336	167.61100000

Continued on Next Page. . .

Table 10 – Continued

$E_\gamma$ (MeV)	$\sigma_{\text{abs}}$ (mb)	$g_n$	$g_n(E_\gamma)$	$\sigma_n = g_n \sigma_{\text{abs}}(\text{mb})$	$\sigma_n = g_n(E_\gamma) \sigma_{\text{abs}}$ (mb)
16.082	182.186	0.865136	1	157.61565997	182.18600000
16.252	178.543	0.865136	1	154.46396967	178.54300000
16.365	181.377	0.865136	1	156.91576498	181.37700000
16.535	177.733	0.865136	1	153.76320954	177.73300000
16.704	183.401	0.865136	1	158.66680016	183.40100000
16.817	188.664	0.865136	1	163.22001072	188.66400000
16.987	170.040	0.865136	1	147.10771860	170.04000000
17.157	176.518	0.865136	1	152.71206935	176.51800000
17.270	167.611	0.865136	1	145.00630336	167.61100000
17.439	168.016	0.865136	1	145.35668342	168.01600000
17.609	142.510	0.865136	1	123.29052563	142.51000000
17.779	140.891	0.865136	1	121.88987051	140.89100000
17.892	125.911	0.865136	1	108.93013383	125.91100000
18.061	123.482	0.865136	1	106.82871859	123.48200000
18.231	126.721	0.865136	1	109.63089396	126.72100000
18.401	108.502	0.865136	0.999999	93.86898191	108.50189150
18.514	102.429	0.865136	0.999999	88.61501123	102.42889757
18.683	105.668	0.865136	0.999999	91.41718660	105.66789433
18.853	92.308	0.865136	0.999999	79.85897018	92.30790769
19.023	88.259	0.865136	0.999999	76.35603468	88.25891174
19.136	86.235	0.865136	0.999998	74.60499949	86.23482753
19.305	83.401	0.865136	0.999998	72.15320418	83.40083320
19.475	75.708	0.865136	0.999998	65.49771324	75.70784858
19.645	78.947	0.865136	0.999997	68.29988862	78.94676316
19.814	70.850	0.865136	0.999997	61.29488275	70.84978745
19.927	62.348	0.865136	0.999996	53.93949682	62.34775061
20.097	63.158	0.865136	0.999995	54.64025695	63.15768421
20.210	62.348	0.865136	0.999995	53.93949682	62.34768826
20.380	63.968	0.865136	0.999994	55.34101708	63.96761619
20.493	61.538	0.865136	0.999994	53.23873669	61.53763077
20.662	59.109	0.865136	0.999993	51.13732145	59.10858624
20.889	60.324	0.865136	0.999991	52.18846164	60.32345708
21.002	59.109	0.865136	0.999991	51.13732145	59.10846802
21.171	53.036	0.865136	0.999989	45.88335076	53.03541660

Continued on Next Page...

Table 10 – Continued

$E_\gamma$ (MeV)	$\sigma_{\text{abs}}$ (mb)	$g_n$	$g_n(E_\gamma)$	$\sigma_n = g_n\sigma_{\text{abs}}(\text{mb})$	$\sigma_n = g_n(E_\gamma)\sigma_{\text{abs}}$ (mb)
21.284	43.320	0.865136	0.999988	37.47768978	43.31948016
21.454	43.725	0.865136	0.999987	37.82806984	43.72443158
21.624	34.818	0.865136	0.999985	30.12230385	34.81747773
21.793	32.794	0.865136	0.999984	28.37126867	32.79347530
21.963	34.413	0.865136	0.999982	29.77192378	34.41238057
22.076	42.105	0.865136	0.999981	36.42654959	42.10420001
22.246	34.818	0.865136	0.999979	30.12230385	34.81726882
22.415	23.077	0.865136	0.999977	19.96474254	23.07646923
22.585	24.292	0.865136	0.999974	21.01588274	24.29136841
22.698	31.579	0.865136	0.999973	27.32012847	31.57814737
22.868	25.911	0.865136	0.999970	22.41653785	25.91022267
23.037	28.745	0.865136	0.999967	24.86833316	28.74405142
23.150	25.506	0.865136	0.999965	22.06615779	25.50510729
23.376	25.506	0.865136	0.999961	22.06615779	25.50500527
23.489	25.911	0.865136	0.999959	22.41653785	25.90993765
23.716	19.433	0.865136	0.999955	16.81218711	19.43212552
24.055	28.340	0.865136	0.999947	24.51795310	28.33849798
24.338	17.409	0.865136	0.999941	15.06115192	17.40797287
24.677	25.101	0.865136	0.999932	21.71577773	25.09929313
24.960	21.457	0.865136	0.999924	18.56322229	21.45536927
25.299	19.838	0.865136	0.999914	17.16256717	19.83629393
25.582	16.194	0.865136	0.999905	14.01001173	16.19246157
25.582	22.672	0.865136	0.999905	19.61436248	22.66984616
25.921	14.170	0.865136	0.999893	12.25897655	14.16848381
26.204	10.526	0.865136	0.999882	9.10642111	10.52475793
26.543	11.741	0.865136	0.999869	10.15756130	11.73946193
26.826	9.312	0.865136	0.999856	8.05614606	9.31065907
27.447	7.287	0.865136	0.999827	6.30424574	7.28573935
27.730	2.834	0.865136	0.999813	2.45179531	2.83347004
28.126	6.073	0.865136	0.999792	5.25397068	6.07173682
28.748	8.097	0.865136	0.999755	7.00500587	8.09501624
29.370	14.170	0.865136	0.999715	12.25897655	14.16596155
29.992	4.049	0.865136	0.999671	3.50293550	4.04766788

Table 11: Cross section values for the reaction  $^{208}\text{Pb}(\gamma, n)$ .

$E_\gamma$ (MeV)	$\sigma_{\text{abs}}$ (mb)	$g_n$	$g_n(E_\gamma)$	$\sigma_n = g_n\sigma_{\text{abs}}(mb)$	$\sigma_n = g_n(E_\gamma)\sigma_{\text{abs}}$ (mb)
8.305	28.632	0.983545	1	28.1608721	28.6320000
8.557	57.263	0.983545	1	56.3207607	57.2630000
9.060	92.632	0.983545	1	91.1077782	92.6320000
9.564	97.684	0.983545	1	96.0766496	97.6840000
9.815	89.263	0.983545	1	87.7942137	89.2630000
9.815	133.053	0.983545	1	130.8636671	133.0530000
10.319	134.737	0.983545	1	132.5199575	134.7370000
10.570	154.947	0.983545	1	152.3974102	154.9470000
10.570	160.000	0.983545	1	157.3672652	160.0000000
10.822	165.053	0.983545	1	162.3371201	165.0530000
10.822	192.000	0.983545	1	188.8407182	192.0000000
11.074	240.842	0.983545	1	236.8790430	240.8420000
11.326	269.474	0.983545	1	265.0399151	269.4740000
11.577	284.632	0.983545	1	279.9484963	284.6320000
11.577	291.368	0.983545	1	286.5736582	291.3680000
11.829	316.632	0.983545	1	311.4219494	316.6320000
11.829	385.684	0.983545	1	379.3377268	385.6840000
12.081	333.474	0.983545	1	327.9868211	333.4740000
12.081	387.368	0.983545	1	380.9940173	387.3680000
12.332	434.526	0.983545	1	427.3760516	434.5260000
12.584	429.474	0.983545	1	422.4071802	429.4740000
12.584	483.368	0.983545	1	475.4143764	483.3680000
12.836	515.368	0.983545	1	506.8878294	515.3680000
13.087	538.947	0.983545	1	530.0788466	538.9470000
13.339	560.842	0.983545	1	551.6135733	560.8420000
13.339	589.474	0.983545	1	579.7744454	589.4740000
13.339	604.632	0.983545	1	594.6830266	604.6320000
13.591	633.263	0.983545	1	622.8429152	633.2630000
13.842	594.526	0.983545	1	584.7433168	594.5260000
13.842	609.684	0.983545	1	599.6518980	609.6840000
14.094	582.737	0.983545	1	573.1483000	582.7370000
14.094	542.316	0.983545	1	533.3924111	542.3160000
14.346	518.737	0.983545	1	510.2013939	518.7370000

Continued on Next Page. . .

Table 11 – Continued

$E_\gamma$ (MeV)	$\sigma_{\text{abs}}$ (mb)	$g_n$	$g_n(E_\gamma)$	$\sigma_n = g_n \sigma_{\text{abs}}(mb)$	$\sigma_n = g_n(E_\gamma) \sigma_{\text{abs}}$ (mb)
14.597	490.105	0.983545	1	482.0405218	490.1050000
14.597	434.526	0.983545	1	427.3760516	434.5260000
14.849	414.316	0.983545	1	407.4985989	414.3160000
14.849	389.053	0.983545	1	382.6512913	389.0530000
15.101	333.474	0.983545	1	327.9868211	333.4740000
15.352	323.368	0.983545	1	318.0471112	323.3680000
15.352	318.316	0.983545	1	313.0782398	318.3160000
15.604	279.579	0.983545	1	274.9786414	279.5790000
15.856	264.421	0.983545	1	260.0700601	264.4210000
15.856	249.263	0.983545	1	245.1614788	249.2630000
16.107	203.789	0.983545	1	200.4357350	203.7890000
16.107	181.895	0.983545	1	178.9019918	181.8950000
16.359	207.158	0.983545	0.999999	203.7492995	207.1577928
16.611	185.263	0.983545	0.999999	182.2145728	185.2628147
16.611	151.579	0.983545	0.999999	149.0848293	151.5788484
16.862	141.474	0.983545	0.999999	139.1461029	141.4738585
17.366	148.211	0.983545	0.999998	145.7722483	148.2107036
17.366	131.368	0.983545	0.999998	129.2063931	131.3677373
17.366	80.842	0.983545	0.999998	79.5117778	80.8418383
17.617	122.947	0.983545	0.999997	120.9239572	122.9466312
18.121	62.316	0.983545	0.999996	61.2906156	62.3157507
18.372	111.158	0.983545	0.999995	109.3289404	111.1574442
18.624	47.158	0.983545	0.999993	46.3820343	47.1576699
18.876	28.632	0.983545	0.999992	28.1608721	28.6317709
19.128	84.211	0.983545	0.999991	82.8253423	84.2102421
19.883	69.053	0.983545	0.999986	67.9167610	69.0520333
20.134	15.158	0.983545	0.999984	14.9085813	15.1577575
20.638	90.947	0.983545	0.999980	89.4505041	90.9451811
20.889	35.368	0.983545	0.999977	34.7860340	35.3671865
21.141	55.579	0.983545	0.999975	54.6644702	55.5776105
21.393	67.368	0.983545	0.999972	66.2594870	67.3661137
21.896	67.368	0.983545	0.999966	66.2594870	67.3657095
22.148	32.000	0.983545	0.999963	31.4734530	31.9988160
22.651	57.263	0.983545	0.999955	56.3207607	57.2604232

Continued on Next Page...

Table 11 – Continued

$E_\gamma$ (MeV)	$\sigma_{\text{abs}}$ (mb)	$g_n$	$g_n(E_\gamma)$	$\sigma_n = g_n \sigma_{\text{abs}}(\text{mb})$	$\sigma_n = g_n(E_\gamma) \sigma_{\text{abs}}$ (mb)
22.651	64.000	0.983545	0.999955	62.9469061	63.9971200
22.903	6.737	0.983545	0.999952	6.6261454	6.7366766
23.406	111.158	0.983545	0.999944	109.3289404	111.1517752
23.658	72.421	0.983545	0.999939	71.2293419	72.4165823
23.909	37.053	0.983545	0.999935	36.4433080	37.0505916
24.161	126.316	0.983545	0.999930	124.2375217	126.3071579
24.664	65.684	0.983545	0.999920	64.6031965	65.6787453
24.916	134.737	0.983545	0.999914	132.5199575	134.7254126
25.168	5.053	0.983545	0.999909	4.9698549	5.0525402
25.419	65.684	0.983545	0.999909	64.6031965	65.6780228
25.671	101.053	0.983545	0.999897	99.3902140	101.0425915
26.175	72.421	0.983545	0.999885	71.2293419	72.4126716
26.426	121.263	0.983545	0.999878	119.2676667	121.2482059

## References

- [1] L.W. Townsend, et al., *Radiat. Prot. Dosimetry* 116 (2005) 135.
- [2] T. Sato, K. Niita, H. Iwase, H. Nakashima, Y. Yamaguchi, L. Sihver, *Radiat. Meas.* 41 (2006) 1142.
- [3] S.K. Suresh, S.R. Blattnig, J.W. Norbury, R.C. Singleterry, *Benchmark Analysis of Pion Contribution From Galactic Cosmic Rays*, NASA Technical Paper 2008 - 21556 (2008).
- [4] G. Battistoni, et al., *Braz. J. Phys.* 34 (2004) 897.
- [5] S. Agostinelli, et al., *Nucl. Instrum. Methods Phys. Res., Sect. A* 506 (2003) 250.
- [6] J.W. Wilson, R.K. Tripathi, F.F. Badavi, F.A. Cucinotta, *Standardized Radiation Shield Design Method: 2005 HZETRN*, Proceedings of the 36th Conference on Environmental Systems (ICES), Norfolk, VA, 2006.
- [7] J.W. Wilson, R. Tripathi, G. Qualls, F. Cucinotta, R. Prael, J.W. Norbury, J. Heinbockel, J. Tweed, *Advances in Space Research*, 34 (2004) 1319.
- [8] J.W. Wilson, *Health Phys.* 79 (2000) 470.
- [9] S. Yoshida, H. Dai, *J. Nucl. Part. Phys.* 24 (1998) 905.
- [10] J.W. Norbury and K. M. Maung, *Acta. Astronautica* 60 (2007) 770.
- [11] G.D. Westfall, et al., *Phys. Rev. C* 19 (1979) 1309.
- [12] J.W. Norbury, L.W. Townsend, *Astrophys. J.* 86 (1993) 307.
- [13] J.W. Wilson, et al., *NUCFRG2: An Evaluation of the Semiempirical Nuclear Fragmentation Database*, NASA Technical Paper 3533 (1995).
- [14] J.W. Norbury, C.M. Mueller, *Astrophys. J. Suppl.* 90 (1994) 115.
- [15] J.W. Norbury, L.W. Townsend, *Astrophys. J. Suppl.* 86 (1993) 307.
- [16] J.W. Norbury, F. Cucinotta, L. Townsend, F. Badavi, *Nucl. Instrum. Methods Phys. Res. B* 31 (1988) 535.
- [17] G. Baur, K. Hencken, D. Trautmann, S. Typel, H.H. Wolter, *The Past And Future Of Coulomb Dissociation in Hadron - And Astrophysics*, lecture given at the NATO Advanced Study Institute, Romania 2000.

- [18] G. Baur, K. Hencken, D. Trautmann, S. Typel, H.H. Wolter, *Prog. Part. Nucl. Phys.* 46 (2001) 99.
- [19] R. Chatterjee, R. Shyam, *Phys. Rev. C* 66 (2002) 061601.
- [20] J. Barrette, et al., *Phys. Rev. C* 45 (1992) 2427 .
- [21] J. Barrette, et al., *Phys. Rev. C* 51 (1995) 865.
- [22] P.E. Hodgson, *Rep. Prog. Phys.* 50 (1987) 1171.
- [23] C.A. Bertulani, *Nuclear Physics in a Nutshell*, Princeton University Press, New Jersey, 2007.
- [24] J. Blatt, V. Weisskopf, *Theoretical Nuclear Physics*, Wiley, New York, 1952.
- [25] C.A. Bertulani, P. Danielewicz, *Introduction to Nuclear Reactions*, Institute of Physics Publishing, Bristol, 2004.
- [26] D. Brink, *Nucl. Phys. A* 519 (1990) 3c.
- [27] E. Gadioli, P.E. Hodgson, *Pre - Equilibrium Nuclear Reactions*, Clarendon Press, Oxford, 1992.
- [28] A.S. Iljinov, M.V. Kazarnovsky, E.Ya. Paryev, *Intermediate - Energy Nuclear Physics*, CRC Press, Boca Raton, 1994.
- [29] H.V. Buttlar, *Nuclear Physics: An Introduction*, Academic Press, New York, 1968.
- [30] V.F. Weisskopf, *Phys. Rev.* 52 (1937) 295.
- [31] K.S. Krane, *Introductory Nuclear Physics*, Wiley, New York, 1988.
- [32] J.R. Huizenga, L.G. Moretto, *Annu. Rev. Nucl. Sci.* 22 (1972) 427.
- [33] [http://cdfesinp.msu.ru/services/calc\\_thr/calc\\_thr\\_help.html](http://cdfesinp.msu.ru/services/calc_thr/calc_thr_help.html)
- [34] G. Audi, A.H. Wapstra, C. Thibault, *Nucl. Phys. A* 729 (2003) 337.
- [35] I. Dostrovsky, P. Rabinowitz, R. Bivins, *Phys. Rev.* 111 (1958) 1659.
- [36] H.A. Bethe, *Rev. Mod. Phys.* 9 (1937) 69.
- [37] H.A. Bethe, E.J. Konopinski, *Phys. Rev.* 54 (1938) 130.
- [38] K.J. LeCouteur, *Proc. Phys. Soc. (London)* A63 (1950) 259.
- [39] I. Dostrovsky, Z. Frankel, G. Friedlander, *Phys. Rev.* 116 (1959) 683.

- [40] V.F. Weisskopf, D. H. Ewing, Phys. Rev. 57 (1940) 672.
- [41] T. Belgya, et al., Handbook for calculations of nuclear reaction data, RIPL - 2 IAEA - TECDOC - 1506, IAEA Vienna, 2006.
- [42] A.V. Ignatyuk, Statistical Properties of Excited Atomic Nuclei, INDC(CCP) - 233/L, IAEA Vienna, 1985.
- [43] M. El Nadi, A. Hashem, Phys. Rev. C 13 (1976) 2189.
- [44] A. Goriely, J. Nucl. Sci. Technol. 2 (2002) 536.
- [45] S.M. Grimes, J. Nucl. Sci. Technol. 2 (2002) 709.
- [46] J. Bardeen, Phys. Rev. 51 (1937) 799.
- [47] V. Weisskopf, U.S. Atomic Energy Commission Report MDDC - 1175, U.S. Government Printing Office, Washington, D.C., 1947.
- [48] N. Page, Proc. Phys. Soc. (London) A63 (1950) 250.
- [49] Harding, Lattimore, Perkins, Proc. Roy. Soc. (London) A196 (1949) 325.
- [50] Y. Fujimoto, Y. Yamaguchi, Progr. Theoret. Phys. (Japan) 4 (1950) 468; 5 (1950) 76; 5 (1950) 787.
- [51] Eisberg, Igo, Wegner, Phys. Rev. 100 (1955) 1309.
- [52] P. Fong, Phys. Rev. 102 (1956) 434.
- [53] J.R. Huizenga, Statistical Properties of Nuclei, Plenum, New York, 1972.
- [54] A.V. Ignatyuk, V.S. Stavisski, Yu.N. Shubin, Nuclear Data for Reactors, IAEA Vienna, 1970.
- [55] V.S. Ramamurthy, S.S. Kapoor, S.K. Kataria, Phys. Rev. Lett. 25 (1970) 386.
- [56] S. Goriely, Nucl. Phys. A605 (1996) 28.
- [57] A.V. Ignatyuk, G.N. Smirenkin, A.S. Tishin, Sov. J. Nucl. Phys. 21 (1975) 255.
- [58] <http://www-nds.ipen.br/RIPL-2/densities/total/shellcor-ms.readme>
- [59] J.O. Newton, Phys. Scr. 24 (1981) 83.
- [60] W.E. Stephens, Nuclear Fission and Atomic Energy, Inman, Pennsylvania, 2008.
- [61] E.V. Weinstock, J. Halpern, Phys. Rev. 94 (1954) 1651.

- [62] E.A. Cherepanov, A.S. Ilijinov, M. V. Mebel, *J. Phys. G: Nucl. Phys* 9 (1983) 1397.
- [63] L.G. Moretto, *Proc. 3rd IAEA Symp. on the Physics and Chemistry of Fission*, Vol. 1, IAEA Vienna, 1973.
- [64] M.A. Preston, *Physics of the Nucleus*, Addison - Wesley, Massachusetts, 1962.
- [65] E.B. Paul, *Nuclear and Particle Physics*, Wiley, New York, 1969.
- [66] G.R. Satchler, *Introduction to Nuclear Reactions*, second ed., Macmillan Education Ltd., New York, 1990.
- [67] *Handbook on photonuclear data for applications - cross sections and spectra*, IAEA - TECDOC - Draft No. 3 (March 2000).
- [68] P. Frobrich, R. Lipperheide, *Theory of Nuclear Reactions*, Clarendon Press, Oxford, 1996.
- [69] H. Feshbach, *Theoretical Nuclear Physics*, Wiley, New York, 1992.
- [70] S. Wolfram, *The Mathematica Book*, Wolfram Research, Illinois, 2006.
- [71] M.R. Spiegel, *Mathematical Handbook*, Mc - Graw - Hill, New York, 1995.
- [72] V.G. Shevchenko, B.A. Yuryev, *Nucl. Phys.* 37 (1962) 495.
- [73] J.W. Norbury, L.W. Townsend, *Electromagnetic Dissociation Effects in Galactic Heavy - Ion Fragmentation*, NASA Technical Paper 2527, 1986.
- [74] J.D. Jackson, *Classical Electrodynamics*, third ed., Wiley, New Jersey, 1999.
- [75] C.A. Bertulani, G. Baur, *Phys. Rep.* 163 (1988) 299.
- [76] J.W. Norbury, *Phys. Rev. C* 40 (1989) 2621.
- [77] M.B. Chadwick, P.G. Young, R.E. MacFarlane, M.C. White, R.C. Little, *Nucl. Sci. Eng.* 144 (2003) 157.
- [78] M.B. Chadwick, P.G. Young, S. Chiba, *J. Nucl. Sci. Tech.* 32 (1995) 1154.
- [79] J.C. McGeorge, G.I. Crawford, R. Owens, M.R. Sene, D. Branford, A.C. Shotter, B. Schoch, R. Beck, P. Jennewein, F. Klein, J. Vogt, F. Zetzl, *Phys. Lett. B* 179 (1986) 212.
- [80] J.R. Wu, C.C. Chang, *Phys. Rev. C* 16 (1977) 1812.
- [81] W.A. Butler, G.B. Almy, *Phys. Rev.* 91 (1953) 58.

- [82] B.C. Diven, G.M. Almy, Phys. Rev. 80 (1950) 407.
- [83] G.A. Price, Phys. Rev. 93 (1954) 1279.
- [84] P.A. Tipler, R.A. Llewellyn, Modern Physics, third ed., Freeman, New York, 1999.
- [85] J.E. Baglin, M.N. Thomson, Nucl. Phys. A 138 (1965) 11.
- [86] J.W. Jury, C.K. Ross, N.K. Sherman, Nucl. Phys. A 337 (1980) 503.
- [87] Y. Birenbaum, Z. Berant, S. Kahane, A. Wolf, Nucl. Phys. A 369 (1981) 483.
- [88] J.G. Woodworth, K.G. McNeill, J.W. Jury, P.D. Georgopoulos, R.G. Johnson, Nucl. Phys. A 327 (1979) 53.
- [89] J.D. Jackson, Classical Electrodynamics, first ed., Wiley, New York, 1972.
- [90] E. Byckling, K. Kajantie, Particle kinematics, Wiley, New York, 1973.
- [91] M. Leon, Particle Physics: An Introduction, Academic Press, New York, 1973.
- [92] C.J. Joachain, Quantum collisions theory, North - Holland, Amsterdam, 1983.
- [93] K.G. Dedrick, Rev. Mod. Phys. 34 (1962) 429.
- [94] J.W. Norbury, F. Dick, Differential Cross Section Kinematics for 3 - dimensional Transport Codes, NASA Technical Paper 2008 - 215543, 2008.
- [95] B.L. Berman, S.C. Fultz, Rev. Mod. Phys. 47 (1975) 713.
- [96] J. Barrette, et al., Phys. Rev. C 41 (1990) 1512.
- [97] H.H. Heckman, P.J. Lindstrom, Phys. Rev. Lett. 37 (1976) 56.
- [98] J.C. Hill, Proc. 23rd Rencontre de Moriond Current Issues in Hadron Physics, ed. J. Tran. Thanh Van, (gif - sur - Yvette: Editions Frontieres), 147, 1988.
- [99] D.L. Olsen, B.L. Berman, D.E. Griener, H.H. Heckman, P.J. Lindstrom, G.D. Westfall, H.J. Crawford, Phys. Rev. C 24 (1981) 1529.
- [100] J. Speth, Electric and Magnetic Giant Resonances in Nuclei, International Review of Nuclear Physics, Vol. 7, World Scientific, New Jersey, 1991.
- [101] R. Hagedorn, Relativistic Kinematics, Benjamin, New York, 1963.
- [102] R. Schmidt, et al., Phys. Rev. C 67 (2003) 044308.